

THESIS FOR THE DEGREE OF LICENTIATE OF ENGINEERING

# Recycling of Antimony and Zinc from Metal Oxide Varistors (MOVs)

Characterization, leaching, purification, and high temperature studies

Toni Y. Gutknecht



Industrial Materials Recycling  
Department of Chemistry and Chemical Engineering  
CHALMERS UNIVERSITY OF TECHNOLOGY  
Gothenburg, Sweden 2015

Recycling of Antimony and Zinc from Metal Oxide Varistors (MOVs)  
*Characterization, leaching, purification, and high temperature studies*

TONI Y. GUTKNECHT

© TONI Y. GUTKNECHT, 2015

Licuppsatser vid Institutionen för kemi och kemiteknik. 2015:10  
ISSN : 1652-943X

Industrial Materials Recycling  
Department of Chemistry and Chemical Engineering  
Chalmers University of Technology  
SE-412 96, Gothenburg  
Sweden  
Telephone: +46 (0) 31-772 1000  
tonig@chalmers.se

Cover:

The cover image shows a SEM micrograph with EDX overlay for detection of zinc (red), antimony (green), and bismuth (blue) on a pulverized particle of MOV

Chalmers Reproservice  
Gothenburg, Sweden, 2015

## Recycling of Antimony and Zinc from Metal Oxide Varistors (MOVs)

TONI Y. GUTKNECHT

Industrial Materials Recycling  
Department of Chemistry and Chemical Engineering  
Chalmers University of Technology

### ABSTRACT

Surge arrestors are an important part of power and rail systems because they protect from overvoltages due to transients such as lightning. Within a surge arrestors lies the metal oxide varistors (MOVs) which are composed mainly of zinc oxide (>90 wt %) and a number of other metals such as antimony (which is both a critical and strategic material), bismuth, cobalt, manganese, and nickel. This work set out to develop a recycling process to recover antimony and zinc from the MOVs and optimize process parameters for economical implementation into an industry acceptable process.

Zinc was leached from the MOVs using acetic, hydrochloric, nitric, and sulfuric acid but not selectively. Co-leaching of cobalt, nickel, and manganese could not be avoided with the conditions studied in this work. The most important acid studied was sulfuric acid because it is used industrially in hydrometallurgical zinc production. Using sulfuric acid avoided co-leaching of antimony and bismuth but required further purification to remove the co-leached metal impurities. It was the intent of the author to develop a recycling scheme for MOVs that could be easily incorporated into a mainstream industrial process.

Purification of the leachate via cementation was investigated, initial findings suggested that the cobalt concentration can be reduced by nearly 45 %, nickel concentration reduced by nearly 60 %, and antimony and copper can be completely removed from the leachate at room temperature. This can be optimized for cobalt removal by adjusting the amount of zinc added, the antimony and copper concentrations, temperature, and the pH. At elevated temperatures and optimized conditions more than 50% of cobalt can be removed from solution. Further investigation into batch addition of zinc and antimony-copper additives needs to be done to determine if cementation is a feasible means of leachate purification.

Leaching of the MOV served two purposes: (1) separated the bulk zinc oxide from the non-leachable metal oxide compounds and (2) concentrated the antimony rich phase into a solid residue. Once the residue was separated from the leachate it was investigated for the possibility of high temperature antimony recycling. The initial findings show that antimony oxide can be recovered at temperature lower than 1100 °C by direct reduction. Carbothermal reduction of the leaching residue leads to the formation of a Sb-Ni-Co alloy making antimony recovery more difficult.

With further improvements to leachate purification a high purity zinc leachate is possible and can be used in zinc electrowinning however the recovery of antimony from the MOV requires further investigation.

**KEYWORDS:** recycling, antimony, zinc, metal oxide varistor, leaching, cementation, direct reduction, carbothermal reduction, hydrometallurgy

## LIST OF PUBLICATIONS

This thesis is based on the work contained in the following paper:

Paper I:

Gutknecht T., Gustafsson A., Forsgren C., Ekberg C., Steenari B.M. *Investigations into Recycling Zinc from Used Metal Oxide Varistors via pH Selective Leaching: Characterization, Leaching, and Residue Analysis*

Accepted to World Scientific Journal

Contribution Report:

All experimental work, data treatment, evaluation and major part of writing the manuscript

## ACKNOWLEDGEMENTS

The author of this work would like to thank:

- Chalmers Area of Advance - Production for providing the funding for this work
- Supervisor Britt-Marie Steenari for her time, guidance, patience, and help
- The Examiner (Prof. Christian Ekberg) and Reviewers
- Christer Forsgren and STENA
- Carina Svenheden for helping to find me a place to live before I came here to Gothenburg (otherwise I might have been living in a box) and for all the work you do at the department
- Sandra Gustafsson for your help in finding answers to all my questions
- Mikael my wonderful Swedish lover and his beautiful but hairy cat Katherine
- Sweden for approving my residency and welcoming me with open arms
- Mother Nature for providing cold and rainy weather which promotes long working hours and difficulty or limited time for outdoor activities
- Most of my current and former colleagues
- Anna and Filip for putting up with me in the office and still being able to hang out later
- Yuda Columbus Chryspian for your excellent lab work and ideas
- OOMK for their equipment and nice people with emphasis on Volkmer, Mohsen, Dongmei, and Pavleta
- Stellan, Marcus and Britt-Marie for help with BET, SEM, and XRD respectively
- Anders Kvist for SEM help
- My friends from the US for the really good times and good memories
- My friends made in Sweden also for the good times and good memories
- The quote, "Do what you like, like what you do!" which I try to follow but sometimes get lost along the way
- Last and most importantly my family! Who are all so much fun and really great people and have taught me the most important things in life!

Thank You All!  
Toni Gutknecht

Gothenburg, Sweden  
October 2015

## TABLE OF CONTENTS

<b>LIST OF FIGURES</b> .....	IX
<b>LIST OF TABLES</b> .....	X
<b>LIST OF ACRONYMS &amp; UNITS</b> .....	XI
<b>1. INTRODUCTION</b> .....	1
<b>2. BACKGROUND</b> .....	1
2.1. Description of MOV .....	1
2.1.1. Composition .....	2
2.1.2. Why recycle MOVs? .....	3
2.2. Antimony .....	4
2.2.1. Uses of Antimony .....	4
2.2.2. Sources of Secondary Antimony .....	4
2.2.3. Recycling of Antimony from MOV .....	5
2.3. Zinc.....	6
2.3.1. Uses of Zinc.....	6
2.3.2. Sources of Secondary Zinc.....	6
2.3.3. Primary Zinc Production .....	6
2.3.4. Recycling of Zinc .....	8
<b>3. THEORY</b> .....	9
3.1. Cementation.....	9
3.2. Carbothermal Reduction.....	10
3.3. Activation Energy.....	11
3.4. Uncertainties.....	12
<b>4. EXPERIMENTAL</b> .....	12
4.1. Analysis Equipment .....	12
4.1.1. ICP-OES .....	12
4.1.2. SEM.....	13
4.1.3. XRD.....	13
4.1.4. TGA.....	13
4.2. Experimental Outline .....	14
4.3. Characterization of MOV .....	15
4.4. Leaching Study.....	16
4.5. Cementation Study .....	18
4.5.1. Cementation Solution – Bulk Leachate of MOV .....	18
4.5.2. Cementation Experiments .....	18
4.6. Antimony Recovery .....	20
4.6.1. Leachate Residue Characterization .....	20

4.6.2.	Reduction Experiments (RT – 1000 °C) .....	21
4.6.3.	Reduction Experiments (RT to 1300 °C) .....	21
<b>5.</b>	<b>RESULTS AND DISCUSSION</b> .....	<b>22</b>
5.1.	Characterization of MOV .....	22
5.2.	Leaching .....	24
5.2.1.	Sulfuric Acid Leaching.....	24
5.2.2.	Analysis of Leaching Residue .....	26
5.3.	Cementation.....	28
5.3.1.	Cementation Solution Preparation - Bulk Leaching of MOV .....	28
5.3.2.	Cementation Experiments .....	29
5.3.2.1.	Influence of Copper Ion Concentration .....	29
5.3.2.2.	Influence of Antimony Concentration.....	31
5.3.2.3.	Influence of Temperature .....	33
5.3.2.4.	Influence of Zinc Dust.....	34
5.3.2.5.	Influence of pH.....	37
5.3.2.6.	Optimized Cementation.....	38
5.4.	Antimony Recovery .....	39
5.4.1.	Characterization of the Sb-rich leaching residue.....	39
5.4.2.	Feasibility Study - Direct and Carbothermal Reduction.....	40
5.4.2.1.	Direct Reduction.....	40
5.4.2.2.	Carbothermal Reduction.....	41
5.4.3.	Direct Reduction of Residue .....	42
5.4.4.	Carbothermal Reduction of Residue.....	43
5.4.5.	Recovery of Antimony from Residue.....	44
5.5.	Antimony Oxide Chemistry – Activation Energy Determination .....	49
<b>6.</b>	<b>SUMMARY &amp; CONCLUSIONS</b> .....	<b>53</b>
6.1.	Leaching .....	53
6.2.	Cementation.....	53
6.3.	Antimony Recovery .....	53
<b>7.</b>	<b>FUTURE WORK</b> .....	<b>54</b>
<b>8.</b>	<b>REFERENCES</b> .....	<b>55</b>

## LIST OF FIGURES

Figure 1: Surge arrester at a) power station in Borås Sweden, b) connected to railway line, c) power lines outside house, and d) portable electronics.....	2
Figure 2: Amount of MOV produced in Sweden during a 5 year period.....	3
Figure 3: Schematic of furnace used in TA Instruments TGA Q500 [73]. .....	14
Figure 4: Process flow diagram for work presented in this licentiate .....	15
Figure 5: Titration vessel with (a) pipet, (b) dosing device, (c) Ag/Ag Cl pH electrode, (d) stir bar, and (e) leaching solution.....	17
Figure 6: Cementation setup with reaction vessel, stir plate, Ag/AgCl pH electrode, dosing device, N <sub>2</sub> line and all non-used ports sealed off. ....	19
Figure 7: SEM/EDX micrograph of pulverized MOV having three phases: Phase I – ZnO grain, Phase II – antimony rich phase, Phase III – bismuth rich phase. (a) EDX map for zinc, (b) EDX map for antimony, (c) EDX map for bismuth (d) combined EDX map for zinc (red), antimony (green) and bismuth (blue) overlay on SEM micrograph for pulverized MOV particle. (e) SEM micrograph of pulverized MOV shown without EDX map overlay.....	23
Figure 8: XRD spectra of the MOV showing peaks for ZnO (●), Bi <sub>2</sub> O <sub>3</sub> (◆), Zn <sub>2.33</sub> Sb <sub>0.67</sub> O <sub>4</sub> (□), Zn <sub>2</sub> Bi <sub>3</sub> Sb <sub>3</sub> O <sub>14</sub> (★), and Zn <sub>7</sub> Sb <sub>2</sub> O <sub>12</sub> (■). .....	24
Figure 9: The leached fraction as given by the left ordinate for zinc (□), bismuth (○) and antimony (△) from the MOV in a) pH 1, b) pH 3, and c) pH 5 solutions. The volume and concentration of sulfuric acid (H <sub>2</sub> SO <sub>4</sub> ) added is shown as a solid black line corresponding to the right ordinate. ....	25
Figure 10: The leached fraction as given by the left ordinate for cobalt (□), manganese (○) and nickel (△) from MOV in a) pH 1, b) pH 3, and c) pH 5 solutions. The volume and concentration of sulfuric acid (H <sub>2</sub> SO <sub>4</sub> ) added is shown as a solid black line corresponding to the right ordinate. ....	25
Figure 11: (a) SEM micrograph of pulverized MOV post leaching in pH 1 sulfuric acid solution for 240 minutes. The antimony-rich phase (phase II) remains along with some undissolved bismuth-rich phase (phase III). (b) SEM micrograph of the MOV prior to leaching showing all three phases: phase I – zinc oxide grains, phase II – antimony rich phase, and phase III – bismuth rich phase. ....	26
Figure 12: XRD spectrum (-----) of leaching residue (pH 1, sulfuric acid) compared to XRD spectrum of non-leached starting material (- - - -). Chemical compounds are represented as follows: Bi <sub>2</sub> O <sub>3</sub> (◆), Zn <sub>2.33</sub> Sb <sub>0.67</sub> O <sub>4</sub> (□) and Zn <sub>7</sub> Sb <sub>2</sub> O <sub>12</sub> (■) .....	27
Figure 13: (a) Amount of 5 M H <sub>2</sub> SO <sub>4</sub> solution added during bulk MOV leaching experiment vs. time. (b) The pH vs. time during the bulk leaching experiments.....	28
Figure 14: Results for the influence of copper concentration on cementation of a.) cobalt, b.) copper, c.) nickel and d.) antimony, with copper concentrations of 0.2, 0.4, 0.8, and 1.2 g·L <sup>-1</sup> at T = 22 °C.....	30
Figure 15: Results for the influence of copper concentration in the presence of 0.4 g·L <sup>-1</sup> antimony on cementation of a.) cobalt, b.) copper, c.) nickel and d.) antimony, with copper concentrations of 0.2, 0.4, 0.8, and 1.6 g·L <sup>-1</sup> at T = 22 °C.....	31
Figure 16: Results for the influence of antimony concentration on cementation for a.) cobalt, b.) copper, c.) nickel and d.) antimony, with copper concentration of 0.4 g·L <sup>-1</sup> and antimony concentrations of 0.1, 0.2, 0.4, 0.8, and 1.6 g·L <sup>-1</sup> at T = 22 °C. ....	32
Figure 17: Results for the influence of temperature (T = 22, 30, 40, 50, 55, 60 °C) on cementation of a.) cobalt, b.) copper, c.) nickel and d.) antimony, with copper and antimony concentrations of 0.4 g·L <sup>-1</sup> .....	33
Figure 18: SEM of zinc dust used in cementation reactions .....	35
Figure 19: Results for the influence of zinc dust addition (0.25, 0.5, 1, 2, 3, 4 g·L <sup>-1</sup> Zn) on cementation of a.) cobalt, b.) copper, c.) nickel and d.) antimony, with copper and antimony concentrations of 0.4 g·L <sup>-1</sup> at T = 22 °C. ....	36
Figure 20: Results for the influence of solution pH on cementation of a.) cobalt, b.) copper, c.) nickel and d.) antimony, with copper and antimony concentrations of 0.4 g·L <sup>-1</sup> at T = 22 °C.....	37
Figure 21: Cementation results for optimized experimental conditions.....	38
Figure 22: SEM micrograph of antimony rich leaching residue surrounded by Bi <sub>2</sub> O <sub>3</sub> . ....	39
Figure 23: XRD spectrum of MOV leaching residue showing many different possible chemical structures present in the MOV leaching residue. ....	40

Figure 24: Direct reduction of antimony Oxide ( $Sb_2O_3$ ), bismuth oxide ( $Bi_2O_3$ ), zinc oxide ( $ZnO$ ), MOV, and leaching residue run in $N_2$ with a heating rate of $10\text{ }^\circ\text{C}\cdot\text{min}^{-1}$ .	41
Figure 25: Carbothermal Reduction of zinc oxide ( $ZnO$ ), Antimony Oxide ( $Sb_2O_3$ ), Bismuth Oxide ( $Bi_2O_3$ ), MOV, and leaching residue in $N_2$ with a heating rate of $10\text{ }^\circ\text{C}\cdot\text{min}^{-1}$ .	42
Figure 26: TGA heating curves for the effect of heating rate on direct reduction of the leaching residue.	43
Figure 27: Effect of carbon to residue ratio on carbothermal reduction of leaching residue	44
Figure 28: XRD spectra for direct reduction of MOV leaching residue in argon atmosphere at $T = 22, 500, 700, 825, 900, 1100$ and $1300\text{ }^\circ\text{C}$ .	46
Figure 29: SEM micrographs of the leachate residue after heating to a.) $T = 500\text{ }^\circ\text{C}$ , b.) $T = 700\text{ }^\circ\text{C}$ , c.) $T = 825\text{ }^\circ\text{C}$ , d.) $T = 900\text{ }^\circ\text{C}$ , e.) $T = 1100\text{ }^\circ\text{C}$ , and f.) $T = 1300\text{ }^\circ\text{C}$ in an argon atmosphere.	47
Figure 30: XRD spectra for carbothermal reduction of MOV leaching residue in argon atmosphere at $T = 22, 500, 700, 825, 900, 1000$ and $1100\text{ }^\circ\text{C}$ .	48
Figure 31: SEM micrographs of the leachate residue and carbon after heating to a.) $T = 500\text{ }^\circ\text{C}$ , b.) $T = 700\text{ }^\circ\text{C}$ , c.) $T = 825\text{ }^\circ\text{C}$ , d.) $T = 900\text{ }^\circ\text{C}$ , e.) $T = 1000\text{ }^\circ\text{C}$ , and f.) $T = 1100\text{ }^\circ\text{C}$ in an argon atmosphere.	49
Figure 32: XRD spectrum of as purchased $Sb_2O_3$ confirming the presence of valentinite ( $\beta\text{-}Sb_2O_3$ ) having an orthorhombic crystal structure. This does not disprove the presence of sermontite ( $\alpha\text{-}Sb_2O_3$ ), which has a cubic crystal structure.	50
Figure 33: Effect of heating rate on direct thermal decomposition of $Sb_2O_3$ in nitrogen atmosphere.	50
Figure 34: Arrhenius plot of the log of heating rate vs. temperature for sublimation of $Sb_2O_3$ with conversion ratios of $\alpha = 0.05, 0.10, 0.15,$ and $0.20$ showing the Arrhenius activation energy for each conversion ratio.	51
Figure 35: First derivative of thermolysis curves (Figure 33) as a function of temperature.	52

## LIST OF TABLES

Table 1: Selected standard reduction potentials in aqueous solutions at $25\text{ }^\circ\text{C}$ vs. SHE [56].	9
Table 2: Particle size fraction by weight of pulverized MOV.	16
Table 3: List of cementation experiments and the parameters which were studied.	20
Table 4: Values of TGA operating parameters.	21
Table 5: Composition of samples used in feasibility study of carbothermal reduction.	22
Table 6: Chemical composition of MOV	22
Table 7: Summary of each metal leached during sulfuric acid leaching for pH 1, pH 3 and pH 5. All values are given in fraction leached.	26
Table 8: Concentration of metals in leachate for the elements found in the MOV along with industrial zinc electrowinning solution concentrations before and after cementation.	29
Table 9: Quantity of zinc dust added during cementation experiments with correlating surface area.	34
Table 10: Concentration of metals in MOV leachate before and after cementation.	38
Table 11: ICP-OES results of leaching residue, tested in triplicate and given in wt %.	39
Table 12: Summary of residue samples for study on antimony recovery.	45

## LIST OF ACRONYMS & UNITS

$\beta$	Heating rate, degree per minute
BET	Brunauer–Emmett–Teller
C	Concentration
$C_0$	Initial concentration
CE	Current efficiency
$E^\circ$	Standard potential
EDX	Energy Dispersive X-ray
ESEM	Environmental Scanning Electron Microscope
EU	European Union
F	Faraday's constant, $96485 \text{ J}\cdot\text{v}^{-1}\cdot\text{mol}^{-1}$
$\Delta G^\circ$	Standard change in Gibb's Free Energy
ICP-OES	Inductively Coupled Plasma – optical emission spectroscopy
ICP-MS	Inductively Coupled Plasma – Mass Spectroscopy
$K_{\text{eq}}$	Equilibrium constant
M	Molarity ( $\text{mol}\cdot\text{L}^{-1}$ )
Me	Metal
$\text{Me}_x\text{O}_y$	Metal oxide
MOV	Metal Oxide Varistor
MT	Metric Ton
RLE	Roast Leach Electrowinning
SEM	Scanning Electron Microscope
SHE	Standard Hydrogen Electrode
TGA	Thermogravimetric Analysis
US	United States
W	Instantaneous mass
$W_0$	Initial mass
$W_\infty$	Final mass
XRD	X-Ray Diffraction

## 1. INTRODUCTION

In waste management it is important to have sustainable development of production as well as disposal and recycling. Sustainable being defined by Brundtland [1] as, “the kind of development that meets the needs of the present without compromising the ability of future generations to meet their own needs.” In the United States and some European countries landfilling has been the most used means for waste disposal [2]. However, nowadays recycling of materials from the products and production waste is recognized as a more sustainable way of managing spent products than landfilling, since reclaiming materials from a landfill is not easily accomplished.

Electrical transmission and distribution equipment such as power poles, insulators, street lamps, transformers and protective equipment is a potentially large source of solid waste. The current power grid and upgrading of deteriorating or obsolete infrastructure will generate a significant amount of potentially valuable material some of which may be suitable for recycling as opposed to landfilling. Of importance for the work presented in this licentiate thesis is scrap from surge arrestors which consists of a polymeric housing and metallic flanges. Within the polymeric housing lies the most important part of the surge arrest, the metal oxide varistor (MOV) [3]. The MOV is a type of resistor with significant non-linear current-voltage characteristics used in power lines to protect transformers against overvoltage from lightning or switching surges during routine operations. The MOV plays an integral role in protecting our power grid with no negative effects on the electrical system during normal conditions [3, 4]. MOVs are sintered disks composed mostly of zinc oxide and to a lesser extent bismuth, antimony or other metal oxides [3].

The recycled, purified products from the MOVs have the potential to be used as the raw starting materials for the production of new MOVs or can be sold as a pure compound and used for production of other consumer goods. The main objective of this investigation was to determine if a suitable process can be developed to recycle antimony and zinc from the MOVs and optimize process parameters for economical implementation into an industry acceptable process. This work has the potential to be extended to electrolytic purification of metals such as zinc. Expected results from this study could provide background information on basic thermodynamics, chemical reactions, physical and chemical properties, experimental setup and design as well as predicted outcomes and potential problems.

## 2. BACKGROUND

### 2.1. Description of MOV

Surge arrestors are important parts of power and rail system because they protect power systems (such as homes, rail systems and businesses) from over voltages due to lightning or transients in the power grid. The need to replace or build power lines is increasing with demand from developing countries. Thus, many surge arrestors need to be replaced to accommodate larger voltage requirements. The end of life surge arrestors can be disassembled giving rise to a material rich in antimony and zinc oxides amongst other metal oxides. Figure 1 shows the different areas where surge arrestors are used. It is clear that surge arrestors containing critical and valuable metals can be found at power stations, rail way lines, power lines, or anywhere the power supply might be affected by a power surge.

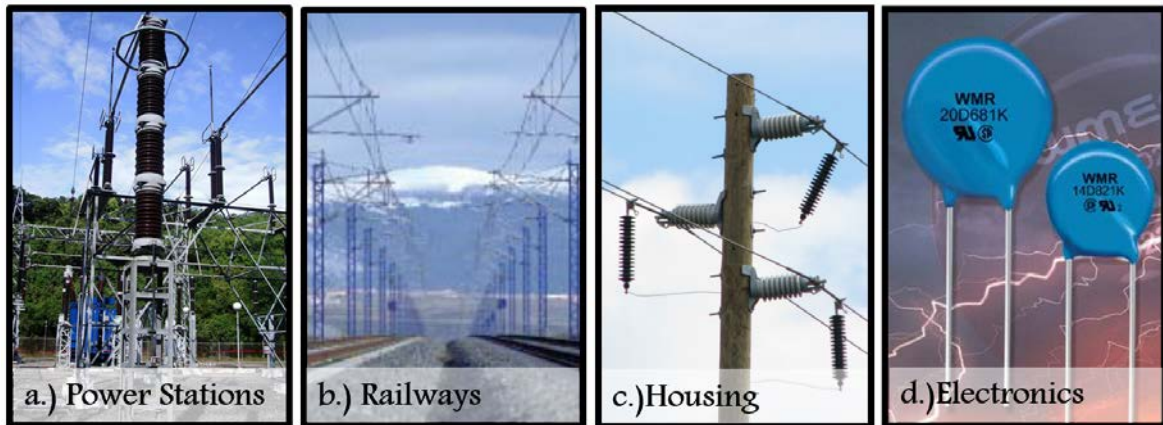


Figure 1: Surge arrester at a) power station in Borås Sweden, b) connected to railway line, c) power lines outside house, and d) portable electronics.

Housed inside the surge arrester is a stack of MOVs, most important to this research are polycrystalline ceramic zinc oxide varistors which are stacked in series and separated by a thin layer of aluminum [5]. The desired property of a MOV is that it be a perfect insulator up to the breakdown voltage above which point it should become highly conductive. The surge arrester contains many parts such as: porcelain insulator, venting duct, spring, desiccant bag, copper sheet, sealing cover, sealing ring, indication plates, ZnO blocks, and flange cover [6]. This work will focus solely on the metal oxide varistor, i.e. zinc oxide varistor.

Zinc Oxide (ZnO) is used in MOVs because of its piezoelectric properties, conductivity, and highly non-linear voltage-current characteristics [7]. Bismuth oxide ( $\text{Bi}_2\text{O}_3$ ) and antimony oxide ( $\text{Sb}_2\text{O}_3$ ) are added to ZnO during construction of the MOVs to enhance its properties. The current-voltage behavior of MOV is attributed mainly to the addition and presence of  $\text{Bi}_2\text{O}_3$  [8]. In addition  $\text{Bi}_2\text{O}_3$  strongly alters the sintering behavior by producing a liquid phase with ZnO and making a eutectic melt at  $738^\circ\text{C}$  and enabling liquid phase sintering.  $\text{Sb}_2\text{O}_3$  is added to decrease the average size of the ZnO grains [8, 9] and therefore increasing the breakdown voltage by increasing the number of barriers and grain boundaries [5].

### 2.1.1. Composition

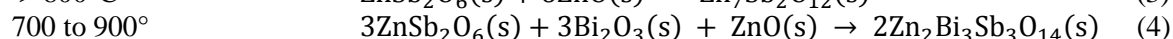
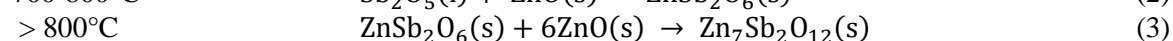
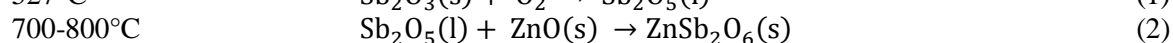
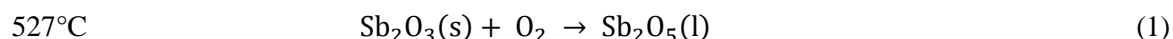
MOVs are produced from raw materials (typically including  $\text{Sb}_2\text{O}_3$ ,  $\text{Bi}_2\text{O}_3$ ,  $\text{MnCO}_3$ ,  $\text{NiO}$ , and  $\text{Co}_2\text{O}_3$ ) which are calcined at around  $700^\circ\text{C}$ . The calcine is mixed with water and milled until the average particle size is around  $1\mu\text{m}$ . The calcine is then mixed with ZnO and spray dried to get granules which are easy to press (homogeneous body). The mixed oxides are then pressed into a green body which is 50-60 % of the theoretical density [10]. The green body is sintered between  $1000$  to  $1300^\circ\text{C}$ . During sintering the MOV experiences linear shrinkage [11, 12]. A glass layer is added to the outside of the MOV and the top and bottom are covered with thin aluminum metallization layer resulting in a useful MOV to be placed in surge arrestors [11, 13].

A MOV has a multiphase polycrystalline microstructure with each phase having different dopants, dopant concentrations, shape and size [9, 14]. MOVs contain primarily ZnO grains in addition to secondary phases such as the antimony-zinc-oxide spinel structure, surrounded by a 3-D network of bismuth rich phase (grain boundaries and pores) [9].

It has been shown that during liquid phase sintering antimony (III) oxide is oxidized to antimony (V) oxide near  $530^\circ\text{C}$  [14]. By heating the antimony (V) oxide with zinc oxide a trirutile,  $\text{ZnSb}_2\text{O}_6$  phase forms [15]. It was shown by Leite et al. that the trirutile phase is most likely an intermediate phase in the formation of the spinel phase [14]. The spinel compound contains two structures: (1) cubic structure with chemical formula  $\text{Zn}_{2.33}\text{Sb}_{0.67}\text{O}_4$  and (2) orthorhombic structure having chemical formula

Zn<sub>7</sub>Sb<sub>2</sub>O<sub>12</sub> [16, 17]. Heating of the trirutile phase, zinc oxide and bismuth oxide forms pyrochlore (Zn<sub>2</sub>Bi<sub>3</sub>Sb<sub>3</sub>O<sub>14</sub>) at sintering temperatures between 700 to 900 °C [8]. Further heating (900 to 1050 °C) of the pyrochlore phase with zinc oxide results in decomposition of the pyrochlore phase to spinel and formation of liquid bismuth oxide phases [14] which promote liquid phase sintering of the zinc oxide with liquid bismuth oxide.

It was suggested by Leite et al. [14] that the following reactions given in Equations 1-4 occur leading to the formation of pyrochlore having the composition, Zn<sub>2</sub>Bi<sub>3</sub>Sb<sub>3</sub>O<sub>14</sub> [8, 14].



Antimony changes its valence from Sb<sup>+3</sup> to Sb<sup>+5</sup> when spinel and pyrochlore are formed from Sb<sub>2</sub>O<sub>3</sub> meaning that additional oxygen is required from the atmosphere during sintering. Typical grain size of ZnO in the MOV is in the range of 20 to 140 μm. The spinel phase has a grain size of 1-2 μm. At room temperature the Bi<sub>2</sub>O<sub>3</sub> phase is crystalline, however, it may exist in several crystalline forms depending on the cooling rate and the presence of transition metal oxides [18]. Other additives may be present such as MnCO<sub>3</sub>, Co<sub>3</sub>O<sub>4</sub>, Cr<sub>2</sub>O<sub>3</sub>, SiO<sub>2</sub> and H<sub>2</sub>O<sub>3</sub> [5, 7, 9, 18, 19].

### 2.1.2. Why recycle MOVs?

In Sweden, there is an initiative to recycle MOVs as opposed to landfilling due to environmental concerns, rising costs of landfilling, awareness of the value of the material in the MOV, and the quantity of material available for recycling. In 2013, one company in Sweden produced 132 tons of MOV [20] and in the last 5 years, 523 tons of MOV have been produced. Shown in Figure 2 is the amount of MOV (in tons) produced from 2009 to 2013 as well as the composition of the MOV in terms of metal oxides. Considering this is only one company in a relatively small country the amount of MOV produced and eventually available for recycling is encouraging as a source of secondary antimony and zinc. The used MOV are primarily not mixed with other types of waste materials (at least in Sweden) but kept in a separate flow. This makes them an ideal case for a dedicated recycling method.

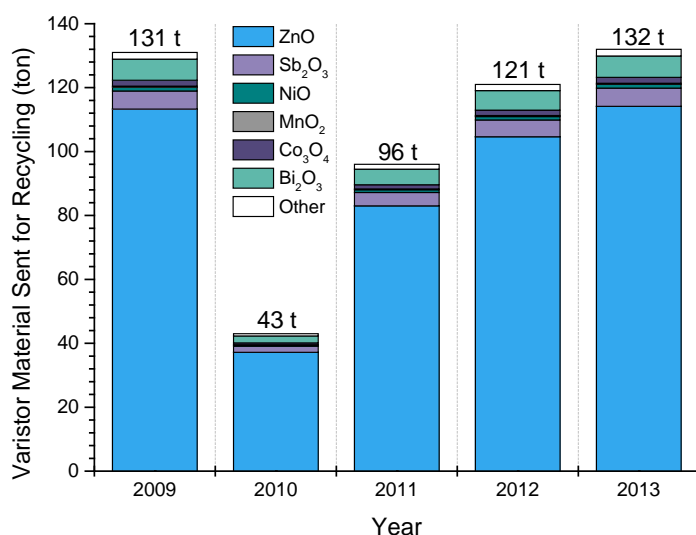


Figure 2: Amount of MOV produced in Sweden during a 5 year period.

Other than zinc which is in the MOV in high concentrations antimony should preferably also be recovered. It is listed as a critical metal for the European Union (EU) as well as strategic metal for the United States Department of Defense [21, 22]. It is predicted that under a national security emergency

in the US there would be severe shortage of antimony along with only three other metals [22]. By recovering the antimony either as a metal or as a metal oxide from the 523 tons of MOV produced, nearly 20 tons of antimony could be recovered and used in lead acid batteries or converted into antimony oxide for a plethora of other uses.

## 2.2. Antimony

Antimony is found in the earth's crust at a concentration of 0.2 g/ton making it one of the rarest elements on earth [23]. Antimony has an atomic mass of 51 and is a silvery white metalloid located in group 5 row 11 of the periodic table and is the 63<sup>rd</sup> most abundant metal in the earth's crust. Even though antimony is considered a metal it is a poor conductor of electricity and heat, is brittle, and has a density of 6.697 g/cm<sup>3</sup> at 26 °C. Antimony has roughly 1/20<sup>th</sup> the thermal conductivity of copper [24] but that can vary depending on grain size and the direction in the crystal. Antimony melts at 630 °C and boils at 1380 °C with a specific gravity between 6.62 and 6.69 [25]. Typically antimony is not found alone in nature because of its high affinity for other metals (i.e. copper, lead, silver) and sulfur [26]. Therefore antimony is typically produced as a byproduct from mining zinc, nickel, and other metals. Antimony has a Mohr's hardness ranging from 3 to 3.5 but is too brittle to be used without alloying [27]. It is typically alloyed with other metals or incorporated into compounds.

The EU is dependent entirely on imports of antimony, though total EU consumption in 2007 (792 tons) only accounted for 0.5% of the world production [21]. The United States (US) in 2013 imported 25,000 metric tons of antimony ores and concentrates, oxides and metal for consumption [25]. The same year the US recycled 3,500 metric tons of antimony for use as secondary antimony recovered by smelting [25]. In total 85% of the antimony used in the US was imported mainly from the People's Republic of China (74%), Mexico (10%) and India (7%). In 2008 a total of 187,000 tons of antimony was produced of that 91% was produced in China.

### 2.2.1. Uses of Antimony

The most important use of antimony industrially is as a flame retardant in cloths, toys, plastics, aircraft and automobile seat covers. Antimony trioxide is used as a polycondensation catalyst in manufacture of PET [28] and in cloths manufacturing as a catalyst for polyester production. Typical antimony concentrations in PET are 150-250 mg/kg [28]. Antimony metal has other uses such as hardeners in lead for storage batteries, additive in glasses and ceramics, ammunition, as an opacifier in pigments and as an alloy in solders. However, the largest single use of antimony industrially is as a flame retardant.

Future uses of antimony may be as a compound in semiconductors and as an antimony-tin-oxide alloy which has the same characteristics as indium-tin-oxide but will be much cheaper [21, 29] it can be used in LCD displays, OLEDs or photovoltaic cells [21]. More and more antimony is being used in industry even though only relatively small amounts are needed. Because more products contain antimony the amount of antimony used annually is increasing and enhances the importance of recycling.

### 2.2.2. Sources of Secondary Antimony

Antimony is typically present in industrial and commercial products in small amounts, because of this recycling of antimony is extremely difficult [30]. Antimony can be classified as a rare or special metal and is not a major metal used industrially, nor is it used in high concentrations. At the moment a very limited amount of recycling is done. The concentration of a metal in a waste stream to be recycled can be a major factor affecting the recycling rate. Conventional recycling routes are typically not applicable for rare metals such as antimony if no prior pretreatment step(s) are done [31]. Pretreatment is done to increase antimony concentration or to allow for proper separation of metals in further hydro- or pyro-metallurgical recycling steps.

In terms of antimony concentration MOVs contain one of the highest concentrations (except lead acid batteries) in consumer goods. However, antimony used in ceramic material consumes the least amount of antimony when compared to other areas such as flame retardants, batteries, plastics and alloys. Over 60 % of antimony used is as a flame retardant [23] in plastics and textiles making it impossible to design a recycling route from this waste stream due to the low amount of antimony available in scrap compared to the large amount of scrap produced [31].

Currently, in the US antimony recycling has been limited to recycling of lead-acid batteries where the secondary antimony is put back into the construction of new lead-acid batteries. In 1990 the US recycled 20,000 tons of antimony while using nearly 39,000 tons/year [32]. In the Netherlands about 375 tons of antimony is recycled per year while their consumption is approximately 1300 tons annually [32].

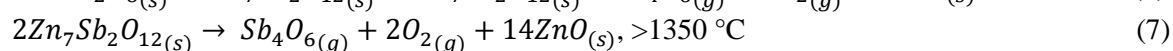
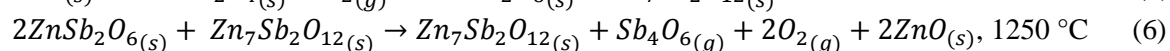
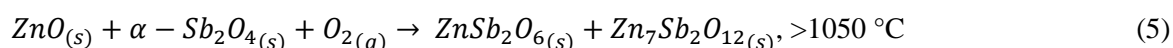
Antimony use in the battery industry is decreasing due to downsizing of automobile batteries. Due to these circumstances the future use of antimony will come from primary antimony and the recycling rate will decline if no new methods to recover antimony from suitable waste streams are developed. Secondary antimony-lead oxide recovered from battery recycling is not suitable for use as a flame retardant [31].

Another potential source of secondary antimony comes from municipal/industrial waste. The major source of antimony in MSW is when it is used as a flame retardant in textiles or non-recyclable plastics which are mainly sent to combustion to date. The concentration of antimony in the waste incinerator feed stream is 42 mg/kg [32]. As previously stated over 60 % of antimony is used as a flame retardant and of that 35% comes as a flame retardant in consumer electrical and electronic equipment. Due to the increased use of electronics and an ever expanding consumer and product base there seems to be no decline in the concentration of antimony in municipal waste incinerator feedstock. This makes the ash a candidate for a secondary source of antimony. There is increased incentive to recycle antimony from incineration residues due to its toxicological and hazardous properties [32].

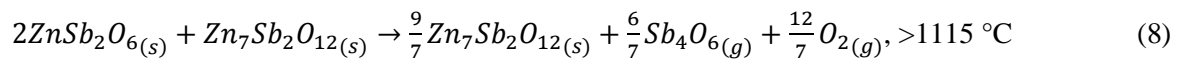
The MOV is a good source of antimony because of its relatively high concentration. Also, the chemical form of antimony containing compounds is known and is relatively simple when comparing it to antimony compounds found for instance in municipal solid waste (MSW) ash. In the MOV the antimony is contained within the spinel structure ( $Zn_7Sb_2O_{12}$  or  $Zn_{2.33}Sb_{0.67}O_4$ ) and the concentration does not vary widely from different MOV or producers of MOV.

### 2.2.3. Recycling of Antimony from MOV

Antimony needs to be concentrated from the MOV for recovery to be feasible. If the zinc oxide portion of the MOV is removed the remaining solid would be the  $Bi_2O_3$  intergranular phase and the antimony rich phase (pyrochlore and spinel) [18]. Work done by Filipek et al. where a sample of  $\alpha$ - $Sb_2O_4$  and ZnO were heated in air to 1500 °C noted that the sample never melted but a change in mass occurred due to the decomposition of  $ZnSb_2O_6$  and  $Zn_7Sb_2O_{12}$ . Their work also showed that in air  $\beta$ - $Zn_7Sb_2O_{12}$  remains in equilibrium with ZnO up to 1225 °C where  $\beta$ - $Zn_7Sb_2O_{12}$  transitions to  $\alpha$ - $Zn_7Sb_2O_{12}$ . At temperature greater than 1350 °C  $\alpha$ - $Zn_7Sb_2O_{12}$  decomposes to ZnO releasing  $Sb_4O_6(g)$  and  $O_2(g)$  [33]. The reactions that Filipek et al. suggest are given by Equations 5 – 8 [34]:



In argon samples with ZnO and  $\beta$ - $Zn_7Sb_2O_{12}$  remain in the solid state until approximately 1115 °C when  $Zn_7Sb_2O_{12}$  starts to decompose according to the reaction given in Equation 8.



Filipek's suggests the breakdown of the spinel phase at temperature above 1115 °C in argon at which temperature it may be possible to recover antimony. It has been shown industrially that adding carbon to both zinc and antimony oxides lowers the reduction temperature [26, 35]. It may be possible to recover the antimony at lower temperature than 1115 °C. However the MOV contains bismuth, cobalt, manganese, and nickel which the samples of Filipek et al. did not have.

### 2.3. Zinc

#### 2.3.1. Uses of Zinc

Zinc is used for a number of reasons but in industry it is mostly used for galvanization which helps reduce the corrosion of steel. Zinc is also used in brass, zinc based alloys, zinc salts and semi-manufacturing for roofing, gutters, and down-pipes [21]. A little over 45% of zinc is used for galvanizing in which a thin layer of zinc is plated on steel to protect from corrosion [21]. Brass and other zinc alloys account for 30% of zinc use, followed to a lesser extent by chemicals such as zinc salts and semi manufacturing [21]. Zinc salts are used in the textile industry, manufacturing of batteries, chemical industry, agriculture and animal feed [21].

Zinc is not used as frequently as other major metals (i.e. iron, copper, aluminum, etc.) but its use continues to trend upward. Nearly half of all the Zn employed in human history was mobilized and put into use in the 1970-2000 timeframe [36].

#### 2.3.2. Sources of Secondary Zinc

The European Union (EU) does not currently consider zinc as one of its critical metals [21] but the point still remains that industrial metals should be recycled, at the very least when economically feasible. Recycling of zinc currently supplies 25-30% of the world's demand for zinc metal and zinc oxide [36]. The major sources of the recycled zinc containing material are:

- Brass scrap, old and new, 32%, recycled as brass
- Galvanizing process residues, 23%
- Scrap die castings, old and new, 16%
- Scrap sheet, old and new, 10%
- Steelmaking EAF dust, 8%

The remainder is made up of chemical industry residues (4%), old smelter slags (3%), other filter dusts (3%), and mine residues (1%). Less than half of this material is reclaimed as metal; the rest goes into ZnO or other chemicals [36]. Zinc can be recycled over and over again without losing its properties and keeping it quality. Over 90% of collected zinc containing products are recycled [36].

The MOV is a source of concentrated zinc as zinc oxide. Because zinc oxide is the major compound in the MOV there should be (in theory) a relatively low cost associated with purification and production of zinc. For this reason the MOV is an ideal candidate for an end of life material which has the potential to be recycled.

#### 2.3.3. Primary Zinc Production

There are generally two industrially used methods for zinc production today (1) pyrometallurgical zinc reduction and (2) roast leach electrowinning (RLE) each is described in brief detail in the following

sections. Hydrometallurgical purification of ZnO feed material produces around 80% of the world's zinc [24, 36] and is typically preferred over pyroprocessing due to the effectiveness, process flexibility and low temperatures. Pyrometallurgical processes are typically energy intensive and often need a dust collection or gas cleaning system [37]. When choosing either a pyro-process or hydro-process for zinc recycling from MOVs the preferred method needs to be economically feasible with respect to the costs of recycling MOV into pure components versus purchasing raw starting material.

In (pyrometallurgical) reduction of zinc the impure metal is exposed to a reducing agent typically any carbon based compound, resulting in metallic zinc and carbon monoxide at temperatures above 1100°C although reduction takes place at temperatures as low as 920°C [24, 38]. Higher temperatures are used to increase the reaction kinetics. The boiling point of zinc in reducing conditions is 907°C [35]. The vapor is collected but must be protected from re-oxidation until it is collected as liquid zinc. Zinc can be lost in the vapor stage if it escapes before being condensed. The horizontal retort process collects 90 – 97% of the zinc along with other impurities [36]. Zinc production by pyrometallurgical reduction is an energy intensive process and is only performed in a few countries.

In RLE mined zinc sulfide is converted to zinc oxide. The ZnO is then leached using H<sub>2</sub>SO<sub>4</sub> to form a ZnSO<sub>4</sub> electrolyte, which is continuously circulated through the leach tanks and an electrolytic cell. All the silicates and other insoluble constituents of the concentrate are removed from the acid leach tanks as solids [36]. Removal of impurities or leachate purification requires several steps. Purification is most commonly done by zinc dust addition which causes the nobler metals in solution to be cemented out leaving a zinc rich sulfate electrolyte. Pb-Ag alloy anodes are used in the cells and zinc forms on aluminum (cathode) starter sheets. After zinc is deposited it is stripped from the cathode, melted, and cast into slabs.

RLE has reduced energy consumption, improved quality of the metal and eliminated the health hazards associated with zinc reduction compared to pyroprocessing [36]. By 1984, 80% of the world zinc was produced by electrowinning [36] and today over 90 % is produced hydrometallurgically [39]. The problem with electrowinning is that the equilibrium potential for zinc is lower than that of hydrogen and the evolution of hydrogen should be thermodynamically preferred over zinc deposition [40]. For this reason zinc should be more difficult to electrowin than other base metals.

Zinc has a high hydrogen evolution over potential making zinc deposition possible [40]. Over potential is directly related to the voltage efficiency and in an electrochemical cell the over potential requires more energy than thermodynamically calculated. To mitigate this problem the over potential must be high enough for zinc deposits to nucleate. Impurities in the electrolyte have the possibility of reducing the hydrogen production potential hindering or eliminating zinc deposition. The concentration of impurities in the ZnSO<sub>4</sub>, even at the ppb level, can affect the deposition of zinc. Some impurities and their characteristic are [40]:

- Ag, Cu, and Cd can co-deposit with zinc at their limiting current density. They can also induce zinc re-dissolution by forming a cathodic area.
- Ni, Co, and Fe can co-deposit with zinc and will lower the hydrogen overvoltage and initiate cyclic zinc deposition and re-dissolution.
- As, Sb and Ge are catalysts for hydrogen production. They will increase the critical current density at which zinc deposition begins but will not cause zinc re-dissolution [24].
- Al and Pb will not cause zinc re-dissolution

Using pure electrolytes with additives hydrogen production can be mitigated. The presence of Sb up to 0.08 ppm increases the limiting current density of Zn<sup>2+</sup> and enhances the hydrogen production reaction and decreases the cathode diffusion layer thickness [40].

The effect of impurity metal ions in solution has a significant effect on the current efficiency (CE) in zinc electrowinning. Even low concentrations of some metal ions can be fatal to the electrolysis step.

The presence of a small amount (less than 2 ppm) of antimony is not acceptable in zinc electrowinning and must be removed from the leach solution because it causes a reduction in CE of nearly 60 % [41]. Cobalt and nickel are also present in the MOV but do not have as pronounced effect on the CE as antimony. Approximately 15 ppm of cobalt and copper will reduce the zinc electrowinning CE by nearly 15 % and 30 % respectively [41].

Even though RLE is the most important zinc production process there are alternatives to RLE such as direct leach electrowinning where the zinc concentrate, the regenerated sulfuric acid from subsequent electrowinning, and oxygen are fed into the electrochemical cell [40]. The main problem in leaching and liquor purification is separation of zinc from other metals which can reduce the hydrogen over potential. Co-leaching of impurity metals in most cases cannot be avoided. Typically the final stage of zinc recovery is electrowinning from a  $ZnSO_4$  solution.

#### 2.3.4. Recycling of Zinc

There are numerous ways to recover secondary zinc from metal waste. Zinc containing wastes from which to recover zinc are zinc ash, dross, electric arc furnace (EAF) dusts brass smelting, automobile shredder scrap, rayon industry, batteries and many more all of which contain zinc at different levels and chemical forms. It is becoming more attractive to recycle zinc from waste due to high disposal costs and increasingly stringent environmental regulations [37]. This has caused an increase in interest in developing processes to recover zinc from secondary materials such as MOVs.

As in zinc production the usual methods for zinc recycling are either pyrometallurgical or hydrometallurgical. Hydrometallurgy is considered more environmentally friendly and economical even for low concentrations of zinc. It gives nearly complete recovery of metals and high purity products [37, 42] whereas pyrometallurgy is more energy intensive and requires cleaning of dust collection systems. Pyrometallurgical systems are also sensitive to chlorides and fluorides which requires the use of equipment made from high cost alloys to avoid corrosion [37]. In hydrometallurgical recovery of zinc sulfuric acid, hydrochloric acid, ammonia/ammonium carbonate, ammonium chloride, caustic soda and others have been used to leach zinc [37].

Not all of the listed leachants are employed on an industrial scale and some are only tested on a bench scale. Sodium hydroxide has been proven to be selective for zinc leaching in the presence of iron but recovery of zinc from the leachate is not done industrially and needs further development [37] and use of hydrochloric acid has high costs associated with it [37].

Recovery of the zinc from solution is done via precipitation, crystallization, solvent extraction (SX), ion exchange and electrowinning [43]. Precipitation is dependent on the solubility of the salt with at a set pH and is commonly used to separate iron from zinc. Cementation uses the nobility of metals to cement out the more noble metals from the zinc leachate. When high concentrations of nickel and cobalt are present in the leachate dimethyl glyoxime and alphanitrosobetanaphthol can be used [37].

In zinc recovery from batteries using the BATENUS process a dilute sulfuric acid leaches the zinc which is then extracted into an organic phase [42]. Subsequent stripping with sulfuric acid yields a pure sulfate solution. In nickel metal hydride battery recycling the zinc from sulfuric acid leaching is extracted using D2EHPA which can extract divalent transition metals such as  $Zn^{2+}$ ,  $Cd^{2+}$ ,  $Mn^{2+}$  [44], and trivalent metal cations such as  $Fe^{3+}$ ,  $Al^{3+}$  [45], as well as trivalent rare earth elements [46] at relatively low pH, but does not extract cobalt and nickel [47]. There are many more processes, both hydro- and pyro-, for recovering zinc from batteries and not all are included in this discussion.

Zinc is recycled from EAF dust where many leaching media have been tested including sulfuric acid [48, 49], sodium hydroxide [50], and many others [51]. Hydrometallurgical treatment of EAF dust can be broken into two paths: acid and alkaline leach treatment. Both paths involve purification of the leachate via cementation [51] where copper and lead are removed from the zinc solution.

There are a plethora of ways to recycling zinc from waste materials and more are being developed. Recycling of zinc from the MOV applies recycling methods which are employed for recovering zinc from other waste streams.

### 3. THEORY

#### 3.1. Cementation

The most common way to produce zinc is by RLE where ZnS is converted (at high temperatures) to ZnO [36], zinc along with other impurities are leached using H<sub>2</sub>SO<sub>4</sub>, impurities are removed via cementation and zinc is electrowon producing a high purity zinc product. In order to maintain the large overpotential, impurities in the sulfate leaching solution must be completely removed [2]. Impurities act as catalysts for hydrogen evolution or co-deposit with zinc, causing large drops in current efficiency [41].

Industrially a more common method is to cement out the impurities using a less noble metal to reduce a more noble metal species in solution. In this case the less noble metal is zinc which serves two purposes: (1) it is needed as a reducing agent and (2) it increases the zinc concentration in solution. Cementation is carried out by addition of a less noble metal usually cheap and nontoxic causing reduction and cementation of the more noble metal from solution.

The somewhat well-known system is the Zn-Co-Sb sulfate system where parameters such as effect of zinc dust amount [52], copper concentration [52], antimony concentration [53], temperature [54], and pH [55] have been studied as a function of time for cobalt concentrations around 20 ppm. However in the leachate solution obtained in this work the concentrations of cobalt, nickel, and manganese are much higher than what has been described in literature in association with RLE. This fact makes this work important in determining the feasibility of incorporating the MOV into the RLE process.

A method for determining the metals which can be electrolytically separated from zinc is to look at the standard reduction potentials ( $E^\circ$ ) of each metal as given in Table 1 versus the standard hydrogen electrode (SHE). Antimony, bismuth, cobalt, manganese and nickel will be considered with respect to zinc reduction. In zinc electrolysis co-deposition of manganese can be avoided by choosing a reduction potential greater than that for  $Mn^{2+}/Mn$  reduction. This can be done electrolytically by selecting a reduction potential higher than -0.762 V but lower than -0.282 V [43] thus reducing bismuth, cobalt, nickel, antimony and leaving zinc in solution. Typically the solution is not cleaned this way as the energy consumption is too large for the process to be economical [41].

Table 1: Selected standard reduction potentials in aqueous solutions at 25 °C vs. SHE [56].

Reaction	Potential, $E^\circ$ (V) vs SHE
$Zn^{2+}/Zn$	-0.762
$Bi^{3+}/Bi$	+0.308
$SbO^+/Sb$	+0.208
$Co^{2+}/Co$	-0.282
$Mn^{2+}/Mn$	-1.182
$Ni^{2+}/Ni$	-0.236

There have been studies on the factors affecting cementation [52, 53, 57-61]. According to thermodynamic calculations it should be possible to cement cobalt, antimony, nickel, and copper from solution by addition of metallic zinc. For cobalt cementation given by Equations 9-11.





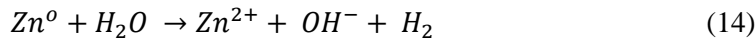
The reduction of cobalt together with the oxidation of the zinc yields a reaction with cell potential difference of 0.48 V. The potential difference can be related to the standard Gibb's free energy,  $\Delta G^o$ , by Equation 13.

$$\Delta G^o = -nFE^o \quad (12)$$

$$\ln k = -\frac{\Delta G^o}{RT} \quad (13)$$

Where, n is the number of electrons transferred in the oxidation-reduction reaction, F is Faraday's constant and  $E^o$  is the standard potential the chemical reaction given in Equation 11. For Equation 11 the standard Gibb's free energy is  $\Delta G^o = -92.7 kJ$  as calculated from Equation 12. From the standard potential the equilibrium constant,  $K_{eq}$ , is determined from Equation 13 to be  $1.7 \times 10^{16}$  [41]. The equilibrium constant suggests the cobalt cementation reaction given in Equation 14 should proceed and not back react. This is not seen experimentally due to slow reaction kinetics of cobalt. To accelerate the cementation of cobalt activators are used. Typically activators are Cu/As or Cu/Sb [54, 62]. Since antimony is already present in the in the MOV leachate in small amounts it is the natural choice for an activator. The mechanisms describing the behavior of the additive in the cementation process is not well understood [41].

In addition to the cementation reaction the zinc dust is also leached in the cementation solution according to the reaction given by Equation 14.

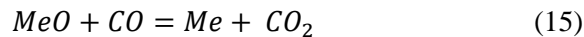


Reaction of the zinc dust with the leachate causes the localized pH to rise and precipitation of basic zinc sulfate with chemical composition  $Zn(OH)_2ZnSO_4 \cdot 4H_2O$  [60]. Zinc salt is fatal in cementation because it coats the zinc dust eliminating the surface area needed for cementation of other metals. Thus, the pH needs to be kept low enough during cementation experiments to ensure no zinc salts are forming. Industrially 4-6 g·L<sup>-1</sup> of zinc dust is used for cementation [41].

The influence of pH on the cementation of the MOV leachate is an important parameter if the pH is too low the hydrogen ion activity will increase leading to hydrogen evolution [41]. But at the same time the pH of the leachate must not precipitate basic zinc sulfate,  $Zn(OH)_2ZnSO_4 \cdot 4H_2O$  [54, 60]. It has been suggested by Borve et al. [54] that on an industrial scale it is more important to avoid hydrogen production than the formation of basic zinc sulfate precipitation although both can be detrimental. The addition of zinc dust causes the pH of the solution to rise as seen in Equation 14.

### 3.2. Carbothermal Reduction

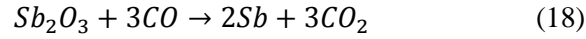
In carbothermal reduction carbon acts as a reducing agent. When solid carbon is present with the metal oxide there are two reactions taking place simultaneously as given by Equations 15-16.



It is known that for high temperature zinc production carbon is added to zinc oxide causing carbothermal reduction of zinc according to the reaction given in Equation 17 [38, 63].



Antimony oxides can be reduced with charcoal in a reverberatory furnace at temperatures near 1200 °C however there is significant loss of antimony due to volatilization. The reaction proceeds according to the following reactions [26]:



Since the MOV is composed mainly of ZnO and many zinc and oxygen containing compounds are present in the material it was thought that addition of carbon would help in the reduction of the leaching residue. But, as antimony is within the spinel structure it was not known at which temperature reduction of antimony would take place.

### 3.3. Activation Energy

Activation energy ( $E_A$ ) is the minimum energy required for a reaction to occur. It is also an empirical parameter that describes the temperature dependence of the rate constant of a reaction [64]. The rate of chemical reactions depend on temperature and how the reaction rate varies with temperature can be described by a rate constant,  $\ln k$ . By using a plot of the logarithm of the rate constant ( $\ln k$ ) against the inverse of the absolute temperature ( $1/T$ ) a straight line is obtained. This was determined by a Svante Arrhenius a Swedish chemist. The Arrhenius equation is shown in Equation 20-21 where A is the pre-exponential factor, R is the gas constant, and T is the absolute temperature.

$$\ln k = \ln A - \frac{E_A}{RT} \quad (20)$$

$$k = Ae^{-\frac{E_A}{RT}} \quad (21)$$

Both  $E_A$  and A are constants known as the Arrhenius parameters and can be determined experimentally [64]. Arrhenius behavior is exhibited when a reaction gives a straight line when  $\ln k$  is plotted against  $1/T$ . The slope of the line taken from an Arrhenius plot is equal to the activation energy of the reaction being studied. Larger slopes (larger  $E_A$ ) means the reaction rate has a higher dependence on temperature than a reaction with a smaller  $E_A$ .

IN high temperature experiments the degree of decomposition of a metal oxides,  $\alpha$  is defined by Equation 22 where  $W_o$ ,  $W$ , and  $W_\infty$  are the initial, instantaneous and final masses of the sample respectively.

$$\alpha = \frac{W_o - W}{W_o - W_\infty} \quad (22)$$

During thermal decomposition a compound is volatilized in one step for example from  $Sb_2O_3(s)$  to  $Sb_2O_3(g)$  the reaction rate can be calculated using the heating rates. Most generally the reaction rate is a function of temperature, reaction area and the activities of the reactants and can be represented mathematically by Equation 23 where t is the reaction time, r is the reaction rate, T is Temperature,  $A(\alpha)$  is the reaction area as a function of reaction fraction, and  $a_A$  and  $a_B$  are activities of reactants A and B respectively.

$$\frac{d\alpha}{dt} = r = fA(\alpha)a_A^m a_B^n \dots \quad (23)$$

For solid reactants the activity is unity. The Arrhenius equation can be used to show the effect of temperature on reaction rate as seen in Equation 24.

$$f(T) = Ae^{\left(\frac{-E_A}{RT}\right)} \quad (24)$$

Using the Ozawa-Flynn-Wall method [65, 66] to determine the activation energy where the first calculation of E, follows Equation 25 where b, on the first iteration = 0.457/K and m is the slope from the Arrhenius plot.

$$E_A = -\left(\frac{R}{b}\right) \cdot m \quad (25)$$

Using a table of numerical integration constants from ASTM E1641-13 reiterations on the calculation of activation energy are done until  $E_A$  changed by less than 1% yielding an activation energy for the decomposition reaction. The pre-exponential factor, A, can be calculated using Equation 26 where  $\beta'$  is the heating rate nearest the midpoint of the exponential heating rates and  $a$  is the logarithm of the approximation derivative (Doyle approximation) and can be taken from a table of values presented in ASTM E1641-13.

$$A = \frac{\beta' \cdot R \ln(1-\alpha) 10^a}{E_A} \quad (26)$$

### 3.4. Uncertainties

Uncertainties calculations are expressed as one standard deviation. The standard deviation (three or more replicates) of an experiment was calculated using Equation 27 where s is the standard deviation,  $\bar{x}$  is the mean value of all samples, and n is the number of samples.

$$s = \sqrt{\frac{\sum(x-\bar{x})^2}{n-1}} \quad (27)$$

The uncertainty propagation for  $C = A+B$  and  $C = A \cdot B$  is expressed by Equation 28 and 29 respectively.

$$s_c = \sqrt{s_A^2 + s_B^2} \quad (28)$$

$$s_c = \sqrt{\left(\frac{s_A}{A}\right)^2 + \left(\frac{s_B}{B}\right)^2} \quad (29)$$

## 4. EXPERIMENTAL

### 4.1. Analysis Equipment

#### 4.1.1. ICP-OES

Inductively coupled plasma (ICP) – Optical Emission Spectroscopy (OES) is a well-established technique used to quantify and qualify elements, typically in an aqueous sample [67]. The liquid sample is injected into an argon plasma by a nebulizer. The sample is turned into a mist in the nebulizer which is then immediately dried, vaporized and energized by the plasma with temperature around 10,000 K [68]. At such high temperatures the free atoms form in a gaseous state. The atoms collide with the plasma causing excitation of the atoms to an excited state. The atoms can then return to ground state via the emission of a photon with characterized energy determined by the atom [68]. The measured wavelength can be used to identify the elements from which they originated [68]. Multiple element analysis can be performed due the combination of a polychromator and an array detector.

For this work an iCAP 6500, Thermo Fisher instrument was used for sample analysis. Sample were diluted in 0.1 or 1.0 M HNO<sub>3</sub>. External calibration curves made by dilution of 1 mg/ml standard solutions were used to quantify metal contents.

#### 4.1.2.SEM

Scanning Electron Microscopy (SEM) is a technique used to analyze the surface of a material. The SEM can magnify samples with a large depth of focus allowing for samples to be visualized on a micro scale as well as in situ chemical information [69]. For the electrons from the sample to be excited and then detected an electron gun emits a beams of electrons which are focused on a point of interest on the sample. The beam is focused by a series of lenses under vacuum. When the primary beam hits the surface of the sample electrons and x-rays are emitted from the sample.

The surface microstructure and morphology of the MOV was investigated as received as well as the leaching residues and studies related to the surface chemistry occurring during cementation of cobalt and other metals. A FEI Quanta 200 environmental SEM equipped with an Oxford Inca energy dispersive X-ray detector (EDX) system. Imaging was done with accelerating voltages between 10 and 20 kV.

#### 4.1.3.XRD

X-ray diffraction (XRD) can be used to determine the crystallographic structure of a sample and for compound identification of solid samples. X-rays are generated by a cathode ray tube and filtered through a monochromator, collimated and then directed towards the sample. The x-rays interact with the sample producing destructive and constructive interferences or a diffracted x-ray. The relationship between the wavelength of the x-ray, diffraction angle, and interatomic spacing (spacing between crystal lattice planes of an atom) is given by Bragg's law shown in Equation 30 [70]:

$$n\lambda = 2d \sin \theta \quad (30)$$

Where  $n$  is an integer,  $\lambda$  is the wavelength of the x-rays,  $d$  is the interatomic spacing, and  $\theta$  is the diffraction angle. Bragg's law shows the relation between the wavelength of electromagnetic radiation to the diffraction angle and the lattice spacing in a crystalline sample [70].

Samples were pulverized and homogenized with an agate mortar and pestle prior to sample analysis. A Bruker 2D Phaser equipped with a characteristic Cu radiation source and a scintillation detector was used to identify crystalline compounds present in the powder samples. Compound identification was made by comparisons with standards in the Joint Committee of Powder Diffraction Standards database [71].

#### 4.1.4.TGA

Thermogravimetry (TG) or Thermogravimetric Analysis (TGA) is a quantitative analysis by weight and is the process of isolating and weighing an element or compound of the element in as pure a form as possible [72] in a specified atmosphere. By studying the effect of heating on a sample mass it is possible to get information on chemical reactions such as reaction temperature, composition, thermal stability, and mass of species involved in the reaction.

The TGA continuously weighs a sample as it is heated. As the temperature increases the sample undergoes changes such as decomposition, oxidation, etc. The resulting weight change of the reacting sample is measured against an empty reference crucible. Results are typically given for weight change as a function of temperature as well as the rate of mass change with time this is known as derivative thermogravimetric (DTG) [72].

Experiments were carried out with a TA Instruments, TGA Q500 equipped with a single control/sample thermocouple positioned immediately adjacent to the sample and a second thermocouple located slightly above in the same sleeve was used for thermal analysis. A quartz-lined furnace which is chemically inert

to products produced from decomposition of the samples. A horizontal purge gas allows N<sub>2</sub> purge gas to flow directly across the sample. A portion of the gas was also directed through the balance chamber. A schematic of the TGA used in this study is shown in Figure 3.

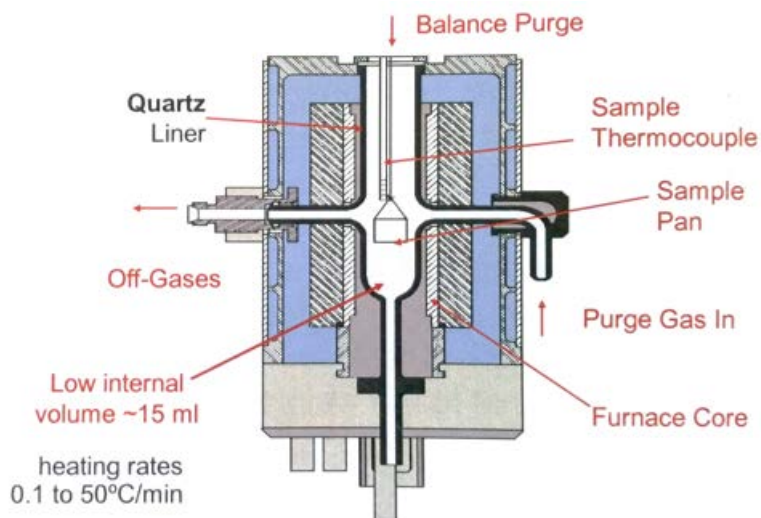


Figure 3: Schematic of furnace used in TA Instruments TGA Q500 [73].

#### 4.2. Experimental Outline

This work will cover a diverse range of topics including leaching, cementation, high temperature (direct) reduction as well as carbothermal reduction. From start to finish the goal of this research project is to recycle the critical metal, antimony from the MOV. However since the major component of the MOV is zinc oxide, recycling of zinc was also investigated. A process flow diagram is shown in Figure 4 for the experiments carried out in this work.



Figure 4: Process flow diagram for work presented in this licentiate

The work started with the MOV as received from the supplier. The as received MOV was pulverized and sieved into different size fractions and characterized prior to and after comminution. A study on pH selective dissolution was done using four acids: acetic acid, hydrochloric acid, nitric acid, and sulfuric acid. Cementation studies were done on the MOV leachate studying a variety of different parameters such as activator concentrations, antimony and cobalt concentrations, temperature, pH, and zinc dust addition. The final step to produce zinc metal would be to use the purified zinc leachate as the electrolyte for zinc electrowinning. Electrolysis of zinc from the leachate is not discussed in this work.

In addition, high temperature studies on  $\text{Sb}_2\text{O}_3$ ,  $\text{Bi}_2\text{O}_3$ ,  $\text{ZnO}$ , MOV and leaching residue were done studying the effect of heating rate (activation energy determination), effect of gas flow rate and effect of carbon to residue ratio for carbothermal reduction reactions.

#### 4.3. Characterization of MOV

The identification and composition of the additives in the specific type of MOV investigated needed to be determined as only the oxides of the major metals: zinc, bismuth, and antimony were known. Additives or impurities (any metal other than zinc or  $\text{ZnO}$ ) in the sample will have an impact on zinc leaching and the possible electrolytic process. New MOV approximately 70 mm in diameter and weighing 1000 g were broken up into pieces approximately 2 cm in diameter. An impact mill (Siebtechnik) was used for further particle size reduction. The crushed MOV was mechanically sieved (CISA, 18, 30, 60, 120, 230 mesh) yielding the particle size fractions shown in Table 2. For all experiments material having a particle size smaller than  $63 \mu\text{m}$  was used (100 %, -250 Mesh) because smaller particle sizes equates to higher surface to volume ratio and thus typically quicker leaching kinetics are observed.

Table 2: Particle size fraction by weight of pulverized MOV.

Particle Size	Particle Size Weight Fraction
> 1.0 mm	0.06
1 mm to > 500 $\mu\text{m}$	0.07
500 $\mu\text{m}$ to >250 $\mu\text{m}$	0.22
250 $\mu\text{m}$ to >125 $\mu\text{m}$	0.20
125 $\mu\text{m}$ to > 63 $\mu\text{m}$	0.11
< 63 $\mu\text{m}$	0.34

Since the MOV is a homogenous mixture with ZnO grains 20-40  $\mu\text{m}$  in diameter surrounded by bismuth rich and antimony rich (2-10  $\mu\text{m}$ ) phases it is likely that the composition of the different size fraction is constant. However, no experiments have been done to confirm this.

To determine the metal content in the pulverized MOV powder (< 63  $\mu\text{m}$ ), complete dissolution of the MOV powder was performed in triplicate using concentrated hydrochloric acid at an elevated temperature. It is not expected for the composition of the different particle size fraction to vary significantly in composition, but this has not been proven experimentally in this work. The varistor material was heated with concentrated hydrochloric acid (37%) at  $70 \pm 3$  °C while being continuously stirred using a magnetic stir bar. Before determination of metal concentrations, aliquots of the solutions were diluted with a 1 M nitric acid solution, prepared from concentrated stock solution (65%, Suprapur®, Merck) and ultrapure water (Milli-Q, Millipore, >18 M $\Omega$ /cm). Analysis was done using ICP-OES

The topography and element distribution of the ground and sieved MOV was analyzed with a scanning SEM-EDX to obtain qualitative data about the elements present in addition to determining the occurrence and distribution of the components XRD was done to identify crystalline compounds present in the MOV powder.

#### 4.4. Leaching Study

Leaching experiments were started by mixing the powdered MOV, with pure water (Milli-Q, Millipore, >18 M $\Omega$ /cm) in a straight wall, 150 mL capacity, titration vessel. The vessel was equipped with a pH electrode, a stir bar and a dosing device connected to a Metrohm 905 Titrando titrator connected to a computer for monitoring and controlling the acid addition. The leaching vessel is shown schematically in Figure 5.

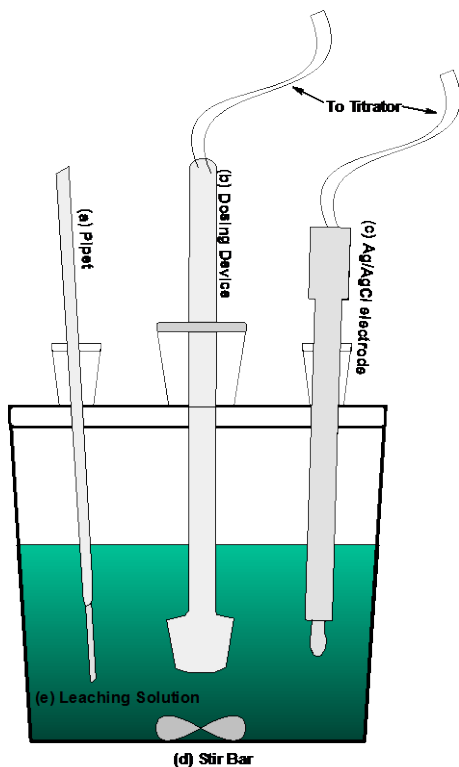


Figure 5: Titration vessel with (a) pipet, (b) dosing device, (c) Ag/Ag Cl pH electrode, (d) stir bar, and (e) leaching solution.

The system was stirred so the stagnant layer around the solid particles could be perturbed ensuring mass transport from the liquid in the pores to the outer leachate where the pH and metal concentrations were measured. The pH was controlled using a silver/silver chloride (Ag/AgCl) glass electrode. Calibration of the pH electrode was done weekly using Metrohm® Ion analysis buffer solutions of pH 1, 4, 7, and 9. The temperature of the system was maintained at  $22\text{ }^{\circ}\text{C} \pm 1$ .

The acid leaching solutions were not initially prepared to the desired pH. Rather the desired pH was entered into the titration program and a more concentrated acid solution was added to the water-MOV system until the desired pH of the system was reached. In total four acid solutions were used for the leaching studies prepared by mixing Milli-Q with: acetic acid ( $\geq 99.7\%$ , Sigma Aldrich), hydrochloric acid (37%, Sigma Aldrich), nitric acid (65%, Suprapur®, Merck) and sulfuric acid (95.0 – 98.0%). The acid solutions were titrated into the MOV-water mixture resulting in a leachate with a specified pH. The leaching experiments were carried out at a constant pH of 1, 3, and 5 for each acid solution with the exception of acetic acid in which leaching experiments were carried out having a pH 2, 3, and 5.

Small aliquots of the leachate were taken at times 0, 2, 10, 30, 60, 120 and 240 minutes in each leaching experiment. To determine the concentration of the metals leached as a function of time an aliquot was taken at each point in time, centrifuged (10 minutes, 5000 RPM), and diluted with  $1\text{ M HNO}_3$  for further analysis using ICP-OES. The following metals were analyzed: bismuth, cobalt, copper, iron, magnesium, manganese, nickel, antimony, and zinc. Leaching experiments were done in triplicates to ensure experimental reproducibility. The concentrations of metals in the leachates were compared to the concentration of the metals from the complete dissolution experiments allowing for data to be given as the fraction of metal leached.

Because the anion of each acid has the ability to form complexes with metal ions the speciation of zinc was also considered in each acid solution. The software used for speciation of metal ions in the leachates, PHREEQC [74] was combined with the *minteq* database [75], to provide data on the metal-anion complexes for zinc. However, the complexation of bismuth or antimony could not be calculated since

thermodynamic data were not available. Concentration of zinc and acid ions in solution at the end of the leaching experiment (pH 1, 3 and 5) were used as input data.

## 4.5. Cementation Study

### 4.5.1. Cementation Solution – Bulk Leachate of MOV

Bulk leaching experiments in 5 M H<sub>2</sub>SO<sub>4</sub> solution were started by mixing pulverized (< 63 μm) MOV to pure water (MilliQ, Millipore, >18 MΩ/cm) in a straight wall, 1000 mL capacity beaker. The beaker was equipped with a pH electrode, a stir bar and a dosing device connected to a Metrohm 905 Titrando titrator connected to a computer for monitoring and controlling the acid addition similar as the setup shown in Figure 5 only on a larger scale. The 5 M sulfuric acid solution was made by dilution of concentrated H<sub>2</sub>SO<sub>4</sub> (95.0 – 98.0%) with milli-Q water. It was titrated into the MOV-water mixture resulting in a leachate with a pH of 3. The pH was controlled using a silver/silver chloride (Ag/AgCl) glass electrode. Calibration of the pH electrode was done using Metrohm® Ion analysis buffer solutions of pH 1, 4, 7, and 9. The temperature of the system was maintained at 20 °C ± 1. The system was again stirred so the stagnant layer around the solid particles could be perturbed ensuring mass transport from the liquid in the pores to the outer leachate where the pH and metal concentrations were measured. Each leaching experiment was performed for 5 hours.

The concentration of the leached metals was determined by taking a small aliquot of the leaching solution, filtering it through a 0.45 μm membrane, and diluted with 0.1 M HNO<sub>3</sub> for analysis using ICP-OES. The following metals were analyzed: bismuth, cobalt, copper, manganese, nickel, antimony, and zinc. Leaching experiments were done in triplicates to ensure experimental reproducibility.

The leachate was separated from the antimony rich residue by filtration with a Büchner funnel to be further used in the cementation study. The residue was washed with milli-Q water and dried in an oven at 60 °C for 48 hours and stored in glass vial for experiments on antimony recovery.

### 4.5.2. Cementation Experiments

The reaction vessel was equipped with an Ag/AgCl pH electrode, a stir bar, and a dosing device connected to a Metrohm 905 Titrando titrator connected to a computer for monitoring and controlling the acid addition and pH. To maintain a set pH, 0.1 M H<sub>2</sub>SO<sub>4</sub> solution was titrated into the reaction vial with cementation solution. Typical cementation experiments were carried out at 20 ± 1 °C. The stirring velocity was constant during all experiments at 600 RPM and nitrogen was bubbled through the cementation solution. Calibration of the pH electrode was done using Metrohm® Ion analysis buffer solutions of pH 1, 4, 7, and 9. A picture of the cementation setup is shown in Figure 6.



Figure 6: Cementation setup with reaction vessel, stir plate, Ag/AgCl pH electrode, dosing device, N<sub>2</sub> line and all non-used ports sealed off.

Copper was added to the leachate as CuSO<sub>4</sub>·5H<sub>2</sub>O (Sigma Aldrich, > 99.0) as an activator for the cementation reactions. When needed antimony was added to the leachate in the form of soluble potassium antimony tartrate trihydrate (K<sub>2</sub>C<sub>8</sub>H<sub>4</sub>O<sub>12</sub>Sb<sub>2</sub>·3H<sub>2</sub>O). For each cementation experiment 25 mL of leachate was used. A summary of cementation parameters studied is given Table 3.

A known amount typically 2 g·L<sup>-1</sup>, of zinc powder (325 mesh, 99.9% Sigma Aldrich) was added to the reaction vessel in one portion initiating the cementation experiment (t = 0). From the time of zinc dust addition (t = 0) samples were taken at t = 5, 10, 20, 30, 60, 90 and 120 minutes. Each sample was filtered through a 25 mm syringe filter with 0.45 μm polypropylene membrane and diluted for ICP-OES analysis of the metal ion concentration. A sample of the starting solution before zinc dust addition was taken for each sample. Dilutions were made using 0.1 M HNO<sub>3</sub> prepared from concentrated HNO<sub>3</sub> (65%, Suprapur®, Merck).

Table 3: List of cementation experiments and the parameters which were studied.

<b>Influence of Cu concentration (no Sb)</b>		<b>Influence of Temperature</b>	
Experiment	Cu Concentration in solution (g·L <sup>-1</sup> )	Experiment	Temperature (°C)
No Sb 2g·L <sup>-1</sup> Zn dust		0.4 g·L <sup>-1</sup> Sb 0.4 g·L <sup>-1</sup> Cu 2g·L <sup>-1</sup> Zn dust	
1A	0.2	4A	30
1B	0.4	4B	40
1C	0.8	4C	50
1D	1.2	4D	55
		4E	60
<b>Influence of Cu Concentration (with Sb)</b>		<b>Influence of Zn Dust Addition</b>	
Experiment	Cu Concentration in solution (g·L <sup>-1</sup> )	Experiment	Zn Dust Addition (g·L <sup>-1</sup> )
0.4 g·L <sup>-1</sup> Sb 2g·L <sup>-1</sup> Zn dust		0.4 g·L <sup>-1</sup> Sb 0.4 g·L <sup>-1</sup> Cu	
2A	0.2	5A	0.25
2B	0.4	5B	0.5
2C	0.8	5C	1
2D	1.6	5D	2
		5E	3
		5F	4
<b>Influence of Sb Concentration</b>		<b>Influence of pH</b>	
Experiment	Sb Concentration in solution (g·L <sup>-1</sup> )	Experiment	Cementation pH
0.4 g·L <sup>-1</sup> Cu 2g·L <sup>-1</sup> Zn dust		0.4 g·L <sup>-1</sup> Sb 0.4 g·L <sup>-1</sup> Cu 2g·L <sup>-1</sup> Zn dust	
3A	0.1	6A	3.0
3B	0.2	6B	3.5
3C	0.4	6C	4.0
3D	0.8	6D	4.5
3E	1.6	6E	5.0
		6F	5.5
		6G	6.0

Experiments were conducted with the amount of zinc dust added being between 0.25 to 4 g·L<sup>-1</sup>. To determine the surface area of the zinc dust a surface area and porosity analyzer (Micrometrics, ASAP 2020) was used. Zinc dust was placed inside a vessel and the surface area was measured as a function of nitrogen gas (adsorbate) adsorbed on the surface of the zinc according to the Brunauer–Emmett–Teller (BET) theory. BET measurements show that the surface area per gram of zinc dust is 0.2268 ± 0.0031 m<sup>2</sup>·g<sup>-1</sup>.

#### 4.6. Antimony Recovery

##### 4.6.1. Leachate Residue Characterization

The residue resulting from bulk leaching experiments (described in section 4.5.1) was used to study the effects of temperature on recovery of antimony. Prior to high temperature experiments characterization was done on the residue which included ICP-OES and XRD analysis.

ICP-OES analysis was used to determine the composition of the MOV leachate residue. The material was mixed with concentrated hydrochloric acid (37%) at 20 ± 1 °C for 24 h while being continuously stirred using a magnetic stir bar resulting in total dissolution of the residue. Before determination of metal concentrations an aliquot of the solution was diluted with a 1 M nitric acid solution, prepared from

concentrated stock solution (65%, Suprapur®, Merck) and pure water (Milli-Q, Millipore, >18 MΩ/cm). The appearance and composition of the dried residue was analyzed with a SEM-EDX and XRD.

#### 4.6.2. Reduction Experiments (RT – 1000 °C)

Reduction of the leaching residue and MOV were tested as well as Sb<sub>2</sub>O<sub>3</sub> (Sigma Aldrich, 99.9%), Bi<sub>2</sub>O<sub>3</sub> (Regentplus®, 99.9%), and ZnO (ACS reagent, ≥ 99.0%). Use of the TGA was limited to temperatures below 1000 °C. Typical operating parameters for TGA work are given in *Table 4*. Thermolysis curves were displayed as % weight loss vs. temperature or when needed the derivative of the thermogravimetric curve. The TGA was calibrated with five high purity standards using their Curie point and peak inflection point as the calibration temperature.

Table 4: Values of TGA operating parameters

Variable	Value
Reaction temperature (°C)	100 -1000
Balance Purge Rate (mL·min <sup>-1</sup> )	10
Sample Purge Rate (mL·min <sup>-1</sup> )	90
Sample Size (mg)	10
Heating Rate (°C·min <sup>-1</sup> )	10
Reaction Gas	N <sub>2</sub>

#### 4.6.3. Reduction Experiments (RT to 1300 °C)

For experiments needing a controlled atmosphere and also requiring temperatures greater than 1000°C a furnace within a glove box (Innovative Technology, Pure Lab HE) was used. The working gas in the glove box was ultra-high purity argon and the gas purification system ensured the atmosphere contained less than 1 ppm O<sub>2</sub> and H<sub>2</sub>O during all experiments unless otherwise noted. The glove box contained an integrated tube furnace with a maximum operating temperature of 1550 °C. The furnace contained a ceramic lining and was closed using formed aluminum silicate fibers as a cover. To monitor the temperature within the furnace a thermocouple was inserted through a bore in the aluminum silicate cover and placed as near to the sample as possible. The temperature was displayed on a separate programmable control unit.

The sample was placed in an alumina crucible during heating experiments. There was no purge gas used during glove box heating experiments however the gas blowers were turned in the on position so that pure argon was constantly circulating during experimentation. Samples were heated at a rate of 10 °C·min<sup>-1</sup>, held at the desired temperature for four hours, and cooled. After heating samples were stored in an inert atmosphere until analysis with XRD and SEM-EDX. A new sample was used for each heating experiment.

For carbothermal reduction reactions activated charcoal (DARCO®, -100 mesh) was mixed with the metal oxides and MOV at multiple molar ratios of O:C until homogenized. Molar calculations for the MOV were made assuming the amount of oxygen available was that of zinc oxide (because the MOV is nearly 90 wt. % ZnO). The O:C ratio is given in Table 5 for the compounds used in carbothermal reduction experiments.

Table 5: Composition of samples used in feasibility study of carbothermal reduction.

Compound	O:C Ratio	O (mol)	C (mol)
Antimony Oxide Sb <sub>2</sub> O <sub>3</sub>	1:0	0.0103	0
	1:2	0.0103	0.0206
	1:4	0.0103	0.0412
Bismuth Oxide Bi <sub>2</sub> O <sub>3</sub>	1:0	0.0064	0
	1:2	0.0064	0.0129
	1:4	0.0064	0.0258
Zinc Oxide ZnO	1:0	0.0123	0
	1:2	0.0123	0.0246
	1:4	0.0123	0.0491
MOV	1:0	0.0123	0
	1:2	0.0123	0.0246
	1:4	0.0123	0.0491

## 5. RESULTS AND DISCUSSION

### 5.1. Characterization of MOV

It has been reported in literature that other metal oxides, than the dominate ZnO, such as MnO<sub>2</sub>, NiO, and Co<sub>2</sub>O<sub>3</sub> and other minor metal oxides may be present in the MOV added to enhance the characteristics of the varistor [5, 7, 9, 18, 19, 76]. Typically MOV contains greater than 90 mol% ZnO and around 3 mol% of both Bi<sub>2</sub>O<sub>3</sub> and Sb<sub>2</sub>O<sub>3</sub> with the other metal oxides accounting for the remaining 4 % [2, 76]. The dissolved MOV investigated in this work contained, in detectable amounts, the metals listed in Table 6. The values in Table 6 are given in weight percent (wt %) and mol % of each metal oxide along with the standard deviation of the measurements.

Table 6: Chemical composition of MOV

Metal Oxide	mol %	wt %
Bi <sub>2</sub> O <sub>3</sub>	2.34 ± 0.06	5.13 ± 0.1
Co <sub>2</sub> O <sub>3</sub>	1.16 ± 0.03	0.94 ± 0.02
MnO <sub>2</sub>	0.76 ± 0.02	0.52 ± 0.01
NiO	0.89 ± 0.02	0.79 ± 0.02
Sb <sub>2</sub> O <sub>3</sub>	3.21 ± 0.08	4.44 ± 0.1
ZnO	91.6 ± 3.3	88.2 ± 3.1

Due to production methods (i.e. sintering) the MOV does not consist strictly of the starting components (ZnO, Bi<sub>2</sub>O<sub>3</sub> and Sb<sub>2</sub>O<sub>3</sub>) instead there are areas high in certain metals. The microstructure of the MOV contains three phases: (1) Phase I which is the most dominant region is the zinc oxide grains, (2) Phase II consisting of the small particles around the zinc oxide, here called the antimony-rich phase, and Phase III is the bismuth-rich phase. A SEM with on overlay of EDX maps for zinc, antimony, and bismuth is shown in Figure 7d for the pulverized MOV and the original SEM micrograph is shown in Figure 7e. The EDX maps for zinc, antimony, and bismuth are shown in Figure 7a, Figure 7b, and Figure 7c respectively.

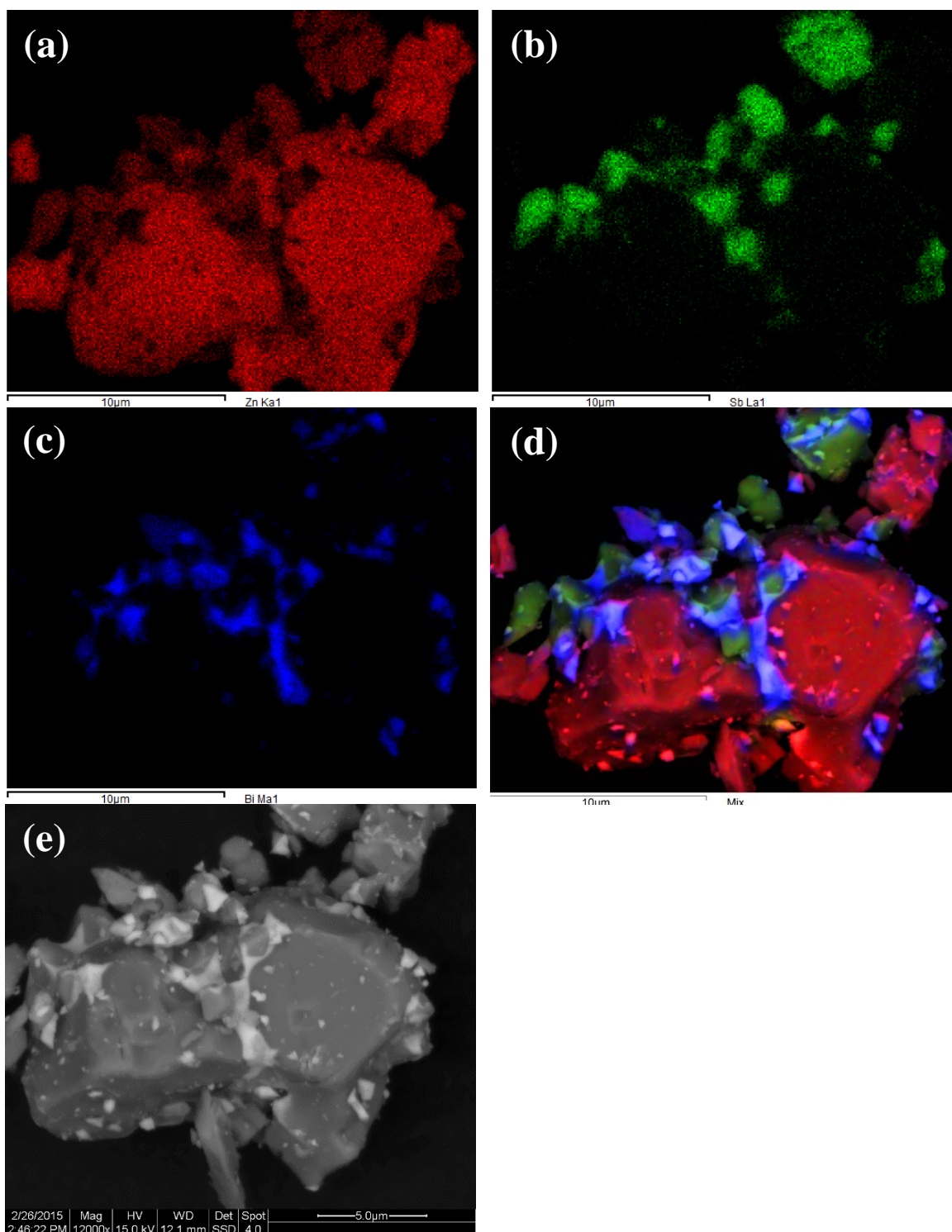


Figure 7: SEM/EDX micrograph of pulverized MOV having three phases: Phase I – ZnO grain, Phase II – antimony rich phase, Phase III – bismuth rich phase. (a) EDX map for zinc, (b) EDX map for antimony, (c) EDX map for bismuth (d) combined EDX map for zinc (red), antimony (green) and bismuth (blue) overlay on SEM micrograph for pulverized MOV particle. (e) SEM micrograph of pulverized MOV shown without EDX map overlay.

As seen in the micrographs in Figure 7 a-e it is clear that a large portion of the MOV consists of the zinc oxide grains. For antimony recovery it will be necessary to invoke a pretreatment step to separate the bulk zinc from the antimony rich region.

The result from qualitative mineralogical analysis of the MOV using XRD was a spectrum as shown in Figure 8. Peaks correlating to ZnO (●), Bi<sub>2</sub>O<sub>3</sub> (◆), Zn<sub>2.33</sub>Sb<sub>0.67</sub>O<sub>4</sub> (□), Zn<sub>2</sub>Bi<sub>3</sub>Sb<sub>3</sub>O<sub>14</sub> (★), and Zn<sub>7</sub>Sb<sub>2</sub>O<sub>12</sub> (■) are labeled. Peaks for compounds containing cobalt, manganese and nickel oxides are not visible due to their low concentrations in the MOV. The majority of peaks shown in Figure 8 are due to the ZnO XRD pattern. There was no peak correlation for antimony oxide confirming that antimony is present in the spinel (Zn<sub>2.33</sub>Sb<sub>0.67</sub>O<sub>4</sub>, Zn<sub>7</sub>Sb<sub>2</sub>O<sub>12</sub>), or pyrochlore (Zn<sub>2</sub>Bi<sub>3</sub>Sb<sub>3</sub>O<sub>14</sub>) phases. Some peaks correspond to multiple compounds and are labeled accordingly.

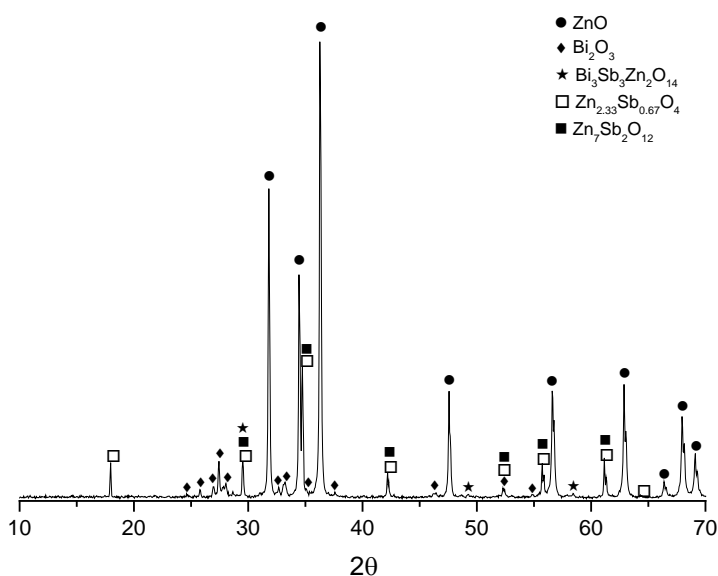


Figure 8: XRD spectra of the MOV showing peaks for ZnO (●), Bi<sub>2</sub>O<sub>3</sub> (◆), Zn<sub>2.33</sub>Sb<sub>0.67</sub>O<sub>4</sub> (□), Zn<sub>2</sub>Bi<sub>3</sub>Sb<sub>3</sub>O<sub>14</sub> (★), and Zn<sub>7</sub>Sb<sub>2</sub>O<sub>12</sub> (■).

## 5.2. Leaching<sup>1</sup>

### 5.2.1. Sulfuric Acid Leaching

Leaching of the MOV in sulfuric acid solutions with pH 1, 3 and 5 gave results as shown in Figure 9a, 8b and 8c respectively. The leached fraction of zinc (□), bismuth (○), and antimony (△) is shown on the left ordinate while the right ordinate along with the solid line shows the amount of the sulfuric acid solution added to the MOV-water slurry to obtain the desired pH. Sulfuric acid solutions were able to leach zinc at each pH level tested. Increasing the pH from 3 to 5 will not change the percent of zinc leached but rather the time needed for leaching will be longer. It seems to be feasible to use pH 5 solutions to selectively leach zinc while avoiding co-leaching of antimony and bismuth. However, for further purification studies the solution should be leached in pH 3 solutions to promote cementation of impurities in the leachate and decrease the time needed for leaching. Bismuth was leached when using pH 1 solution and the dominant species should be Bi<sup>3+</sup> based on the E<sub>h</sub>-pH diagrams [77]. In these conditions less than 5% of antimony was leached which is consistent with published data stating oxidizing, acidic solutions should not react with Sb<sub>2</sub>O<sub>3</sub> [77].

<sup>1</sup> The work presented in this section (section 5.2) is based on the article published in *The Scientific World Journal*, special edition *Recycling of Industrial and Municipal Solid Waste into New Products* titled: *Investigations into Recycling Zinc from Used Metal Oxide Varistors via pH Selective Leaching: Characterization, Leaching, and Residue Analysis*. Submitted May, 2015

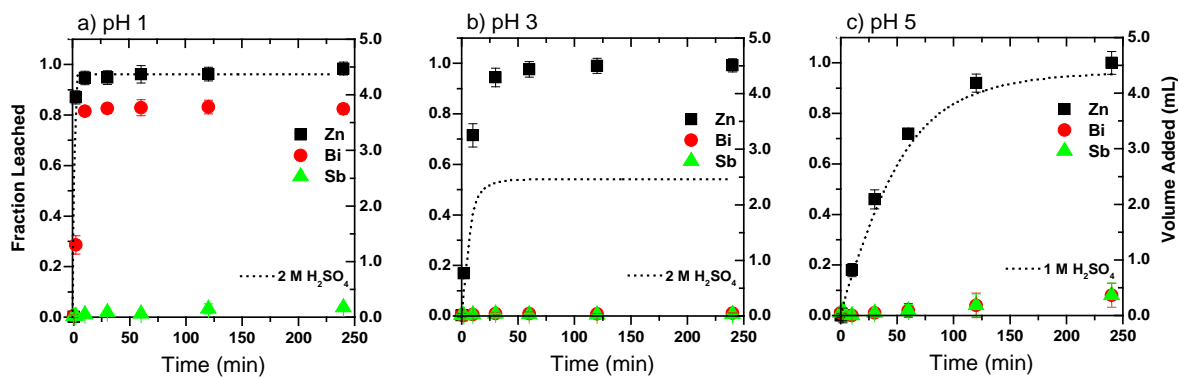


Figure 9: The leached fraction as given by the left ordinate for zinc ( $\square$ ), bismuth ( $\circ$ ) and antimony ( $\triangle$ ) from the MOV in a) pH 1, b) pH 3, and c) pH 5 solutions. The volume and concentration of sulfuric acid ( $\text{H}_2\text{SO}_4$ ) added is shown as a solid black line corresponding to the right ordinate.

PHREEQC calculations showed that approximately 65% of the zinc in the pH 1 leachate occurred as  $\text{Zn}^{2+}$  with the remaining 35% of zinc in solution as  $\text{ZnSO}_4$  soluble complex. As the pH increased the fraction of zinc as  $\text{Zn}^{2+}$  ions decreased to 55% for pH 5.

Impurities in the zinc leachate include cobalt of which approximately 65 % was leached in all solutions investigated. Manganese and nickel were approximately 25 % leached in pH 1 solution, 17% at pH 3 solution and 27% at pH 5. It is not known what causes a lower leaching fraction in pH 3 solution but it could be due to a change in speciation or precipitation of the metals in secondary compounds. The fraction leached of the minor metals versus time is shown in Figure 10.

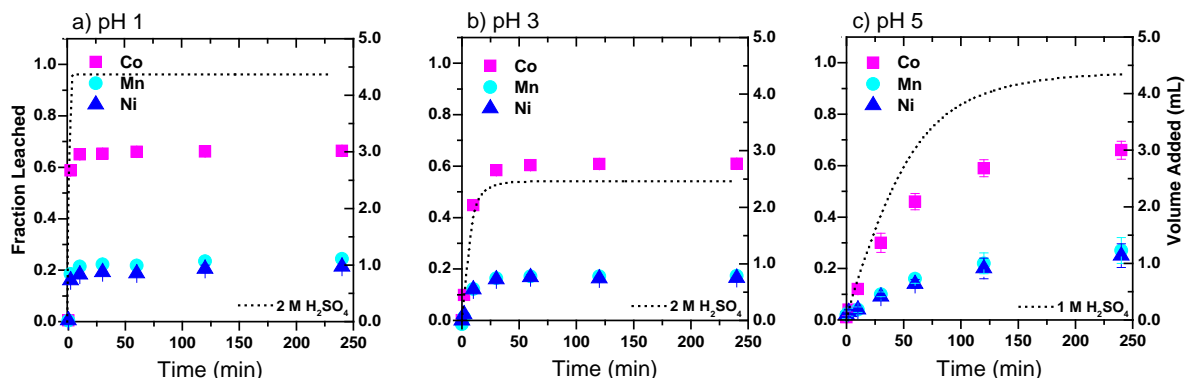


Figure 10: The leached fraction as given by the left ordinate for cobalt ( $\square$ ), manganese ( $\circ$ ) and nickel ( $\triangle$ ) from MOV in a) pH 1, b) pH 3, and c) pH 5 solutions. The volume and concentration of sulfuric acid ( $\text{H}_2\text{SO}_4$ ) added is shown as a solid black line corresponding to the right ordinate.

A summary of the fraction of each metal leached versus time (minutes) in the sulfuric acid leachate is given in Table 7. These data that are the same used to construct the plots in Figure 9 and Figure 10 only shown in numerical form. All standard deviations were less than or equal to 0.05.

Table 7: Summary of each metal leached during sulfuric acid leaching for pH 1, pH 3 and pH 5. All values are given in fraction leached.

pH	Metal	Time (minutes)						
		t = 0	t = 2	t = 10	t = 30	t = 60	t = 120	t = 240
pH 1	Bi	ND	0.29 ± 0.04	0.82 ± 0.02	0.83 ± 0.02	0.83 ± 0.02	0.83 ± 0.03	0.82 ± 0.02
	Co	ND	0.59 ± 0.01	0.65 ± 0.01	0.65 ± 0.01	0.66 ± 0.01	0.66 ± 0.01	0.66 ± 0.01
	Mn	ND	0.18 ± 0.01	0.21 ± 0.01	0.22 ± 0.01	0.22 ± 0.01	0.24 ± 0.01	0.24 ± 0.01
	Ni	ND	0.16 ± 0.01	0.18 ± 0.01	0.19 ± 0.01	0.19 ± 0.01	0.21 ± 0.01	0.21 ± 0.01
	Sb	ND	ND	ND	0.02 ± 0.01	0.01 ± 0.01	0.03 ± 0.02	0.04 ± 0.01
	Zn	ND	0.87 ± 0.03	0.95 ± 0.03	0.95 ± 0.03	0.96 ± 0.03	0.96 ± 0.03	0.98 ± 0.03
pH 3	Bi	ND	ND	ND	ND	ND	ND	ND
	Co	ND	0.10 ± 0.01	0.45 ± 0.01	0.58 ± 0.01	0.60 ± 0.01	0.61 ± 0.01	0.61 ± 0.01
	Mn	ND	0.01 ± 0.01	0.12 ± 0.01	0.16 ± 0.01	0.17 ± 0.01	0.17 ± 0.01	0.17 ± 0.01
	Ni	ND	0.02 ± 0.01	0.12 ± 0.01	0.16 ± 0.01	0.17 ± 0.01	0.16 ± 0.01	0.16 ± 0.01
	Sb	ND	ND	ND	ND	ND	ND	ND
	Zn	ND	0.17 ± 0.01	0.72 ± 0.05	0.94 ± 0.04	0.98 ± 0.03	0.99 ± 0.03	0.99 ± 0.03
pH 5	Bi	ND	ND	ND	ND	ND	ND	ND
	Co	ND	0.04 ± 0.01	0.12 ± 0.02	0.30 ± 0.04	0.46 ± 0.03	0.59 ± 0.03	0.66 ± 0.04
	Mn	ND	0.03 ± 0.02	0.04 ± 0.01	0.10 ± 0.01	0.16 ± 0.02	0.22 ± 0.04	0.27 ± 0.05
	Ni	ND	0.03 ± 0.01	0.04 ± 0.01	0.09 ± 0.01	0.14 ± 0.02	0.20 ± 0.04	0.25 ± 0.05
	Sb	ND	ND	ND	ND	0.02 ± 0.02	0.04 ± 0.05	0.08 ± 0.05
	Zn	ND	0.00 ± 0.03	0.18 ± 0.03	0.46 ± 0.04	0.72 ± 0.02	0.92 ± 0.04	1.00 ± 0.05

ND = metal not present in high enough concentration to be detected by ICP-OES

### 5.2.2. Analysis of Leaching Residue

The residue left after leaching of the MOV in a pH 1 sulfuric acid solution for 240 minutes is shown in Figure 11a. This specimen corresponds to the leaching data in Figure 9a and Figure 10a where nearly all of the zinc, 80% of the bismuth and very little antimony had been leached from the MOV. In Figure 11a the dominating structure present is the antimony-rich phase where as in the original MOV the dominating phase was zinc oxide as shown in Figure 11b. The antimony rich particles are approximately 2  $\mu\text{m}$  in diameter with some residual, undissolved bismuth-rich phase is still attached.

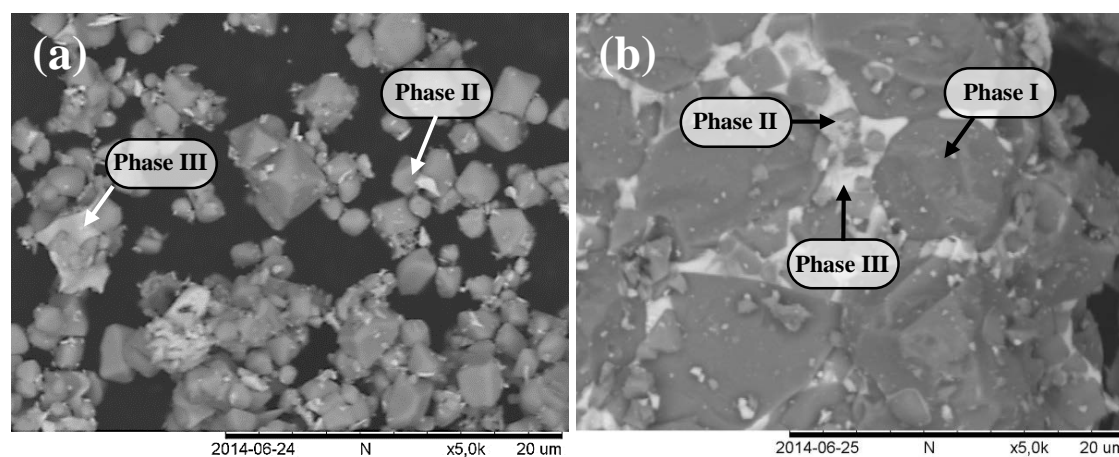


Figure 11: (a) SEM micrograph of pulverized MOV post leaching in pH 1 sulfuric acid solution for 240 minutes. The antimony-rich phase (phase II) remains along with some undissolved bismuth-rich phase (phase III). (b) SEM micrograph of the MOV prior to leaching showing all three phases: phase I – zinc oxide grains, phase II – antimony rich phase, and phase III – bismuth rich phase.

XRD analysis results for the pH 1 sulfuric acid leaching residue (Figure 9a and Figure 10a) is shown in Figure 12 as the solid black line (----). The majority of the peaks can be identified as originating from

antimony containing compounds, such as  $Zn_{2.33}Sb_{0.67}O_4$  ( $\square$ ),  $Zn_7Sb_2O_{12}$  ( $\blacksquare$ ),  $ZnCo_{1.33}Sb_{0.67}O_4$  ( $\circ$ ), and  $Zn_{1.66}Ni_{0.67}Sb_{0.67}O_4$  ( $\bullet$ ). The four aforementioned chemical compounds all share the same peaks and are all possibly present in the MOV. It might be possible that the concentrations of the minor metals (Co, Ni and Mn) in the leaching residue identify the presence of some compounds containing Ni, Co and Mn. However, XRD only suggest the presence is possible not that the compound is actually in the sample.

Also present in the MOV is  $Zn_2Bi_3Sb_3O_{14}$  ( $\star$ ) and  $Bi_2O_3$  ( $\blacklozenge$ ) both having identical peaks. It is logical based on characterization and literature data that pyrochlore ( $Zn_2Bi_3Sb_3O_{14}$ ), spinel both cubic ( $Zn_{2.33}Sb_{0.67}O_4$ ) and orthorhombic ( $Zn_7Sb_2O_{12}$ ) as well as some residual  $Bi_2O_3$  are present in the sample. It is also probable to have the presence of cobalt, nickel, and manganese in the sample however, the chemical form of those metals is not known. It should also be noted that the presence of the trirutile phase ( $ZnSb_2O_6$ ) was not identified in the spectrum in Figure 12. This supports Leite et al. that this compound is only an intermediary phase between the formation of the pyrochlore and spinel phases [14].

The XRD pattern in Figure 12 suggests all ZnO has been leached while some bismuth-rich compound was not fully leached. These results correlate with the leaching curves of Figure 9 and Figure 10. The residue can be compared to the starting material, dashed gray line (---) in Figure 12. The spectrum for the starting material contained prominent peaks for ZnO whereas the appearance of ZnO peaks in the leaching residue was non-existent. The XRD spectrum also indicates that it will be difficult to solubilize the zinc that is present in the combined zinc-antimony oxides.

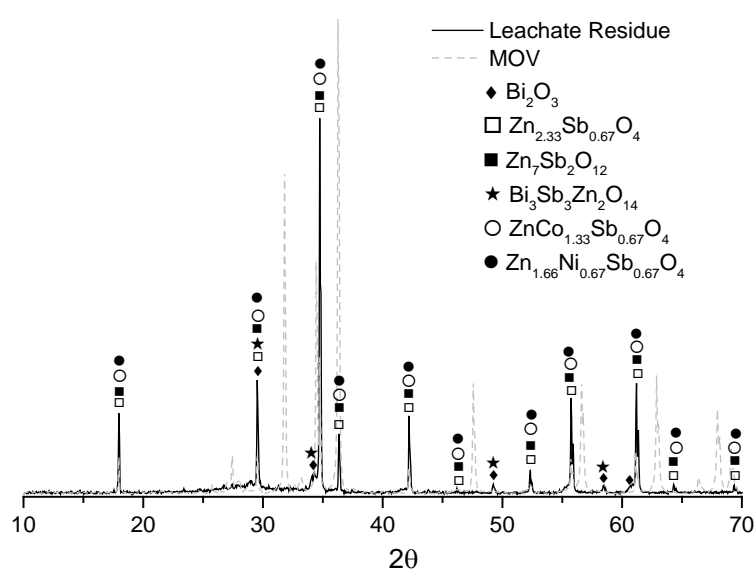


Figure 12: XRD spectrum (-----) of leaching residue (pH 1, sulfuric acid) compared to XRD spectrum of non-leached starting material (---). Chemical compounds are represented as follows:  $Bi_2O_3$  ( $\blacklozenge$ ),  $Zn_{2.33}Sb_{0.67}O_4$  ( $\square$ ) and  $Zn_7Sb_2O_{12}$  ( $\blacksquare$ )

Leaching in sulfuric acid solutions was highly effective for zinc leaching at each of the three pH values investigated. Sulfuric acid solutions showed the lowest leaching efficiency of minor metal in the MOV such as cobalt, nickel, and manganese compared to other acids studied. Co-leaching of the minor metals indicates that further purification will be needed before zinc electrowinning.

It can be concluded that it was possible to selectively leach zinc from the MOV without significant co-leaching of bismuth and antimony by selecting a suitable pH, mainly pH 3 or higher in all acids investigated [78]. Results of leaching with acetic acid, hydrochloric acid, and nitric acid are described in detail in Paper I [78]. The results for all acids are similar, in that zinc can be leached, but not selectively with respect to minor metals. No matter the leachate used: acetic, hydrochloric, nitric, or sulfuric acid, further purification of the leach liquor would be required if the leachate is to be used in the industrial zinc electrowinning process.

A purification method such as cementation could be effective for removing antimony, bismuth, nickel, and cobalt from the leaching solution. The added benefit of antimony is that it acts as an activator, increasing the kinetics of the cementation reaction [52].

### 5.3. Cementation

Cementation is carried out by addition of a less noble metal usually cheap and nontoxic causing reduction and deposition of the more noble metal from solution. As discussed in section 5.2 the sulfuric acid leaching solution needs to be purified of metals other than zinc in order to be usable in zinc electrowinning.

#### 5.3.1. Cementation Solution Preparation - Bulk Leaching of MOV

After four hours the pH remained constant at pH 3 indicating the solution had reached equilibrium. Results for the leaching are shown in Figure 13a for the volume of 5 M  $H_2SO_4$  added during the leaching experiment and Figure 13b showing the pH change as a function of time for the three bulk MOV leaching experiments.

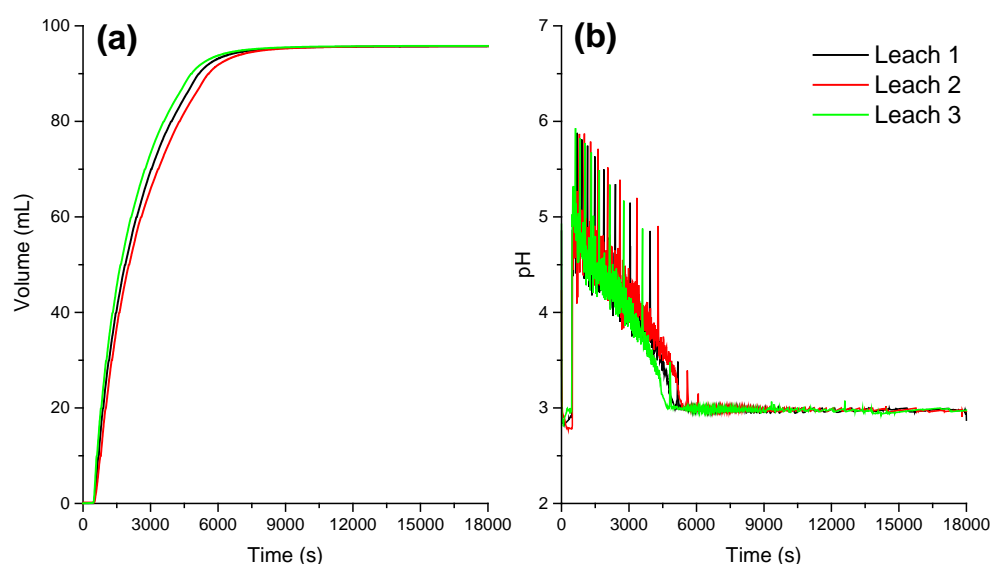


Figure 13: (a) Amount of 5 M  $H_2SO_4$  solution added during bulk MOV leaching experiment vs. time.  
(b) The pH vs. time during the bulk leaching experiments.

The average volume of 5 M  $H_2SO_4$  added during the leaching experiments was  $95.75 \pm 0.04$  mL. All leaching curves showed the same trend and very similar leaching results. Once the bulk leaching was done the leachate was separated from the residue and analyzed by ICP-OES yielding a leachate solution having concentrations found in column 2 of Table 8.

Table 8: Concentration of metals in leachate for the elements found in the MOV along with industrial zinc electrowinning solution concentrations before and after cementation.

Element	MOV Leachate Conc. (mg/L)	Industrial Conc. Before cementation [41] (mg/L)	Industrial Conc. after cementation [41] (mg/L)
Bi	0	0	0
Co	437 ± 8	15	1 – 0.05
Cu	0	1000	0.1 – 0.15
Mn	68 ± 1	0	0
Ni	106 ± 2	0	0
Sb	0	0	0.01 – 0.02
Zn	81 g/L	150 g/L	150 g/L

Along with the metal concentrations in the MOV leachate, typical metal concentrations in industrial solution prior to cementation reactions and after cementation reaction during the RLE process are shown in Table 8, column 3 and 4 respectively. It can be concluded by comparing the bulk MOV leachate metal concentrations (column 2) to the concentrations of the metals in industrial solution before cementation (column 3) that the MOV system has much higher concentrations of cobalt and nickel than the industrial solution.

Industrial removal of cobalt via cementation is complex and depends on a number of parameters such as the influence of additives, temperature, pH, zinc dust addition, etc. Some important parameters have been studied with respect to RLE but never on the MOV leaching system where the cobalt concentration is over 25 times higher than in common cementation systems. For the MOV leachate to be easily integrated into the zinc electrowinning process it needs to be as clean from impurities as possible. It has been reported that 15 ppm of cobalt, copper, and nickel can reduce the current efficiency by 10%, 15% and 40% respectively [41].

### 5.3.2. Cementation Experiments

#### 5.3.2.1. Influence of Copper Ion Concentration

Work by Van der Pas et al. showed that cementation of cobalt without antimony or copper resulted in less than 10% of cobalt being removed from solution [59]. Their results also show that addition of copper to the cementation solution did not result in improved cementation of cobalt. However it has been reported that the effect of copper improves the cementation rate if only slightly [41].

Experiments were carried out to show the influence of copper on cementation reactions. The results are shown in Figure 14. Initially nitrogen was bubbled through 25 mL of cementation solution, also known as the leachate having composition given in Table 8, column 2. In addition to the metal ions in the leaching solution copper was added in four different concentrations: 0.2, 0.4, 0.8, and 1.2 g·L<sup>-1</sup> Cu. For each experiment 2 g·L<sup>-1</sup> of zinc powder was added to the leachate, similar amounts have been reported in literature [54] and this parameter will be further investigated. The initial pH of the cementation solution was pH 3 but increased due to the addition of zinc. The cementation solution was kept at pH 4 during the cementation experiments by titration with 0.1 M H<sub>2</sub>SO<sub>4</sub> solution. Cementation results are shown in Figure 14 for a.) cobalt, b.) copper, c.) nickel, and d.) antimony. Results are given in terms of C/C<sub>0</sub>, where C, is the concentration of metal in solution at that point in time and C<sub>0</sub>, is the initial concentration of the metal in solution at t = 0. The results show the fraction of metals removed from solution as a function of time.

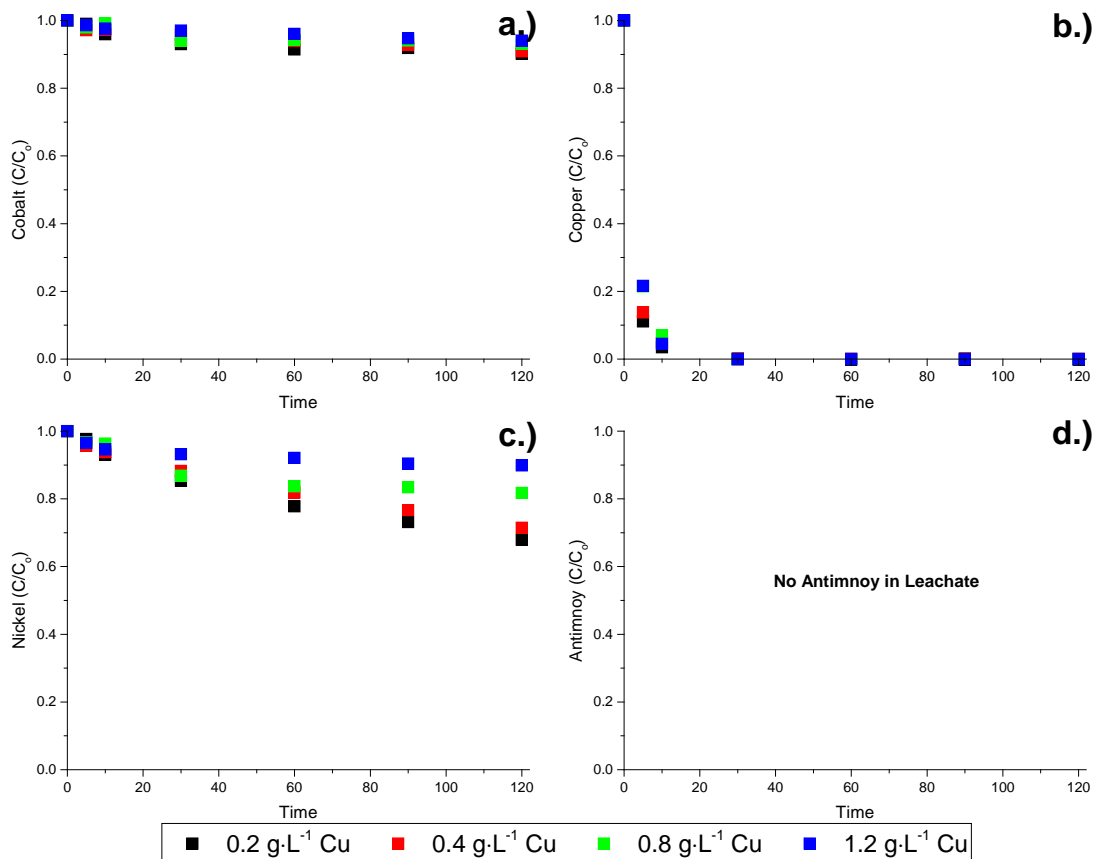


Figure 14: Results for the influence of copper concentration on cementation of a.) cobalt, b.) copper, c.) nickel and d.) antimony, with copper concentrations of 0.2, 0.4, 0.8, and 1.2 g·L<sup>-1</sup> at T = 22 °C.

The results in this work is in agreement with Van der Pas et al. [59] in that the addition of copper did not improve cobalt cementation. From Figure 14a the amount of cobalt cemented from solution is never more than 10%. From Figure 14b it can be concluded that copper is cemented from solution within 20 minutes, no matter the amount added, it is easily removed from solution. It is interesting to note the effect of copper concentration on the cementation of nickel shown in Figure 14c where the cementation rate of nickel is inversely related to the copper concentration in solution. This cannot currently be explained. No data was obtained on the amount of antimony that could be cemented from the solution as antimony was not present in the leachate.

Therefore, the same cementation experiments shown in Figure 14 were repeated with the addition of 0.4 g·L<sup>-1</sup> Sb and yielded results shown in Figure 15. Addition of 0.2 and 0.4 g·L<sup>-1</sup> Cu with 0.4 g·L<sup>-1</sup> Sb resulted in nearly 40 % of cobalt and 60 % of nickel being removed from solution; much higher than comparing results for the same copper concentration with no antimony present in solution. Addition of copper over 0.8 g·L<sup>-1</sup> to the cementation solution resulted in low removal of cobalt, nickel, antimony, and copper itself. This is due to the limited zinc dust surface area available for cementation reactions to occur.

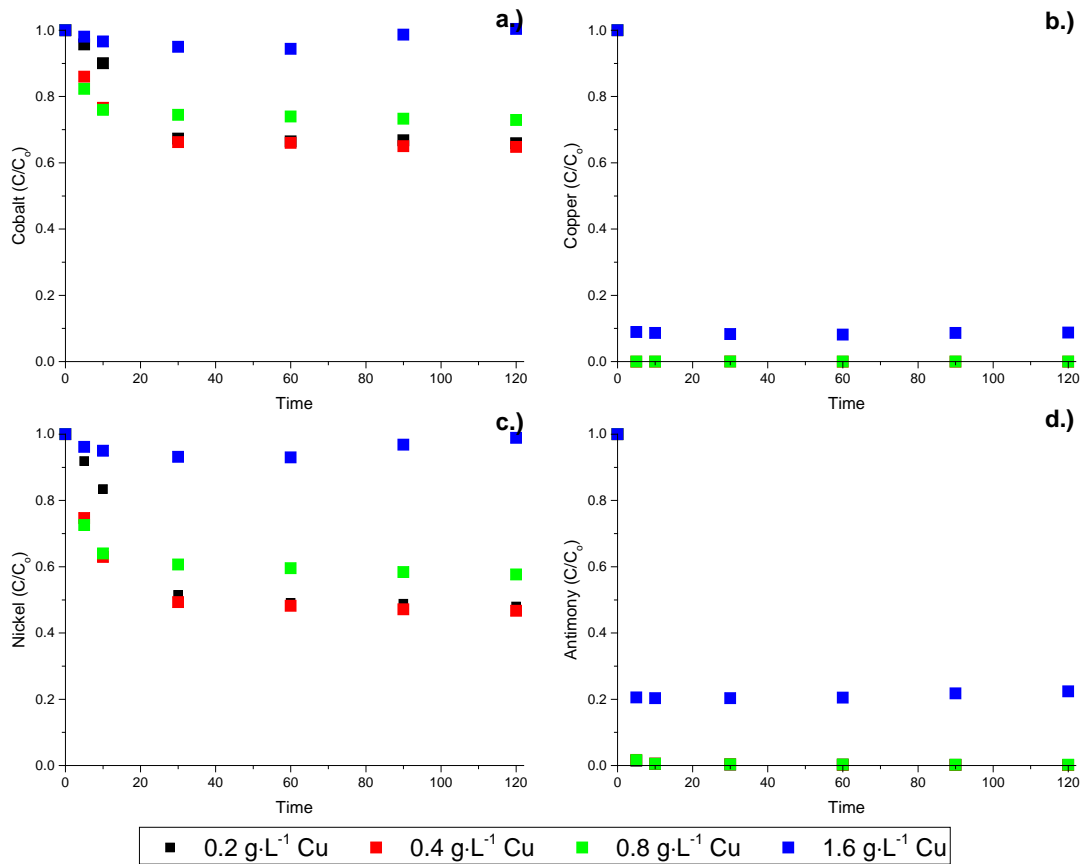


Figure 15: Results for the influence of copper concentration in the presence of 0.4 g·L<sup>-1</sup> antimony on cementation of a.) cobalt, b.) copper, c.) nickel and d.) antimony, with copper concentrations of 0.2, 0.4, 0.8, and 1.6 g·L<sup>-1</sup> at T = 22 °C.

All concentrations were chosen based on concentrations of impurities reported in literature but scaled up to accommodate the increased cobalt and nickel concentrations in the MOV leachate. Boyanov et al. determined that when  $G_{Sb} : G_{Co}$  ratio is between 0.5 : 1 and 2 : 1 the solution is purified from cobalt and nickel to the greatest degree [52, 79]. This work used a 1 : 1 ( $G_{Sb} : G_{Co}$ ) ratio.

### 5.3.2.2. Influence of Antimony Concentration

From previous results (Figure 14 and Figure 15) it can be concluded that antimony needs to be present in the solution if cementation reactions are to occur to a large degree. Furthermore, antimony needs to be in solution with copper ions present. In industry, antimony is known as an activator which helps to speed up the slow kinetics of cobalt cementation on zinc making this type of purification process feasible [62]. Copper together with antimony forms a substrate favorable for cobalt cementation. It is known to do so by copper forming a larger cathodic area on the zinc dust and antimony increasing the amount of cobalt in the deposit by forming an Sb-Co alloy [41].

In addition to the metal ions in the leaching solution (Table 8) copper was added having a concentration of 0.4 g·L<sup>-1</sup>. Antimony was added at five different concentrations: 0.1, 0.2, 0.4, 0.8, and 1.6 g·L<sup>-1</sup>. For each experiment 2 g·L<sup>-1</sup> of zinc powder was added to the leachate. The cementation solution was kept at pH 4 by titration of 0.1 M H<sub>2</sub>SO<sub>4</sub> solution. Cementation results are shown in Figure 16 for a.) cobalt, b.) copper, c.) nickel, and d.) antimony.

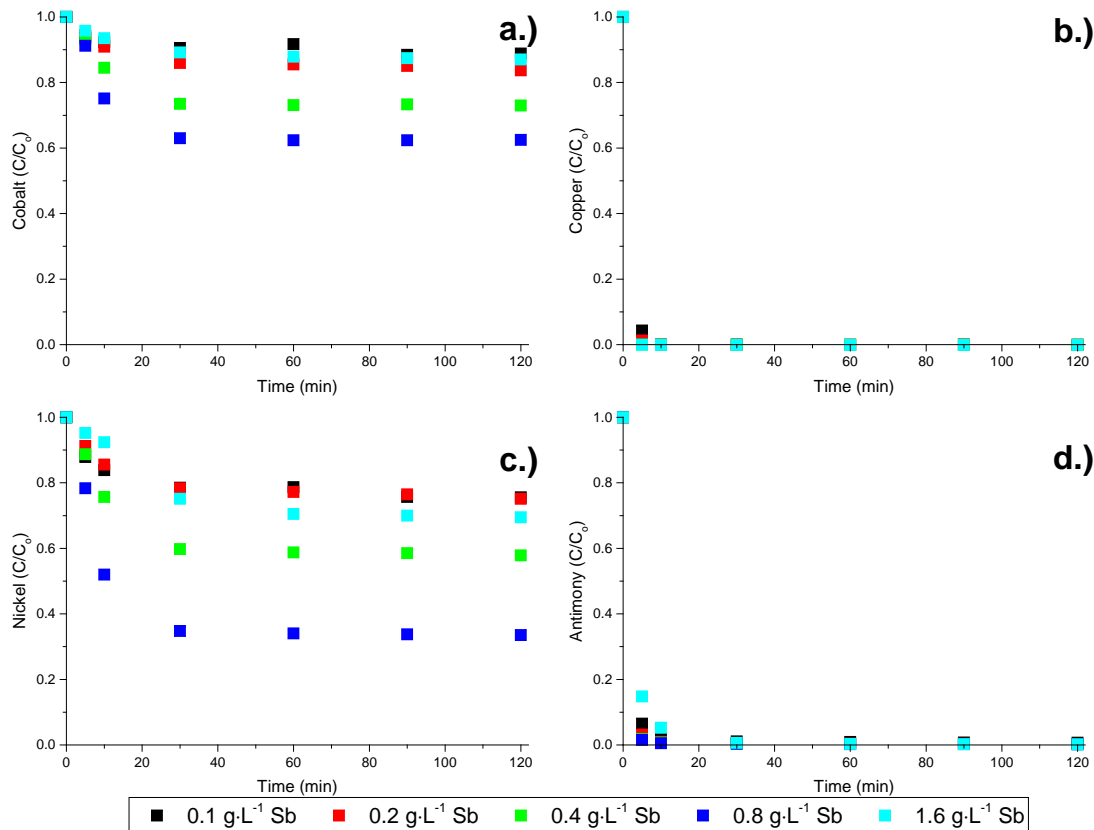
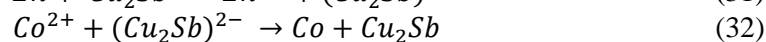


Figure 16: Results for the influence of antimony concentration on cementation for a.) cobalt, b.) copper, c.) nickel and d.) antimony, with copper concentration of 0.4 g·L<sup>-1</sup> and antimony concentrations of 0.1, 0.2, 0.4, 0.8, and 1.6 g·L<sup>-1</sup> at T = 22 °C.

An addition of antimony increased the amount of cobalt cemented from less than 10 % (no antimony) to nearly 40 % of cobalt removal using 0.8 g·L<sup>-1</sup> of antimony as seen in Figure 16a. Addition of 1.6 g·L<sup>-1</sup> antimony to the cementation solution had adverse effects on the cementation. This trend is not reported in literature where antimony was always added in lower concentrations than in our experiments. However a trend was seen in work done by Dai et al. [53] where addition of more than 5 mg·L<sup>-1</sup> of antimony to the solution did not increase the rate of cobalt cementation in a 24 g·L<sup>-1</sup> solution of cobalt. This can be explained by the zinc dust surface area available for cementation being completely coated with copper and antimony allowing no surface for cobalt cementation or electron exchange. After the first 10 minutes all the copper had been cemented from solution. Similar reaction kinetics of copper and antimony were also seen by Van der Pas et al [59].

From Figure 16 it is seen that after 30 minutes all of the copper and antimony have been cemented from solution. Similarly after 30 minutes the amount of cobalt cemented from solution does not increase. This could indicate the formation of an alloy of copper-antimony-cobalt-nickel promoting the cementation of cobalt and nickel. Analysis of the residue would need to be done to confirm this. Work has been done by Kroleva et al. [80] suggesting the formation of a deposition enhancing Cu<sub>2</sub>Sb alloy according to Equations 31-32:



### 5.3.2.3. Influence of Temperature

This is by far the most influential parameter in cementation as reported in the work of others [81, 82]. Higher temperature result in a greater amount and faster rate of cobalt cemented from the solution due to increased reaction kinetics. Literature suggests the optimal temperature for cobalt cementation is between 75 and 90 °C [53, 58, 60]. Industrially, temperatures higher than 70 °C are used for cobalt cementation but it has been seen by Van der Pas et al. [59] that once above 85 °C hydrogen evolution retards the cobalt cementation.

The cementation solution contained copper and antimony having a concentration of 0.4 g·L<sup>-1</sup> each. Experiments were run at temperatures of 22, 30, 40, 50, 55, 60 °C. For each experiment 2 g·L<sup>-1</sup> of zinc powder was added to the leachate. The cementation solution was kept at pH 4 by titration of 0.1 M H<sub>2</sub>SO<sub>4</sub> solution. Cementation results are shown in Figure 17 for a.) cobalt, b.) copper, c.) nickel, and d.) antimony.

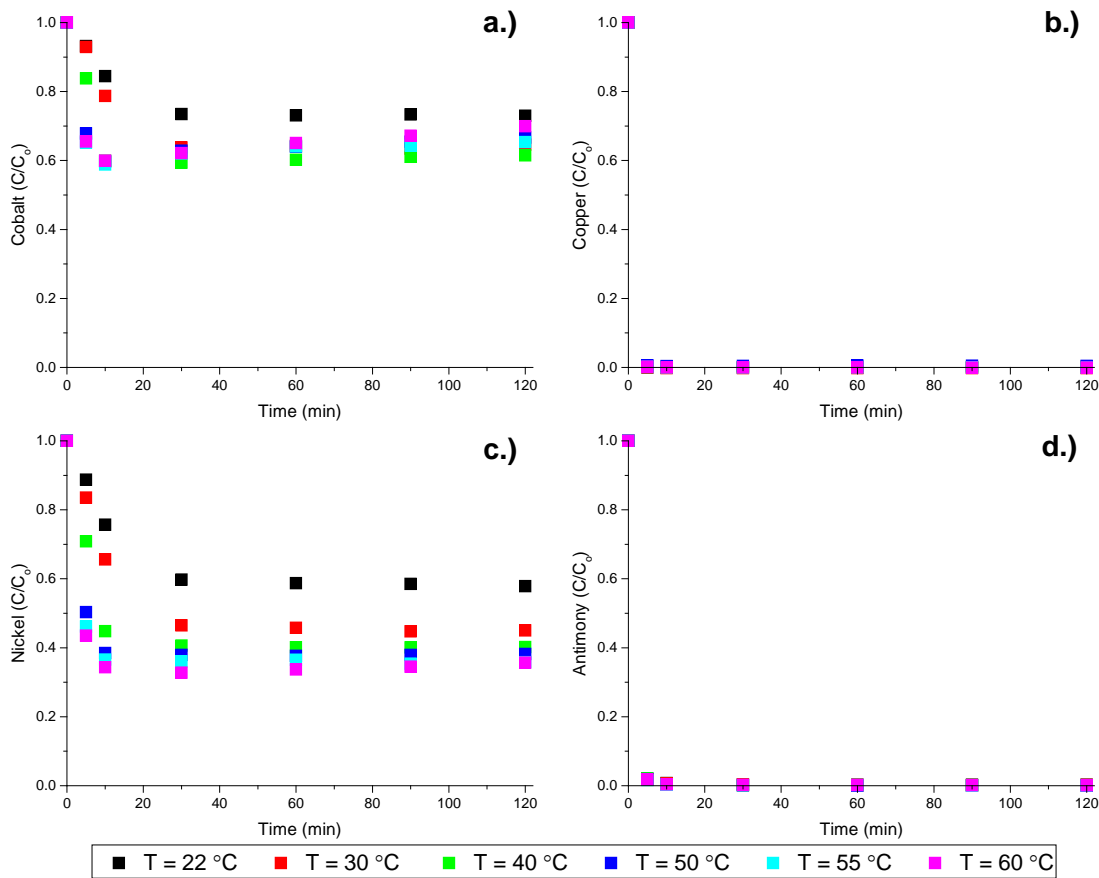


Figure 17: Results for the influence of temperature ( $T = 22, 30, 40, 50, 55, 60$  °C) on cementation of a.) cobalt, b.) copper, c.) nickel and d.) antimony, with copper and antimony concentrations of 0.4 g·L<sup>-1</sup>.

Literature suggests the optimal temperature for cobalt cementation is near 80 °C. It was not possible to perform cementation reactions at such high temperatures in the present work due to evaporation. However, over 40 % of the cobalt in solution was successfully cemented out, reducing the concentration in solution by over 160 ppm, at  $T = 60$  °C. It is clear from Figure 17a that increasing the temperature also increased the kinetics of cobalt cementation but it did not have a significant effect on the total amount of cobalt cemented from solution. All copper and antimony and nearly 70 % (70 ppm) of nickel were cemented from solution at  $T = 60$  °C.

It has been reported in literature [52, 83] that cobalt re-dissolves after reaching a concentration minimum in the solution. It is also stated that increasing temperature also reduces the time in which the minima is experienced. It should be noted that temperature also increases the production of hydrogen and thus reduces the volume in solution. It was not seen in any article that this loss in volume was accounted for in data processing. In summary, our work also showed that with higher temperature a minima of cobalt in solution was seen however it cannot be concluded that this minima is explained by re-dissolution of the cobalt or simply evaporation (due to heating and hydrogen evolution) of the cementation solution. Further investigation is needed.

#### 5.3.2.4. Influence of Zinc Dust

The influence of the amount of zinc dust added on this (MOV) system was largely unknown due to the higher concentration of impurities versus industrial zinc electrolyte. Industrially 4-6 g·L<sup>-1</sup> of zinc dust is used for cementation [41]. Experiments were conducted with the amount of zinc dust added being between 0.25 to 4 g·L<sup>-1</sup>. However, it is not the amount of zinc added but rather the surface area that affects the cementation reactions. BET measurements show that the surface area per gram of zinc dust is 0.2268 ± 0.0031 m<sup>2</sup>·g<sup>-1</sup>. The amount of zinc dust and the equivalent surface area of the zinc dust added to the cementation solution is given in Table 9.

Table 9: Quantity of zinc dust added during cementation experiments with correlating surface area.

Concentration of Zn Dust Added (g·L <sup>-1</sup> )	Surface Area of Zn Dust (cm <sup>2</sup> )
0.25	14.5 ± 0.2
0.5	28.4 ± 0.4
1	56.9 ± 0.8
2	113 ± 2
3	171 ± 2
4	228 ± 3

It should be noted that most literature data (and all of the articles cited within this text) give the amount of zinc dust added not in surface area (cm<sup>2</sup>) but in concentration (g·L<sup>-1</sup>). This does not allow accurate comparison of results between studies as the geometry and particle size distribution since the zinc dust varies from supplier to supplier and depends on the preparation method. For this work a zinc powder with spherical particles was used as seen in Figure 18. By using surface area it would be able for experiments performed in different studies to be more accurately compared.

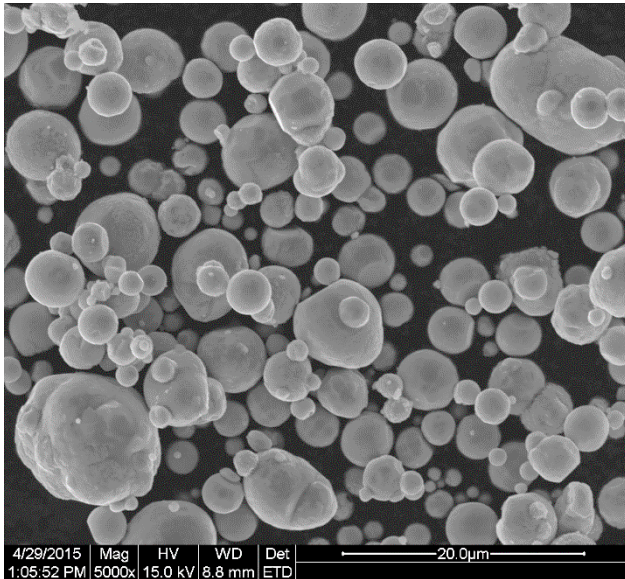


Figure 18: SEM of zinc dust used in cementation reactions

Previous experiments were done using zinc flakes which were laminar and did not mix well with the cementation solution without the help of surfactants due to surface tension. Its use was discontinued and spherical zinc dust was used successfully without the use of surfactants. It has been reported that smaller zinc dust particles (less than  $38\ \mu\text{m}$ ) result in faster kinetics and lower cobalt concentrations [54]. For this work the particle size of the zinc used is below  $20\ \mu\text{m}$ .

The cementation solution in these experiments contained copper and antimony at a concentration of  $0.4\ \text{g}\cdot\text{L}^{-1}$  each. Experiments were carried out at  $22\ ^\circ\text{C}$ . The solution was kept at pH 4 by titration of  $0.1\ \text{M}$   $\text{H}_2\text{SO}_4$  solution. Cementation results are shown in Figure 19 for a.) cobalt, b.) copper, c.) nickel, and d.) antimony.

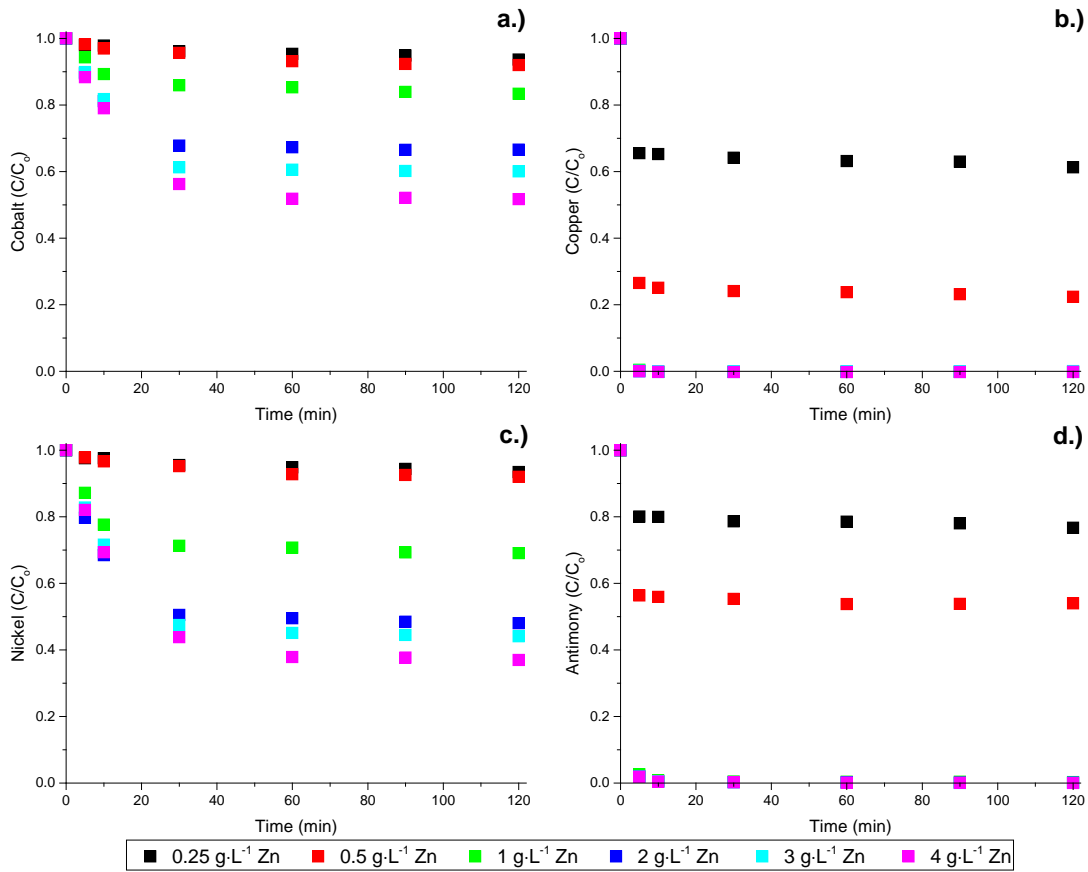


Figure 19: Results for the influence of zinc dust addition (0.25, 0.5, 1, 2, 3, 4 g·L<sup>-1</sup> Zn) on cementation of a.) cobalt, b.) copper, c.) nickel and d.) antimony, with copper and antimony concentrations of 0.4 g·L<sup>-1</sup> at T = 22 °C.

When using less than 1 g·L<sup>-1</sup> of zinc dust ( $56.9 \pm 0.78$  cm<sup>2</sup>) not enough surface area was available for cementation reactions to take place. The zinc surface was fully covered with antimony and copper thus stopping the cementation reaction. This can be seen from results in Figure 19 where antimony and copper remained in solution using low concentrations of zinc dust. Addition of more zinc dust resulted in better cobalt and nickel removal. The cobalt concentration was reduced from 400 ppm to 200 ppm and the nickel concentration was reduced from 100 ppm to nearly 35 ppm.

### 5.3.2.5. Influence of pH

Cementation experiments were carried out to show the influence of pH on cementation of Co, Cu, Ni, and Sb. The cementation solution contained copper and antimony having a concentration of  $0.4 \text{ g}\cdot\text{L}^{-1}$  each. For each experiment  $2 \text{ g}\cdot\text{L}^{-1}$  of zinc powder was added to the leachate. The cementation solution was kept at the desired pH by titration of  $0.1 \text{ M H}_2\text{SO}_4$  solution. Cementation results are shown in Figure 20 for a.) cobalt, b.) copper, c.) nickel, and d.) antimony.

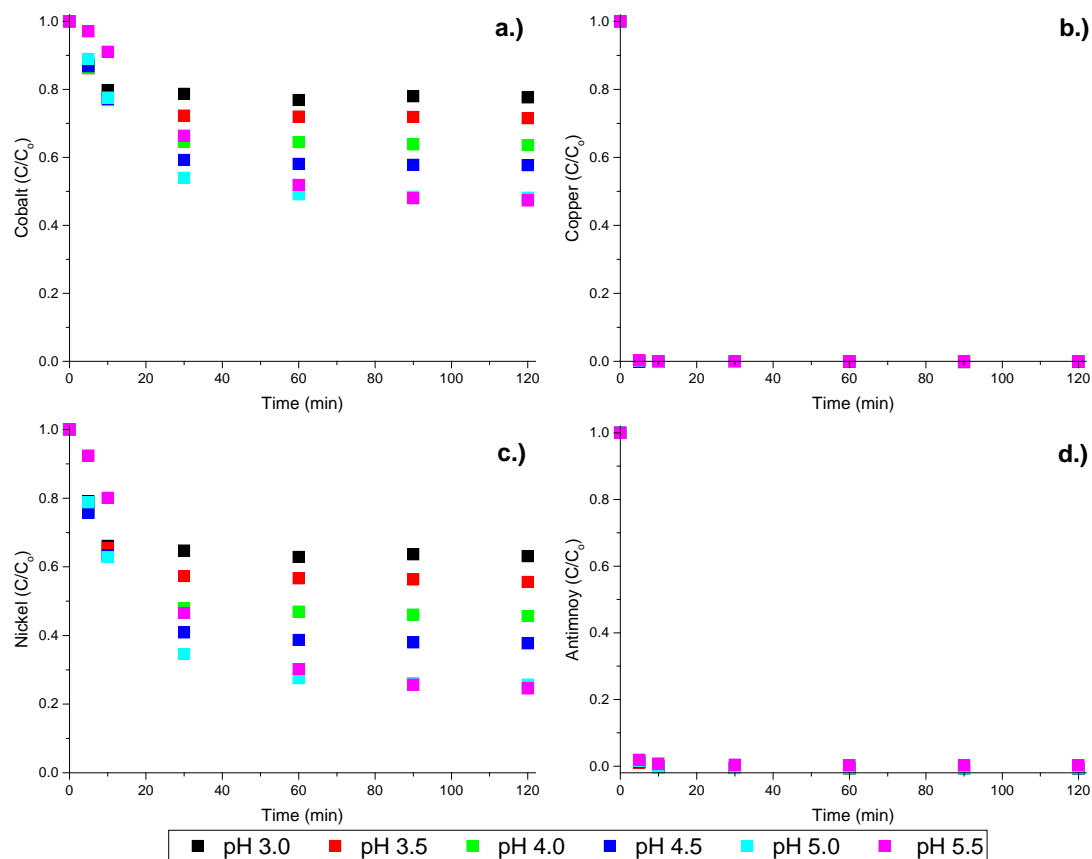


Figure 20: Results for the influence of solution pH on cementation of a.) cobalt, b.) copper, c.) nickel and d.) antimony, with copper and antimony concentrations of  $0.4 \text{ g}\cdot\text{L}^{-1}$  at  $T = 22 \text{ }^\circ\text{C}$ .

For this work the pH of the solution was between pH 3 and pH 6.0. Results show that using pH 5 is most effective in removal of cobalt and nickel with over 50 % and 75 % removal respectively. Higher pH however slowed the reaction kinetics for cementation of both cobalt and nickel. Using a pH higher than 6 had a negative impact in cementation and the results are not shown in Figure 20. These results are in good agreement with work done by Van der Pas et al showing that low pH is worse for cementation reactions than a higher pH. Using pH 5 cementation solution 50% of the cobalt ( $200 \text{ mg}\cdot\text{L}^{-1}$ ) was removed from solution. If the pH of the solution is too high (typically greater than pH 5.0) the formation of basic sulphate or zinc hydroxide inhibit the reaction kinetics by forming a passivating layer on the zinc powder [62, 84]. Once again copper and antimony were removed from solution within 10 minutes.

### 5.3.2.6. Optimized Cementation

From the experiments described in sections 5.3.2.1 to 5.3.2.5 where the influence of parameters such as copper concentration, antimony concentration, zinc dust addition, temperature and pH were studied; it can be concluded that the optimal conditions for cementation of cobalt are:  $0.8 \text{ g}\cdot\text{L}^{-1}$  Sb,  $0.4 \text{ g}\cdot\text{L}^{-1}$  Cu,  $T = 40 \text{ }^\circ\text{C}$ ,  $0.2 \text{ g}\cdot\text{L}^{-1}$  Zn addition and a solution pH of 5.0. Using these parameters on the MOV leachate yields results shown in Figure 21. The copper is not seen in Figure 21 but its values lie behind those of antimony.

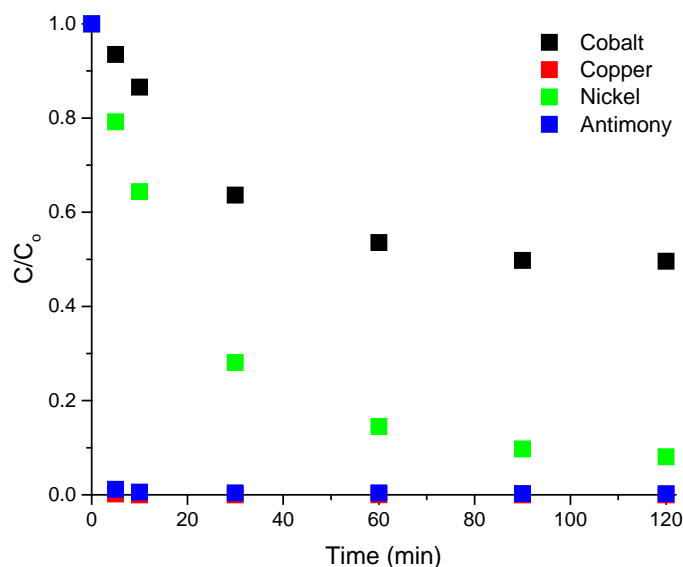


Figure 21: Cementation results for optimized experimental conditions.

Cementation results show that it is possible to purify MOV leaching solutions via cementation reactions. Even though copper and antimony are added to the cementation solution as activators they are easily removed causing no contamination of the leachate. The concentration of cobalt in solution was reduced from 400 over ppm to 215 ppm and nickel was reduced from 106 ppm to 9 ppm. The starting and final concentration of metals in the leachate are shown in Table 10.

Table 10: Concentration of metals in MOV leachate before and after cementation.

Metal	MOV leachate pre-cementation ( $\text{g}\cdot\text{L}^{-1}$ )	MOV leachate post-cementation ( $\text{g}\cdot\text{L}^{-1}$ )
Bi	0	ND
Co	$437 \pm 8$	$215 \pm 4$
Cu	0	ND
Mn	$68 \pm 1$	$68 \pm 1$
Ni	$106 \pm 2$	$9 \pm 1$
Sb	0	ND

ND = not detected

It was also realized that the cementation of cobalt and nickel is dependent on having copper and antimony in solution. From cementation experiment it was seen that copper and antimony were consumed within 10 minutes of the cementation reaction. Batch addition of these two metals needs to be investigated further.

## 5.4. Antimony Recovery

### 5.4.1. Characterization of the Sb-rich leaching residue

Antimony changes its valence from  $\text{Sb}^{+3}$  to  $\text{Sb}^{+5}$  when spinel and pyrochlore are formed from  $\text{Sb}_2\text{O}_3$  requiring additional oxygen from the atmosphere, see Equations 1-4 [8]. The typical grain size of ZnO in the MOV is in the range of 20 to 140  $\mu\text{m}$ . But it is removed via leaching, leaving the pyrochlore and spinel phases having a grain size smaller than 5  $\mu\text{m}$ . The  $\text{Bi}_2\text{O}_3$  phase is crystalline at room temperature, however, it can exist in several different crystalline forms depending on the cooling rate and the presence of transition metal oxides [18]. ICP-OES analysis of the dissolved leaching residue is shown in Table 11.

Table 11: ICP-OES results of leaching residue, tested in triplicate and given in wt %.

	Bi	Co	Mn	Ni	Sb	Zn
Residue 1	24.5	1.2	1.5	2.6	17	36
Residue 2	24.8	1.2	1.5	2.6	18	36
Residue 3	24.8	1.2	1.5	2.6	19	36
Average	$25 \pm 0.2$	$1.2 \pm 0.01$	$1.5 \pm 0.01$	$2.6 \pm 0.01$	$18 \pm 0.8$	$36 \pm 0.1$
MOV	$5.7 \pm 0.1$	$0.86 \pm 0.02$	$0.44 \pm 0.01$	$0.77 \pm 0.02$	$4.6 \pm 0.1$	$87 \pm 3.0$

By leaching and thus removing the soluble zinc oxide portion from MOV it was possible to concentrate the antimony from 4.6 wt % to nearly 18 wt % after leaching. Similarly, the wt % of zinc decreased from 87 wt % to nearly 35 wt % in the sample. The concentration of the other metals increased in the residue after leaching as seen by comparing row 5 and 6 in Table 11. SEM-EDX analysis showed mostly the antimony rich compound as well as the  $\text{Bi}_2\text{O}_3$  phase, the SEM micrograph is seen in Figure 22.

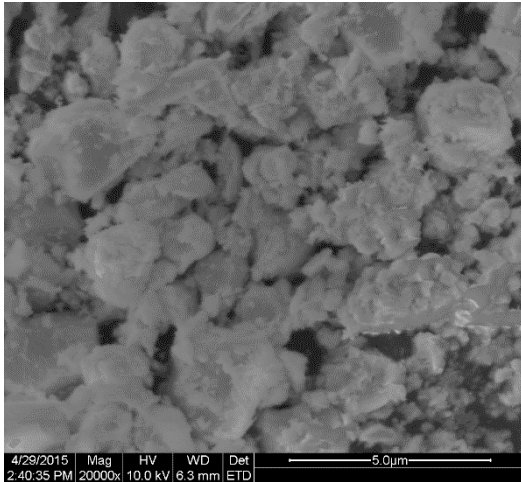


Figure 22: SEM micrograph of antimony rich leaching residue surrounded by  $\text{Bi}_2\text{O}_3$ .

The chemical composition of the leaching residue is complex. An XRD analysis of the residue is presented in Figure 23 showing the possible presence of many different chemical compounds in the leaching residue. The exact chemical compounds in the MOV residue cannot be determined by XRD and SEM-EDX alone but would require further investigation. However, from results reported in literature it can be assumed that the composition of the leaching residue is mainly  $\text{Bi}_2\text{O}_3$ ,  $\text{Zn}_2\text{Bi}_3\text{Sb}_3\text{O}_{14}$  (pyrochlore),  $\text{Zn}_{2.33}\text{Sb}_{0.67}\text{O}_4$  (spinel-cubic), and  $\text{Zn}_7\text{Sb}_2\text{O}_{12}$  (spinel-orthorhombic) [8, 17].

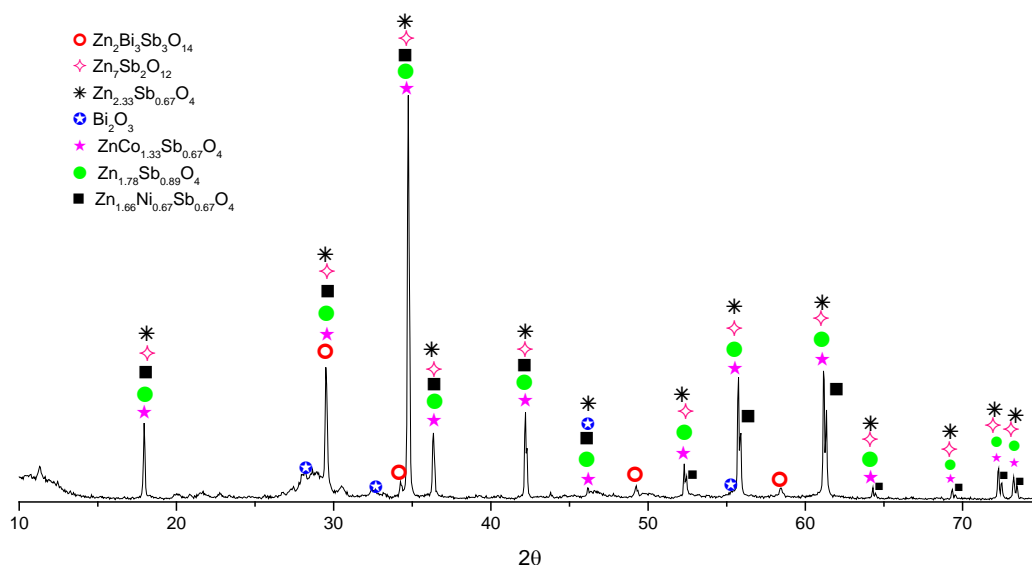


Figure 23: XRD spectrum of MOV leaching residue showing many different possible chemical structures present in the MOV leaching residue.

From the XRD spectra it is shown that the pyrochlore and spinel phases are present in the residue along with bismuth oxide. The bismuth is also confirmed from the ICP-OES and SEM data. The XRD data also shows that some peaks match for Zn-Co-Sb-O, Zn-Ni-Sb-O, and other similar compounds. This is to be expected as the MOV is sintered during manufacturing and several products can be formed during this process.

#### 5.4.2. Feasibility Study - Direct and Carbothermal Reduction

Initially a TGA study was done on pure compounds as well as the MOV and residue. This was done to see if the leaching residue followed the decomposition of simple metal oxides or if the decomposition of the residue was more complex.

The reaction system consisting of pure oxides ( $\text{Sb}_2\text{O}_3$ ,  $\text{Bi}_2\text{O}_3$ , and  $\text{ZnO}$ ) is a much simpler system than the MOV leaching residue. However, it can provide a good fundamental understanding of the behavior of antimony oxide. Two types of experiments were performed: (1) direct reduction where the metal oxides are heated in a nitrogen atmosphere and (2) carbothermal reduction where charcoal is added to the metal oxides to lower the reduction temperature also done in oxygen free atmosphere. Carbothermal reduction has been proven to work in zinc production [36] but the effect on the oxides of antimony and bismuth as well as the MOV and residue are not well known.

##### 5.4.2.1. Direct Reduction

Experiments on pure metal oxides of antimony, bismuth and zinc along with the MOV and leaching residue were carried out to determine if a high temperature separation of antimony oxide from zinc oxide was feasible. Within the spinel and pyrochlore structures the coordination of the antimony and zinc is not related to the pure metal oxides. Nonetheless the results shown in Figure 24 for the direct reduction of antimony(III) oxide, bismuth(III) oxide, zinc oxide, MOV and residue give results that are comparable to those reported in literature ( $\text{Sb}_2\text{O}_3$ ,  $\text{Bi}_2\text{O}_3$ , and  $\text{ZnO}$ ) as well as information on relatively unknown systems.

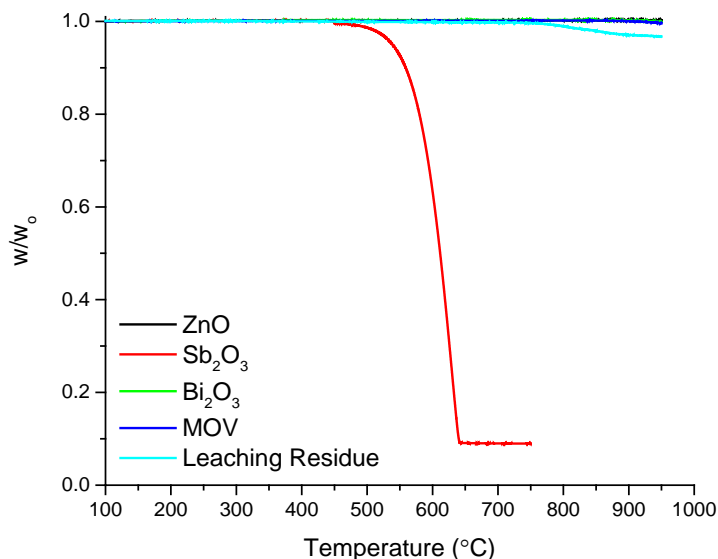


Figure 24: Direct reduction of antimony Oxide ( $\text{Sb}_2\text{O}_3$ ), bismuth oxide ( $\text{Bi}_2\text{O}_3$ ), zinc oxide ( $\text{ZnO}$ ), MOV, and leaching residue run in  $\text{N}_2$  with a heating rate of  $10\text{ }^\circ\text{C}\cdot\text{min}^{-1}$ .

The oxides of more noble metals can be reduced to directly produce the metals by simple thermal decomposition [35]. This is the case for antimony oxide which is shown in Figure 24 to volatilize at temperatures near  $600\text{ }^\circ\text{C}$  with nearly all  $\text{Sb}_2\text{O}_3$  converted to gaseous antimony at  $650\text{ }^\circ\text{C}$ . The oxides of zinc and bismuth are stable at temperatures lower than  $1000\text{ }^\circ\text{C}$ . The percent weight loss for the MOV indicates that it is stable at temperatures below  $1000\text{ }^\circ\text{C}$  as well. This is to be expected as the MOV is over 90 wt % zinc oxide, which has a melting temperature well above  $1000\text{ }^\circ\text{C}$ . The leaching residue experienced a 3 % weight loss with an onset reaction temperature near  $700\text{ }^\circ\text{C}$ . Which confirms that antimony is not present in the leaching residue as  $\text{Sb}_2\text{O}_3$  but as something more resistant to thermal decomposition.

#### 5.4.2.2. Carbothermal Reduction

The composition of the samples used in the TGA carbothermal reduction study are given in Table 5. The carbon to leaching residue ratio (based on weight) was 1:2. It was not possible to calculate the molar ratio of carbon to oxygen in the leaching residue. The effect of temperature on weight loss for the metal oxides with charcoal addition is shown in Figure 25 for a heating rate of  $10\text{ }^\circ\text{C}\cdot\text{min}^{-1}$  in nitrogen atmosphere. The peak reduction temperature for  $\text{Sb}_2\text{O}_3$  was reduced  $40\text{ }^\circ\text{C}$  by addition of charcoal when compared to direct reduction. It was not possible to directly reduce  $\text{ZnO}$  but addition of charcoal caused the onset of  $\text{ZnO}$  reduction to occur around  $900\text{ }^\circ\text{C}$  as is commonly reported in literature [85, 86].

Carbothermal reduction of the MOV resulted in a weight loss of nearly 10% while the carbothermal reduction of the leaching residue resulted in a weight loss of nearly 30%. From the thermolysis curve for the leaching residue several inflection points can be see indicating multiple reactions. From TG data alone it is not possible to determine the products of the reactions and further investigation is needed.

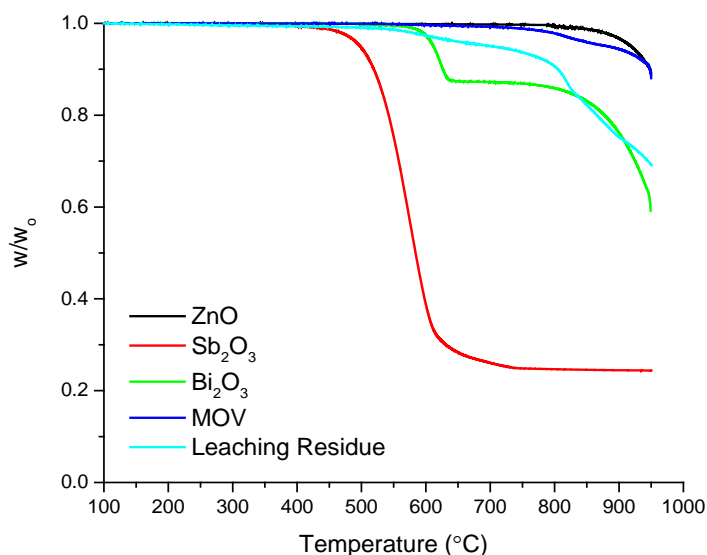


Figure 25: Carbothermal Reduction of zinc oxide (ZnO), Antimony Oxide ( $\text{Sb}_2\text{O}_3$ ), Bismuth Oxide ( $\text{Bi}_2\text{O}_3$ ), MOV, and leaching residue in  $\text{N}_2$  with a heating rate of  $10\text{ }^\circ\text{C}\cdot\text{min}^{-1}$ .

In the Carbothermic reduction of  $\text{Bi}_2\text{O}_3$ , where the carbon which accounts for 13.5 wt % of the sample was combusted starting around  $600\text{ }^\circ\text{C}$ . This conclusion was reached because TGA results from Figure 25 show 13 wt % of the sample had decomposed. It is possible that there was contamination of oxygen from impurities in the purge gas. Inspection of the sample after TGA analysis indicated carbon was not present in the sample. This was not experienced in other samples. Another reaction occurred during the heating of  $\text{Bi}_2\text{O}_3$  near  $800\text{ }^\circ\text{C}$  and is most likely due to melting of  $\text{Bi}_2\text{O}_3$ ; the melting temperature of  $\text{Bi}_2\text{O}_3$  is  $820\text{ }^\circ\text{C}$  [27].

#### 5.4.3. Direct Reduction of Residue

From the feasibility study it was clear that neither the MOV nor the leaching residue followed decomposition reactions relating to pure metal oxides. However, further analysis of the residue was done by investigating parameters such as the heating rate and carbon to residue ratio. The rate at which the sample is heated can affect the onset of the transition and peak temperatures of the reaction. This can be seen in Figure 26 where lower heating rates result in a lower onset of the first transition in the residue. This is because at higher heating rates there is lower heat conduction through the sample [87]. The residue heated at  $1\text{ }^\circ\text{C}\cdot\text{min}^{-1}$  shows three transitions in Figure 26, which are more clear when taking the derivative of the weight with respect to temperature of the heating curve. The first transition has a peak temperature of  $740\text{ }^\circ\text{C}$ , the second transition occurs near  $810\text{ }^\circ\text{C}$ , and the third transition has started but

not finished within the temperature range studied and therefore cannot be determined. It is also not known what happens during the transitions and further investigation is needed.

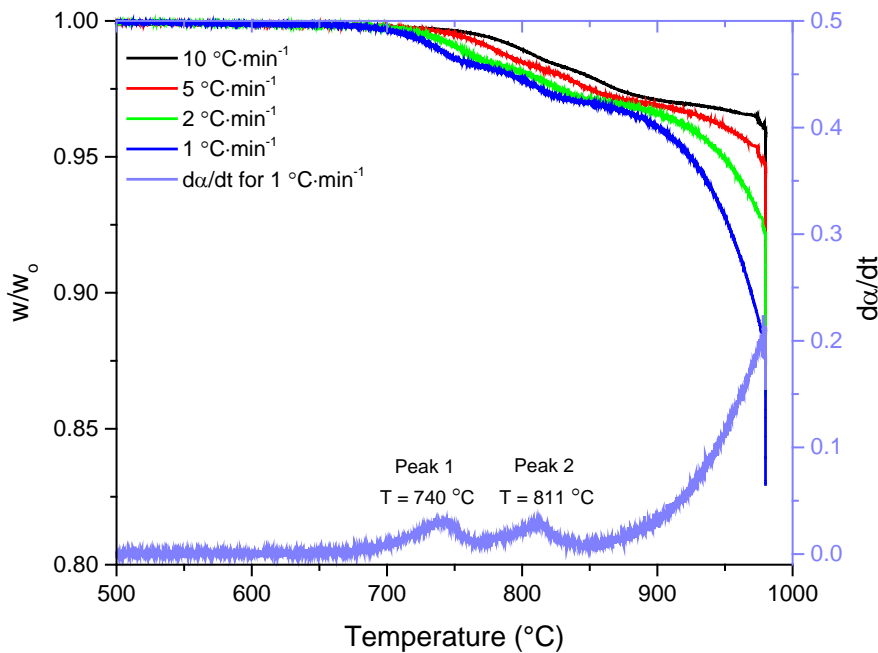


Figure 26: TGA heating curves for the effect of heating rate on direct reduction of the leaching residue.

Activation energy is the minimum energy required for a reaction to take place. From TGA thermolysis curves taken at multiple heating rates it is possible to determine the activation energy from the Arrhenius equation. Most generally the reaction rate is a function of temperature, reaction area and the activities of the reactants. For solid reactants the activity is unity. The Arrhenius equation can be used to show the effect of temperature on reaction rate.

From the curves in Figure 26 it should be possible to calculate the activation energy. But due to multiple reactions taking place as depicted by multiple inflection points on the thermolysis curves it is not yet known how this is done. For first order reactions the activation energy can be calculated as discussed in section 3.3.

#### 5.4.4. Carbothermal Reduction of Residue

Carbothermal reduction reactions were done using multiple carbon to residue ratios (by weight). The ratios were based on the weight of residue and weight of carbon not the molar ratio of carbon to oxygen. Several ratios were used as seen in Figure 27. Carbothermal reduction of the leaching residue from 500 °C to 700 °C resulted in mass loss of 6 wt % and a peak reaction temperature of 606 °C. The next transition occurred between 700 °C and 830 °C resulting in a weight loss of 13.2 wt % and had a peak temperature of 814 °C. The next reaction started near 830 °C and had a peak temperature of 901 °C and accounted for a weight loss of 17.6 wt %. It appears that more reactions are occurring at higher temperatures but due to instrument limitations those could not be investigated using the TGA.

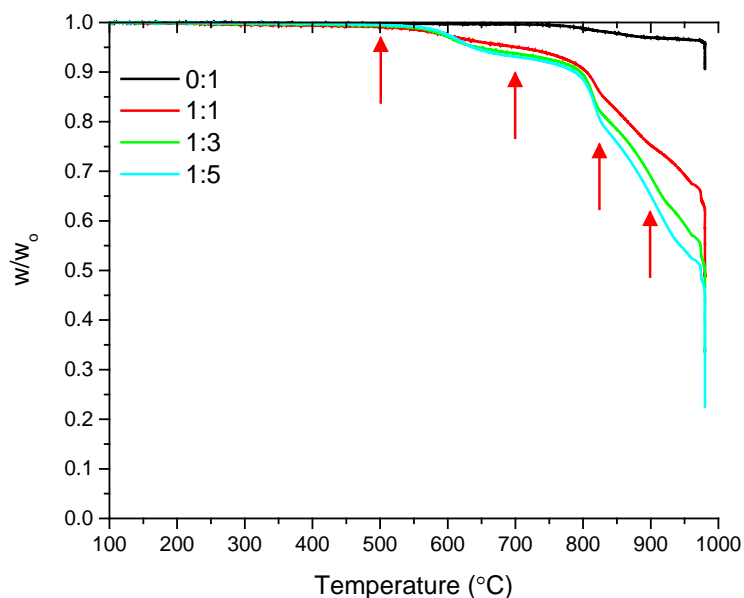


Figure 27: Effect of carbon to residue ratio on carbothermal reduction of leaching residue

Once the sample was heated to 980 °C it was held at that temperature for 30 minutes. This is indicated in Figure 27 as the vertical drop in weight at 980 °C. The lower carbon to residue ratio resulted in a greater weight loss. This is because more residue and thus more oxygen was available to react with the carbon.

Mass balance calculations were conducted to no avail due to the multiple phases present in the leachate. It is also not known how much of each phase is present making mass balance calculations difficult. In future experiments analyzing the evolved gas phase could help in identification of the reactions specific to each temperature. In future TGA experiments an experimental setup will be done allowing for calculation of the mass of carbon present in the sample allowing for calculations of amount of carbon involved in reactions. It was previously not known how to do this.

#### 5.4.5. Recovery of Antimony from Residue

It is known that the leaching residue contains  $Zn_7Sb_2O_{12}$  amongst other compounds. Therefore, to liberate antimony from the structure temperatures greater than 1350 °C are needed if done in air and temperatures greater than 1115 °C are needed in argon atmospheres. To verify work done by Filipek et al. experiments have been setup to be done in an argon atmosphere glove box equipped with a furnace capable of reaching temperatures of 1500 °C.

In total six samples were analyzed for direct reduction and carbothermal reduction. A summary of the samples analyzed is given in Table 12. The temperatures were chosen based on TGA results (Figure 27) and literature data. The red arrows in Figure 27 show the temperatures that were chosen and it is clear that some reaction resulting in weight loss has occurred near these points.

Table 12: Summary of residue samples for study on antimony recovery.

	Sample Name	Reduction Temp. (°C)	Sample weight prior to heating (g)	Sample weight after heating (g)	Weight loss (%)
Direct Reduction	DR-500	500	1.0066	0.9744	3.2
	DR-700	700	1.0022	0.9608	4.1
	DR-825	825	1.0078	0.9459	6.1
	DR-900	900	1.0060	0.8943	11.1
	DR-1100	1100	0.9997	0.4235	57.6
	DR-1300	1300	1.0129	0.1857	81.7
Carbothermal Reduction	CR-500	500	1.0097	0.9871	2.2
	CR-700	700	1.0086	0.9202	8.8
	CR-825	825	1.0028	0.8006	20.2
	CR-900	900	0.9969	0.6728	32.5
	CR-1000	1100	1.0063	0.2461	75.5
	CR-1100	1300	1.0044	ND	

ND = not determined.

The direct decomposition temperature of the residue and therefore the antimony recovery temperature was investigated. After heating the residue in an inert atmosphere, furnace samples were analyzed using XRD. Results for direct reduction of the MOV leaching residue are shown in Figure 28. Red circles are used to mark when a new peak has appeared (compared to the previous XRD at lower temperature), grey circles represent when a peak is absent when comparing results from the XRD spectrum of lower temperature, and green circles signify when there is a significant change in peak height. The spectrum for  $T = 22\text{ °C}$  is the same as Figure 23 where the compounds present are identified. It can be concluded from Figure 28:

- There is no change when the leaching residue is heated from room temperature ( $T = 22\text{ °C}$ , Figure 23) to  $500\text{ °C}$ .
- Heating from  $500\text{ °C}$  to  $700\text{ °C}$  causes a change in the crystal structure of  $\text{Bi}_2\text{O}_3$  and can be seen from the XRD spectra
- At temperatures over  $900\text{ °C}$   $\text{Bi}_2\text{O}_3$  no longer exists except for possibly as metallic bismuth
- At  $900\text{ °C}$  peaks can be confirmed for pyrochlore ( $\text{Zn}_2\text{Bi}_3\text{Sb}_3\text{O}_{14}$ ), spinel ( $\text{Zn}_{2.33}\text{Sb}_{0.67}\text{O}_4$  and  $\text{Zn}_7\text{Sb}_2\text{O}_{12}$ ), ZnO, and phases containing Zn-Co-Sb-O and Zn-Ni-Sb-O such as  $\text{ZnCo}_{0.133}\text{Sb}_{0.67}\text{O}_4$  and  $\text{Zn}_{1.33}\text{NiSb}_{0.67}\text{O}_4$
- At  $900\text{ °C}$  it is possible that bismuth metal and  $\text{Sb}_2\text{O}_3$  (valentinite) are present.
- At  $1100\text{ °C}$ , XRD peaks for ZnO are present meaning that antimony has been liberated from the spinel ( $\text{Zn}_{2.33}\text{Sb}_{0.67}\text{O}_4$  and  $\text{Zn}_7\text{Sb}_2\text{O}_{12}$ ) and pyrochlore phases.
- At  $1300\text{ °C}$  peaks for ZnO were seen along with some other peaks for CoO or Cobalt (II) Aluminate which was also indicated by the blue color of the residue and in the alumina crucible.

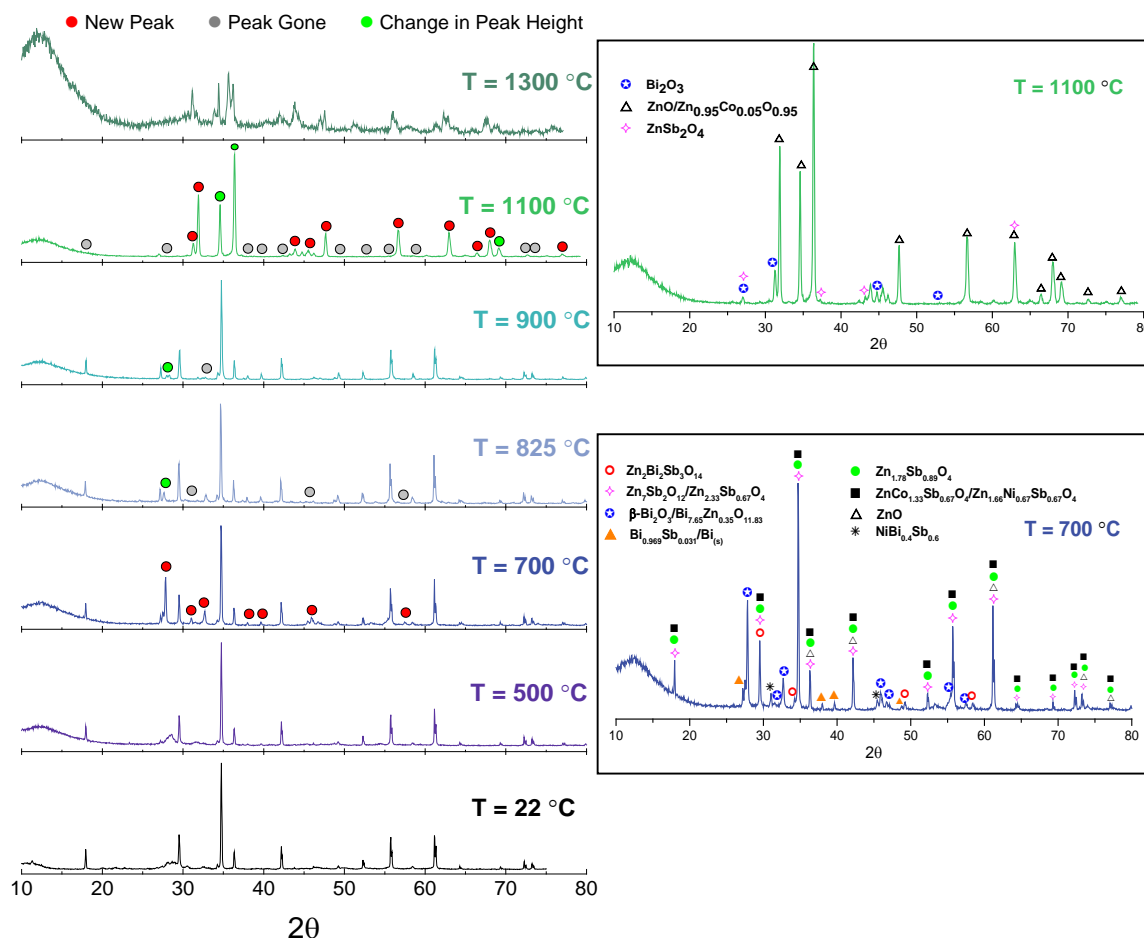


Figure 28: XRD spectra for direct reduction of MOV leaching residue in argon atmosphere at T = 22, 500, 700, 825, 900, 1100 and 1300 °C.

Results of direct reduction of the MOV leaching residue show that antimony containing compounds are present at 900 °C but not above 1100 °C. This differs from work reported by Filipek et al. [33] where temperatures greater than 1115 °C were needed to break down the  $Zn_7Sb_2O_{12}$  compound. The difference can be explained by Filipek et al. [33] prepared samples containing  $ZnO-Sb_2O_3-Bi_2O_3-CrO_3$ , while the material used in this study contained  $ZnO-Sb_2O_3-Bi_2O_3-MnCO_3-NiO-Co_2O_3$ . It can be concluded that antimony can be recovered from direct reduction of the MOV leaching residue between 900 – 1100 °C.

Following XRD analysis each sample was analyzed with SEM-EDX and the micrographs are shown in Figure 29 for each temperature studied. The material used in Figure 29 is the same as the samples analyzed by XRD in Figure 28. From the micrographs and EDX it can be said that at T = 500 °C no change has occurred to the leaching residue. The bismuth oxide phase as well as the antimony rich phases are present. Heating the sample to T = 700 °C causes a change in the bismuth phase. Now small spheres can be seen but the antimony rich phase appears unaffected and is confirmed from the XRD spectrum. Further heating to T = 825 °C melts the bismuth oxide phase; leaving the antimony rich phase. At T = 900 °C the antimony phase starts to decompose as can be seen in the micrograph from Figure 29d and is fully decomposed at T = 1100 °C. Decomposition of the antimony phase either reveals or causes formation of a nickel-antimony compound which can be seen in Figure 29e as small lighter in color particles less than 1 µm in diameter. EDX analysis of the remaining sample in Figure 29f shows what remains of the leachate residue after heating to T = 1300 °C and contained mainly cobalt and nickel but also EDX indicated chromium.

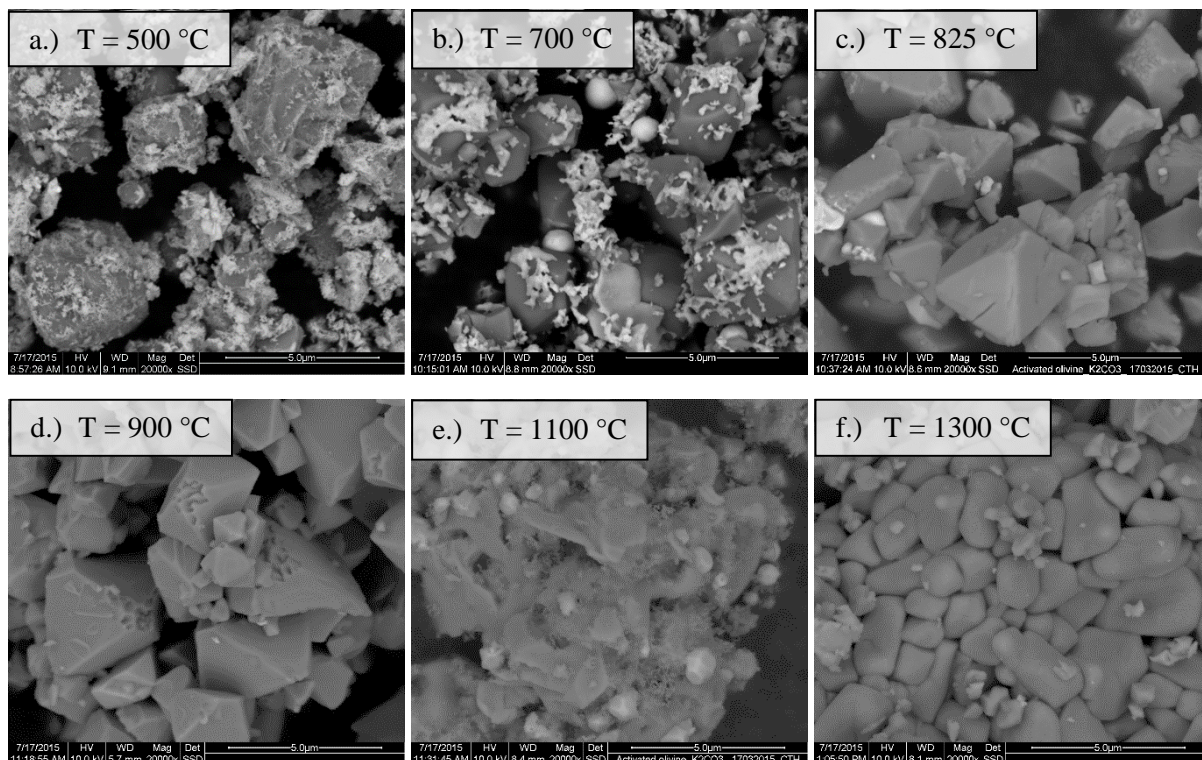


Figure 29: SEM micrographs of the leachate residue after heating to a.)  $T = 500\text{ }^{\circ}\text{C}$ , b.)  $T = 700\text{ }^{\circ}\text{C}$ , c.)  $T = 825\text{ }^{\circ}\text{C}$ , d.)  $T = 900\text{ }^{\circ}\text{C}$ , e.)  $T = 1100\text{ }^{\circ}\text{C}$ , and f.)  $T = 1300\text{ }^{\circ}\text{C}$  in an argon atmosphere.

It was also investigated if carbothermal reduction could lower the decomposition temperature of the phases present in the MOV leaching residue. After heating the residue and carbon at a 1:10 (carbon to residue) ratio by weight in an inert atmosphere furnace samples were analyzed using XRD. Results for direct reduction of the MOV leachate residue are shown in Figure 30. Red circles are used to mark when a new peak has appeared (compared to the previous XRD at lower temperature), grey peaks represent when a peak is absent when comparing results from the XRD spectrum of lower temperature, and green circles signify when there is a significant change in peak height. It can be concluded from Figure 30 that:

- There is no change when the leaching residue is heated from room temperature ( $T = 22\text{ }^{\circ}\text{C}$ ) to  $500\text{ }^{\circ}\text{C}$
- Heating from  $500\text{ }^{\circ}\text{C}$  to  $700\text{ }^{\circ}\text{C}$  forms a Bi-Sb alloy similar to  $\text{Bi}_{0.944}\text{Sb}_{0.056}$
- Heating from  $700\text{ }^{\circ}\text{C}$  to  $825\text{ }^{\circ}\text{C}$  causes changes in the residue leaving ZnO and a Bi-Sb alloy
- No change in the XRD spectra was seen when heating from  $825\text{ }^{\circ}\text{C}$  to  $900\text{ }^{\circ}\text{C}$
- At  $900\text{ }^{\circ}\text{C}$  the data suggests phases containing ZnO, Sb-Co alloy, Bi-Sb alloy, and possibly  $\text{Bi}_2\text{O}_3$  and  $\text{Bi}_3\text{Sb}_3\text{Zn}_2\text{O}_{14}$  in the sample.
- At temperatures over  $900\text{ }^{\circ}\text{C}$  the predominant phase is a Sb-Co alloy as well as the possibility of Ni-Sb alloy and bismuth metal. ZnO is not present in the sample. It is possible that some  $\text{Bi}_3\text{Sb}_3\text{Zn}_2\text{O}_{14}$  remains in the sample.

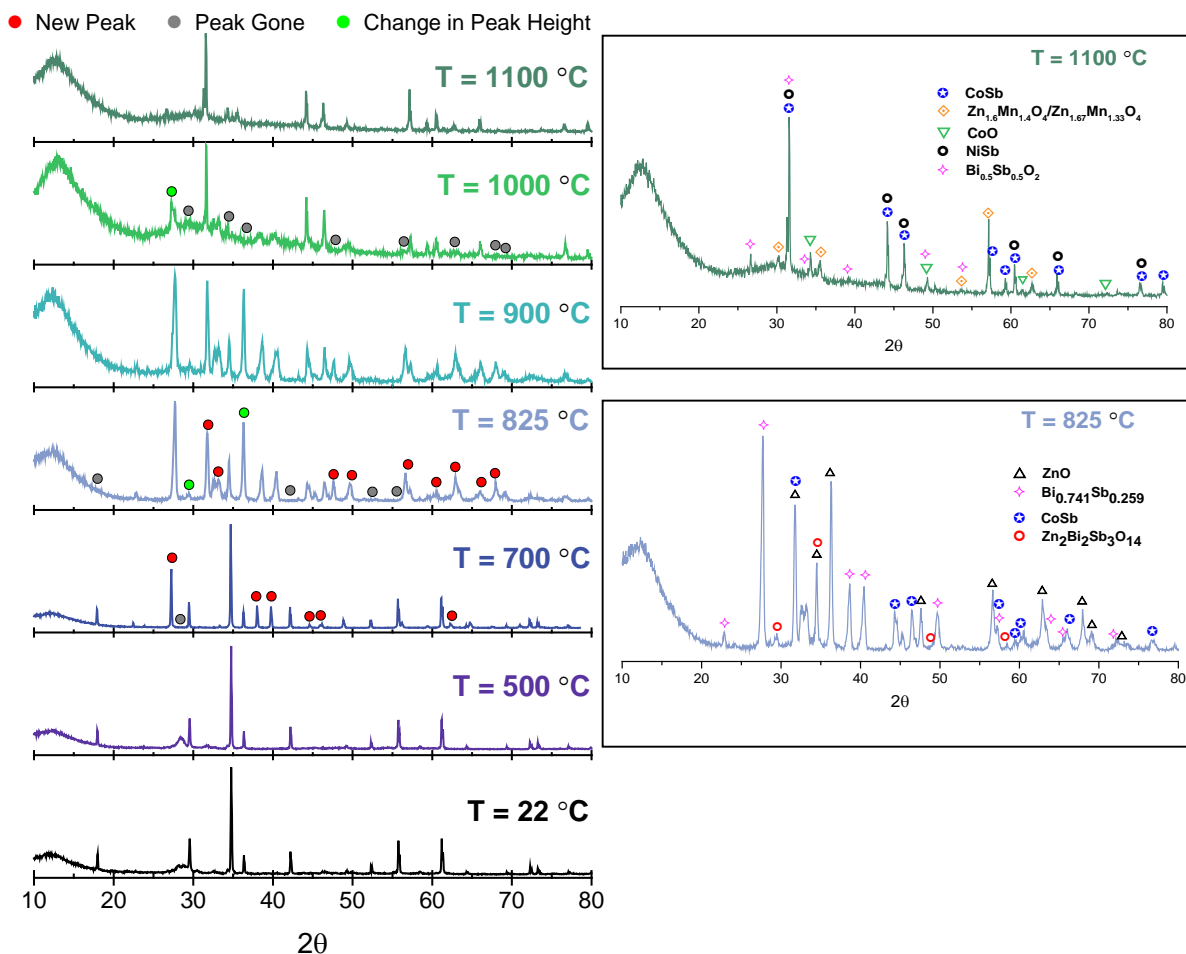


Figure 30: XRD spectra for carbothermal reduction of MOV leaching residue in argon atmosphere at  $T = 22, 500, 700, 825, 900, 1000$  and  $1100\text{ }^{\circ}\text{C}$ .

XRD Results of carbothermal reduction of the MOV leaching residue show that antimony containing compounds are present above  $1100\text{ }^{\circ}\text{C}$ . Following XRD analysis each sample was analyzed with SEM-EDX and the micrographs are shown in Figure 31 for each temperature studied. The material used in Figure 31 is the same as the samples analyzed by XRD in Figure 30. From the micrographs and XRD it can be said that at  $T = 500\text{ }^{\circ}\text{C}$  no change has occurred to the leaching residue. The bismuth oxide phase and the antimony rich phases are present. Heating the sample to  $T = 700\text{ }^{\circ}\text{C}$  causes a change in the bismuth phase most likely melting as seen by bismuth sphere in Figure 31b. The antimony rich phase appears unaffected but as seen from the XRD spectrum there are peaks suggesting a Bi-Sb alloy has formed and EDX also confirmed this.

Further heating to  $T = 825\text{ }^{\circ}\text{C}$  caused thermal degradation or breakdown of the antimony rich phases yielding ZnO and small particles of Sb-Co-Ni in a zinc oxide matrix according to EXD results. No change was noticed from  $825\text{ }^{\circ}\text{C}$  to  $900\text{ }^{\circ}\text{C}$  as also seen by XRD spectrum. At temperatures greater than  $1000\text{ }^{\circ}\text{C}$ , large circular “blobs” are seen composed of Sb-Ni-Co as seen in Figure 31e and Figure 31f. ZnO is now gone from the sample. Carbothermal reduction data suggest that it may not be possible to recover the antimony from the MOV leaching residue as it is alloyed with nickel and cobalt and further purification would be needed.

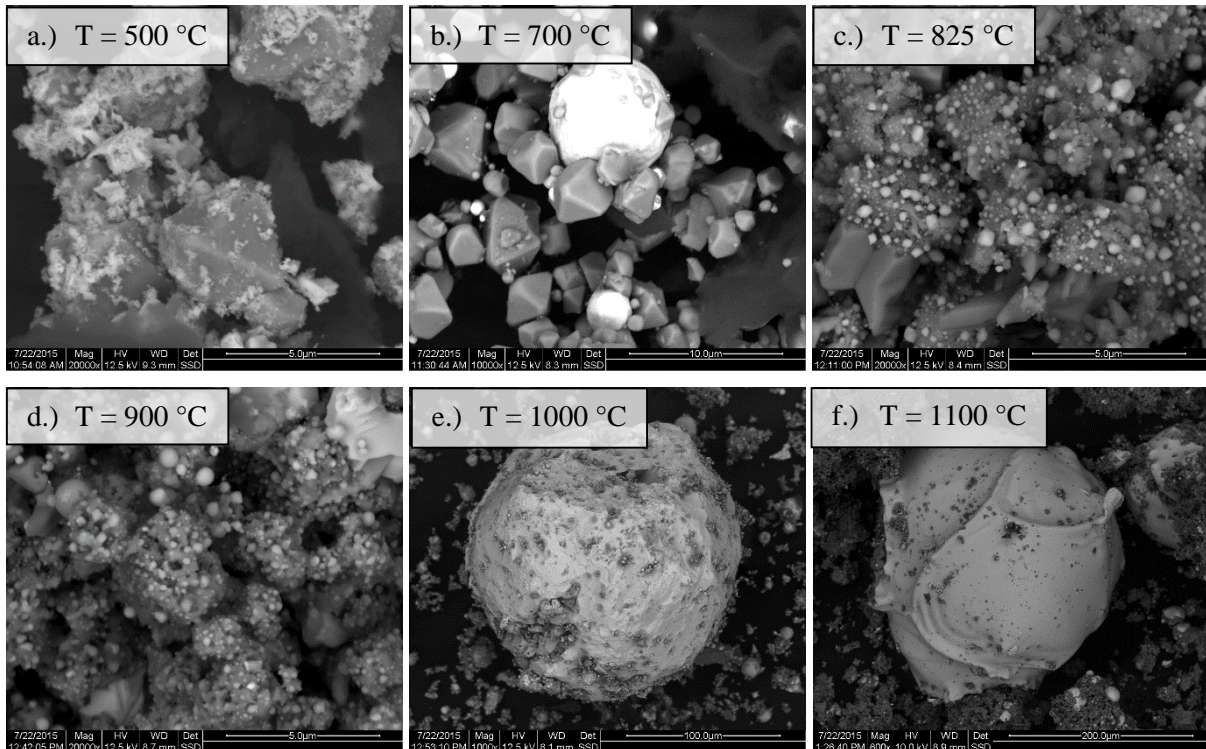


Figure 31: SEM micrographs of the leachate residue and carbon after heating to a.) T = 500 °C, b.) T = 700 °C, c.) T = 825 °C, d.) T = 900 °C, e.) T = 1000 °C, and f.) T = 1100 °C in an argon atmosphere.

### 5.5. Antimony Oxide Chemistry – Activation Energy Determination

In literature there exists a plethora of data about  $\text{Sb}_2\text{O}_3$ , however, some report different melting temperatures. This portion of work is not related to the MOV directly but rather to expand on antimony chemistry and determine such things as decomposition of  $\text{Sb}_2\text{O}_3$  along with the activation energy needed for the decomposition reaction to take place. The method for determining activation energy could be applied to the reaction occurring within the MOV.

The as purchased  $\text{Sb}_2\text{O}_3$  is most likely a mixture of senarmonite ( $\alpha\text{-Sb}_2\text{O}_3$ ) and valentinite ( $\beta\text{-Sb}_2\text{O}_3$ ) as confirmed by the XRD spectrum shown in Figure 32. The spectrum confirms the presence of  $\alpha\text{-Sb}_2\text{O}_3$  but does not eliminate the possibility of  $\beta\text{-Sb}_2\text{O}_3$ . This is not unusual as commercial samples typically contain both allotropes [88]. The peak melting temperature of the  $\text{Sb}_2\text{O}_3$  was 644 °C at a heating rate of 20 °C·min<sup>-1</sup>. This is in close agreement to previous work by Golunski et al. [88] with a reported melting temperature for  $\beta\text{-Sb}_2\text{O}_3$  of 643 ± 2 °C and Jones et al. [89] reported a melting temperature of 640 to 655 °C depending on the heating rate. This work differs from reported melting temperature of  $\text{Sb}_2\text{O}_3$  of 655 °C by Trofimov et al. [90] and Centers et al. [91] both of which used  $\beta\text{-Sb}_2\text{O}_3$ .

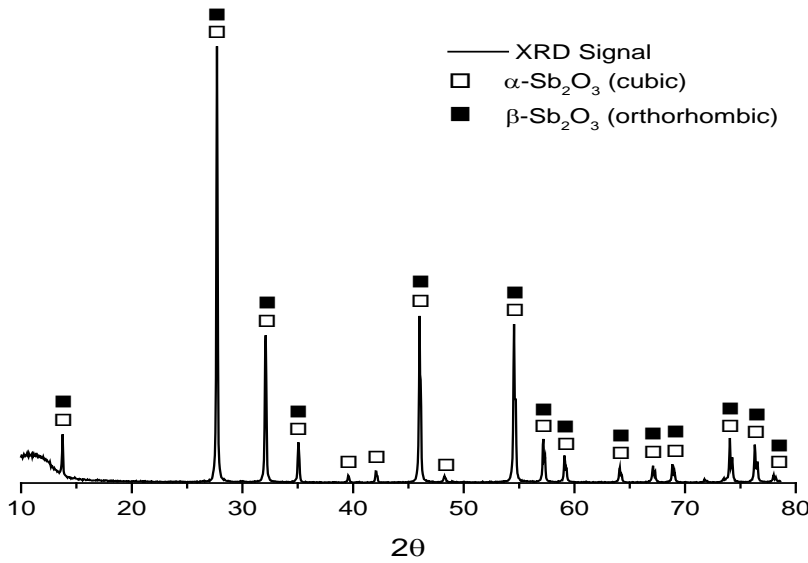


Figure 32: XRD spectrum of as purchased  $\text{Sb}_2\text{O}_3$  confirming the presence of valentinite ( $\beta\text{-Sb}_2\text{O}_3$ ) having an orthorhombic crystal structure. This does not disprove the presence of sermontite ( $\alpha\text{-Sb}_2\text{O}_3$ ), which has a cubic crystal structure.

The assumption was made that the decomposition of  $\text{Sb}_2\text{O}_3$  follows first order reaction kinetics, where the reaction depends on a single reactant,  $\text{Sb}_2\text{O}_3$ . The data in Figure 33 represents the amount of antimony oxide sublimed as a function of temperature. The heating rates ( $\beta$ ) used are 20, 15, 10, 5 and 1  $^\circ\text{C}\cdot\text{min}^{-1}$ . The temperature range in which  $\text{Sb}_2\text{O}_3$  sublimes is 673 to 923 K. For lower heating rates the amount of  $\text{Sb}_2\text{O}_3$  subliming at a specific temperature is greater than at higher heating rates. This is because the time interval the sample is exposed to the temperature decreases with increased heating rate. The thermolysis curve for a heating rate of  $\beta = 20 \text{ K}\cdot\text{min}^{-1}$  is in good agreement with work by Cody et al. [92] claiming the onset temperature of sublimation occurs near 775 K.

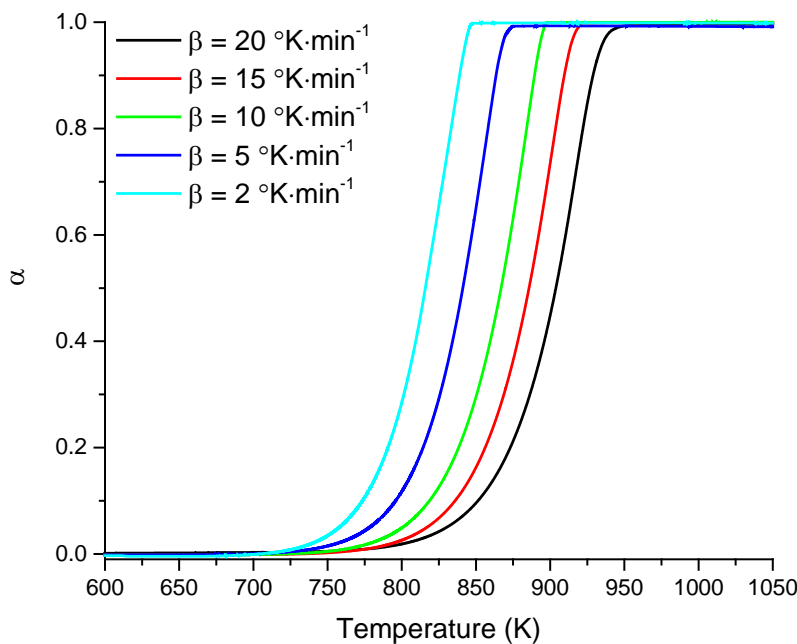


Figure 33: Effect of heating rate on direct thermal decomposition of  $\text{Sb}_2\text{O}_3$  in nitrogen atmosphere.

During thermal decomposition it was observed that  $\text{Sb}_2\text{O}_3$  was volatilized in one step directly from  $\text{Sb}_2\text{O}_3(\text{s})$  to  $\text{Sb}_2\text{O}_3(\text{g})$  this is seen from Figure 33 as there is only smooth continuous curves for each heating rate. This is also reported by Orman et. Al [93] for  $\alpha\text{-Sb}_2\text{O}_3$ . The  $\text{Sb}_2\text{O}_3$  was analyzed using multiple heating rates as shown in Figure 33 and the Arrhenius plot of heating is given in Figure 34. The average Arrhenius activation energy and pre-exponential factor for  $\alpha = 0.05$  was calculated to be:  $E_A = 160.4 \text{ kJ}\cdot\text{mol}^{-1}$  ( $38.7 \text{ kcal}\cdot\text{mol}^{-1}$ ) and  $A = 10^{7.4} \text{ s}^{-1}$ .

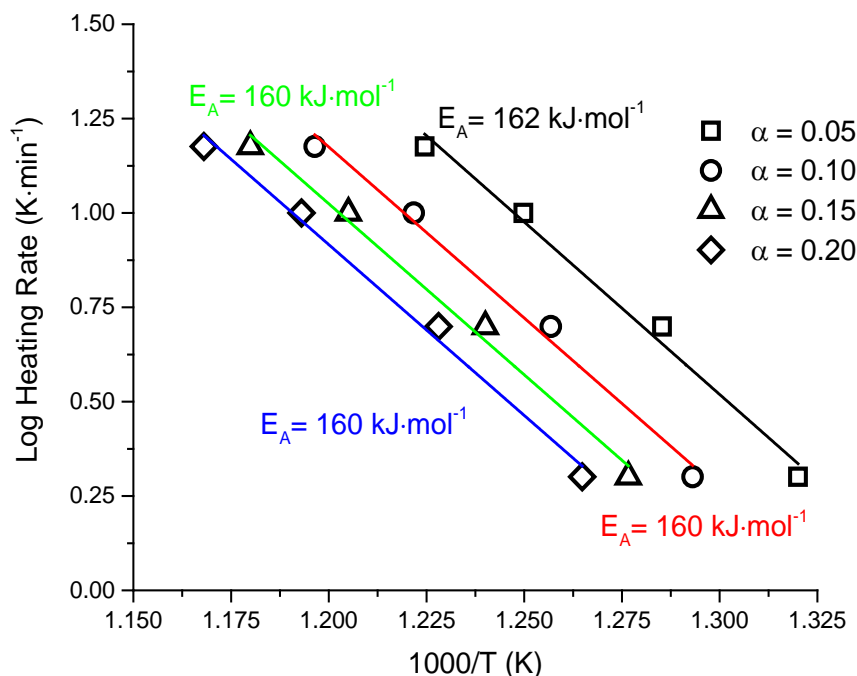


Figure 34: Arrhenius plot of the log of heating rate vs. temperature for sublimation of  $\text{Sb}_2\text{O}_3$  with conversion ratios of  $\alpha = 0.05, 0.10, 0.15,$  and  $0.20$  showing the Arrhenius activation energy for each conversion ratio.

It was reported by Agrawal et al. [94] that  $\text{Sb}_2\text{O}_3$  when heated in Ar or  $\text{N}_2$  does not undergo any transitions until 703 K (430 °C) at which point there is a slow but continuous mass loss until approximately 823 K (550 °C) at which point an enormous mass loss occurs. This is due to volatilization of  $\text{Sb}_2\text{O}_3$ . TGA curves for this work are in good agreement with Agrawal et al. [94] as seen in Figure 35 showing the rate of mass loss as a function of temperature.

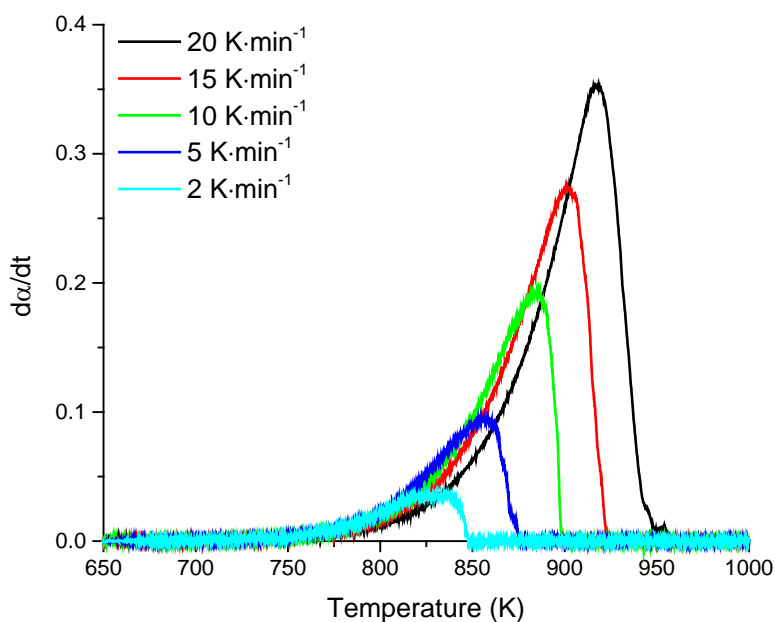


Figure 35: First derivative of thermolysis curves (Figure 33) as a function of temperature.

Agrawal et al. [94] analyzed the  $\text{Sb}_2\text{O}_3$  before heating and also after collecting and condensing the volatilized  $\text{Sb}_2\text{O}_3$ . They found that the residue was mostly senarmontite, the cubic crystal structure of  $\text{Sb}_2\text{O}_3$  while the collected, condensed residue is valentinite, the orthorhombic form of  $\text{Sb}_2\text{O}_3$ .

Senarmontite directly sublimates at a temperature of 775 K [92, 95] while valentinite is stable to 903 K where sublimation and oxidation  $\text{Sb}_2\text{O}_4$  are competing reactions. It is not known what the rate controlling step is in the oxidation of valentinite but it has been speculated by Centers [91] to be sublimation controlled by senarmontite subliming to low-energy valentinite nucleation site before oxidizing. This work is in reasonable agreement with work by Centers [91] where the calculation of  $E_A$  gave values between 180 – 196  $\text{kJ}\cdot\text{mol}^{-1}$  confirming that oxidation of  $\text{Sb}_2\text{O}_3$  is controlled by sublimation of  $\text{Sb}_2\text{O}_3$ . This work obtained slightly lower values (160.4  $\text{kJ}\cdot\text{mol}^{-1}$ ) for  $E_A$ . Lower values could be due to differences in calculation techniques and in particle size of the antimony sample.

## 6. SUMMARY & CONCLUSIONS

The overall goal of this work was to recover antimony, a critical and strategic metal, from the MOV. Because of the low concentration of antimony in the MOV a leaching pretreatment step needed to be done before it was feasible to recover antimony. Investigations into leachate purification were also done so the leachate could be easily incorporated into a zinc electrolyte for industrial production of zinc. The antimony remained in the leaching residue and was heat treated to volatilize the antimony from the pyrochlore and spinel phases. This was done by direct and carbothermal reduction.

### 6.1. Leaching

This work set out to determine whether it is possible to separate metal components of the MOV via pH selective leaching in acetic, nitric, hydrochloric and sulfuric acidic solutions having pH 1, 3 and 5. Initially the composition of the MOV was determined in order to quantify the metal and metal oxides within the MOV. The MOV contains simple oxides such as zinc oxide but it also contains more complex oxides such as  $Zn_7Sb_2O_{12}$  as shown using the SEM and XRD.

Experimental data showed that lower pH acid solutions gave higher percent of zinc leaching except for the case where  $H_2SO_4$  was used and zinc was shown to be fully leached at pH 5 and below. It was possible to selectively leach zinc from the MOV without significant co-leaching of bismuth and antimony by selecting a suitable pH, mainly higher than 3 in all acids investigated here. It was not possible to leach zinc without co-leaching of manganese, cobalt and nickel. Even though these metals are present in small amounts in the leachates production of pure zinc metal will require their removal. Sulfuric acid leaching is also preferred because nearly 80% of zinc is produced by electrowinning in sulfate solutions.

This investigation concludes that either acetic, nitric, hydrochloric or sulfuric acid solutions at pH 3 can be used to selectively leach zinc from the MOV without significant co-leaching of antimony or bismuth. However, the efficiency of zinc leached decreases with increasing leaching pH except in the case of sulfate solution. No matter the pH in sulfate leaching 100% of the zinc in the MOV was leached making this the ideal selective leaching solution for leaching zinc from MOV. Selective zinc leaching with respect to minor metals such as cobalt, nickel and manganese could not be successfully done with the acids and pH range under investigation in this study.

### 6.2. Cementation

Cementation of cobalt and nickel from the zinc electrolyte can be done using cementation as demonstrated in this work. Running an optimized cementation experiment removed over 50 % (>200 ppm) of the cobalt and over 90 % (> 80 ppm) of the nickel from the leachate. A study on the effect of batch addition of zinc will also be done to see if these numbers can be improved. It was seen that adjusting the pH of the cementation had the largest influence on the amount of material cemented from solution with pH 5.5 being the most effective while temperature had the largest effect on the rate at which the metals were cemented from solution. Other parameters influencing cementation include additive concentration (Sb/Cu) and zinc dust addition. Also, experiments will be produced in triplicate to account for uncertainty.

### 6.3. Antimony Recovery

It is possible to recover antimony from the MOV leaching residue by direct reduction at temperatures between 900 to 1100 °C. Addition of carbon in a 1:10 ratio of carbon to residue results in a metallic alloy of antimony-cobalt-nickel making the recovery of antimony unfeasible as removal of cobalt and nickel would be needed to obtain a pure antimony product. With respect to direct recovery of antimony

no work has been done with regards to reaction kinetics but this is important and would be a valuable extension of this work. Based on data from the feasibility it is clear there are many parameters which could be optimized to lower the temperature at which antimony can be recovered such as gas flow rate, reaction gas, particle size, carbon to residue ratio, etc. From collected data it is possible to calculate the activation energy related to the recovery of antimony however, further data analysis and experimental work is needed.

The results of this work indicate that zinc leaching in a slightly acidic sulfuric acid solution yield a leachate with high concentrations of zinc along with minor impurities of cobalt, manganese, and nickel. The impurities can be over 50 % removed via cementation with experiments/research suggesting further purification is possible. The recovery of antimony has proven difficult and further investigation is required.

## 7. FUTURE WORK

There are many areas of interesting studies to be continued with respect to this work. A more fundamental understanding of chemical processes and reaction mechanisms associated with antimony recovery would be interesting for this work and also the electronics industry. To determine the exact phases formed and the actual composition and structure including bond lengths of the MOV using EXAFS. This work uses characterization techniques such as SEM-EDX, XRD, and ICP-OES of the MOV material. Since it has been shown in this work that it is possible to isolate the Sb-rich phases it would be interesting to examine them further in order to gain a more fundamental understanding of the structures.

With respect to leaching an investigation into the leaching kinetics is needed. Some parameters would need to be modified and perhaps alkaline leaching would result in a selective leaching of antimony directly from the MOV. Experiments to determine if leaching of the MOV was a chemically controlled process or a diffusion controlled process are of importance and need to be developed. Also, it would be useful to use Factsage® or HSC® software to develop  $E_h$ -pH diagrams specific to the MOV system and get more into the thermodynamics of the aqueous system. Determination of the activation energy of leaching system is also interesting because the rate of the reaction can be determined at a given temperature.

It was not possible to completely remove all cobalt from the leachate but over 50 % (220 ppm) can be removed from solution under optimal conditions at room temperature. Increasing the temperature above ~40 °C has proven hard with the experimental setup used. A new reaction vessel needs to contain a condensing column. One thing that should be investigated more is the mechanism by which cementation occurs. It would be relevant to this work but also to industrial zinc production and not much work has been done in this area therefore the reactions are not known. There are other means of purification such as solvent extraction but it is very difficult to find an extractant that would remove the cobalt from the leachate rather than the zinc. Another problem if zinc is extracted then a stripping step could be needed to remove the zinc from the organic phase.

High temperature separation of antimony from the MOV seems to be promising but requires temperatures between 900 and 1100 °C for direct and carbothermal reduction. It would be interesting to investigate what parameters can be changed to lower the antimony recovery temperature. This could include things such as changing the environment by purging with a reducing gas. It would be very interesting to determine and investigate the reaction mechanism for the liberation of antimony or antimony species from the pyrochlore and spinel structures. This would be useful in both the recycling of old and production of new MOV.

In general the reaction mechanisms of antimony in this system are not well-known and often conflicting data exists. It would also be scientifically interesting to investigate more chemical reactions of antimony, antimony oxides and mixed metal antimony oxides found in this and other industrial systems.

## 8. REFERENCES

1. Brundtland, G., et al., *Our Common Future ('Brundtland report')*. 1987: Oxford University Press, USA.
2. Sekula, R., M. Wnek, and S. Slupek, *Potential Utilization Method of Scrap Ceramic Insulators*. Journal of Solid Waste Technology and Management, 1999. **26**(2): p. 6.
3. Sekula, R., et al., *For a better environment: recycling opportunities for insulating components in ABB Review*, P. Terwiesch, et al., Editors. 2009, ABB Asea Brown Boveri Ltd: Zurich Switzerland.
4. Ankara, S.B. *POLiPAR The Power of Future*. HP Series Medium Voltage Polymer Surge Arrester (HP serisi polimer parafudr) 2010 [cited 2013 July 25 2013]; HP Series Medium Voltage Polymeric Housed Surge Arresters]. Available from: [http://www.polipar.com.tr/urun\\_detay.aspx?urun\\_id=17](http://www.polipar.com.tr/urun_detay.aspx?urun_id=17).
5. Ashraf, M.A., et al., *Microstructure and electrical properties of Ho<sub>2</sub>O<sub>3</sub> doped Bi<sub>2</sub>O<sub>3</sub>-based ZnO varistor ceramics*. Physica B: Condensed Matter, 2010. **405**(17): p. 3770-3774.
6. ABB, *High Voltage Surge Arresters, Buyer's Guide, ABB High Voltage Products Surge Arrestors*. 2014: Ludvika, Sweden.
7. Huang, Y., et al., *The effect of secondary phases on electrical properties of ZnO-based ceramic films prepared by a sol-gel method*. Journal of Materials Science: Materials in Electronics, 2004. **15**(8): p. 549-553.
8. Arefin, M.L., et al., *Phase formation during liquid phase sintering of ZnO ceramics*. Ceramics International, 2009. **35**(8): p. 3313-3320.
9. Bernik, S., S. Maček, and A. Bui, *The characteristics of ZnO–Bi<sub>2</sub>O<sub>3</sub>-based varistor ceramics doped with Y<sub>2</sub>O<sub>3</sub> and varying amounts of Sb<sub>2</sub>O<sub>3</sub>*. Journal of the European Ceramic Society, 2004. **24**(6): p. 1195-1198.
10. Forsberg, P., *Development Engineer, ABB Ludvika*, T. Gutknecht, Editor. 2014.
11. AB, A.P.T.P., *Physical properties of zinc oxide varistors*, A.P.T.P.A.-H.V. Products, Editor.
12. Al-Tounsi, A., R. Puyané, and M.S.J. Hashmi, *Rate-controlled shrinkage of ZnO varistors*. Journal of Materials Processing Technology, 1996. **56**(1–4): p. 891-896.
13. Levinson, L.M., Philipp, H.R., *Zinc Oxide Varistors - A Review*. Ceramic Bulletin, 1986. **65**(4): p. 639-646.
14. Leite, E.R., et al., *Microstructural development of ZnO varistor during reactive liquid phase sintering*. Journal of Materials Science, 1996. **31**(20): p. 5391-5398.
15. Kim, J., T. Kimura, and T. Yamaguchi, *Sintering of Zinc Oxide Doped with Antimony Oxide and Bismuth Oxide*. Journal of the American Ceramic Society, 1989. **72**(8): p. 1390-1395.
16. Inada, M., *Formation Mechanism of Nonohmic Zinc Oxide Ceramics*. Japanese Journal of Applied Physics, 1980. **19**(3): p. 409.
17. Kumari, K.G.V., et al., *Formation of Zinc–Antimony-Based Spinel Phases*. Journal of the American Ceramic Society, 2002. **85**(3): p. 703-705.
18. Kim, J.C. and E. Goo, *Morphology and Formation Mechanism of the Pyrochlore Phase in ZnO Varistor Materials*. Journal of Materials Science, 1989. **24**(1): p. 76-82.
19. Huang, Y.Q., et al., *Preparation and properties of ZnO-based ceramic films for low-voltage varistors by novel sol-gel process*. Materials Science and Engineering: B, 2001. **86**(3): p. 232-236.
20. Hultgren, H., *Varistor Material Information*, T. Gutknecht, Editor. 2014: Microsoft Outlook. p. 1.
21. *Critical Raw Materials for the EU - Report of the Ad-hoc Working Group on defining critical raw materials*. 2010; Available from: [http://ec.europa.eu/enterprise/policies/rawmaterials/documents/index\\_en.htm](http://ec.europa.eu/enterprise/policies/rawmaterials/documents/index_en.htm).
22. *Reconfiguration of the National Defense Stockpile Report to Congress*. 2009, [http://www.acq.osd.mil/mibp/docs/nds\\_reconfiguration\\_report\\_to\\_congress.pdf](http://www.acq.osd.mil/mibp/docs/nds_reconfiguration_report_to_congress.pdf). p. 10.
23. Kirk-Othmer, *Kirk-Othmer Encyclopedia of Chemical Technology*. 1992, John Wiley & Sons: New York. p. 367-407.

24. Habashi, F., *Handbook of Extractive Metallurgy* Primary metals, secondary metals, light metals, ed. F. Habashi. Vol. 2. 1997, Weinheim, Federal Republic of Germany: VCH Verlagsgesellschaft. 641-681.
25. Guberman, D.E., *U.S. Geological Survey, Mineral Commodity Summaries*, in *Antimony*. 2014. p. 196.
26. Anderson, C.G., *The metallurgy of antimony*. *Chemie der Erde - Geochemistry*, 2012. **72**, **Supplement 4(0)**: p. 3-8.
27. Norman, N.C., *Chemistry of Arsenic, Antimony and Bismuth*. 1998: Springer.
28. *International Antimony Association VZW*, in *Safe use of antimony catalysts in PET*. (2014) <http://www.antimony.com/en/publications.aspx>.
29. Commission, E., *Annex V to the Report of the Ad-hoc Working Group on defining critical raw materials*. 2010.
30. Graedel, T.E. and B.K. Reck, *Chapter 3 - Recycling in Context*, in *Handbook of Recycling*, E. Worrell and M.A. Reuter, Editors. 2014, Elsevier: Boston. p. 17-26.
31. Rombach, E. and B. Friedrich, *Chapter 10 - Recycling of Rare Metals*, in *Handbook of Recycling*, E. Worrell and M.A. Reuter, Editors. 2014, Elsevier: Boston. p. 125-150.
32. van Velzen, D., H. Langenkamp, and G. Herb, *Antimony, its sources, applications and flow paths into urban and industrial waste: a review*. *Waste Management & Research*, 1998. **16(1)**: p. 32-40.
33. Filipek, E. and G. Dąbrowska, *Phase relations up to the solidus line in the part of the Sb-Zn-O system*. *Central European Journal of Chemistry*, 2009. **7(2)**: p. 192-196.
34. Filipek, E. and G. Dąbrowska, *Unknown thermal properties of ZnSb<sub>2</sub>O<sub>6</sub> and Zn<sub>7</sub>Sb<sub>2</sub>O<sub>12</sub> compounds*. *Journal of Thermal Analysis and Calorimetry*, 2008. **94(1)**: p. 195-201.
35. Rosenqvist, T., *Reduction of Metal Oxides* in *Principles of extractive metallurgy*, B.J. Clark, Editor. 1974, McGraw-Hill: New York. p. 264-298.
36. Gordon, R.B., et al., *The characterization of technological zinc cycles*. *Resources, Conservation and Recycling*, 2003. **39(2)**: p. 107-135.
37. Jha, M.K., V. Kumar, and R.J. Singh, *Review of hydrometallurgical recovery of zinc from industrial wastes*. *Resources, Conservation and Recycling*, 2001. **33(1)**: p. 1-22.
38. Rosenqvist, T., *Volatile Metals* in *Principles of extractive metallurgy*, B.J. Clark, Editor. 1974, McGraw-Hill: New York. p. 299-321.
39. Wilkinson, S., *Zinc Environmental Profile - Life Cycle Assessment*. International Zinc Association
40. Bard, A. and M. Stratmann, *Encyclopedia of Electrochemistry*, in *Electrochemical Engineering*, D. MacDonald and P. Schmuki, Editors. 2007, WILEY-VCH Verlag GmbH & Co. KGaA: Federal Republic of Germany.
41. Nelson, A., et al., *The Removal of Cobalt from Zinc Electrolyte by Cementation: A Critical Review*. *Mineral Processing and Extractive Metallurgy Review*, 2000. **20(4-6)**: p. 325-356.
42. Fröhlich, S. and D. Sewing, *The BATENUS process for recycling mixed battery waste*. *Journal of Power Sources*, 1995. **57(1-2)**: p. 27-30.
43. Shamsuddin, M., *Metal Recovery from Scrap and Waste*. *JOM*, 1986. **38(2)**: p. 24-31.
44. Sato, T., et al., *The extraction of divalent manganese, iron, cobalt, nickel, copper and zinc from hydrochloric acid solutions by di-(2-ethylhexyl) phosphoric acid*. *Journal of Applied Chemistry and Biotechnology*. **28(2)**: p. 85-94.
45. Cattrall, R., *The Extraction of Beryllium and Aluminium from Aqueous Sulphate Solutions with Di-(2-ethylhexyl) Phosphoric Acid*. *Australian Journal of Chemistry*, 1961. **14(1)**: p. 163-165.
46. Pierce, T.B. and P.F. Peck, *The extraction of the lanthanide elements from perchloric acid by di-(2-ethylhexyl) hydrogen phosphate*. *The Analyst*, 1963. **88(1044)**: p. 217-221.
47. Zhang, P., et al., *Recovery of metal values from spent nickel-metal hydride rechargeable batteries*. *Journal of Power Sources*, 1999. **77(2)**: p. 116-122.
48. Havlik, T., et al., *Atmospheric leaching of EAF dust with diluted sulphuric acid*. *Hydrometallurgy*, 2005. **77(1-2)**: p. 41-50.
49. Cruells, M., A. Roca, and C. Núnñez, *Electric arc furnace flue dusts: characterization and leaching with sulphuric acid*. *Hydrometallurgy*, 1992. **31(3)**: p. 213-231.

50. Frenay, J., S. Ferlay, and J. Hissel, *Zinc and lead recovery from EAF dusts by caustic soda process* *Electric Furnace Proceedings, Treatment Options for Carbon Steel Electric Arc Furnace Dust*. Iron Steel Society, 1986. **43**: p. 417-421.
51. Palencia, I., et al., *Recycling EAF dust leaching residue to the furnace: A simulation study*. JOM, 1999. **51**(8): p. 28-32.
52. Boyanov, B.S., V.V. Konareva, and N.K. Kolev, *Purification of zinc sulfate solutions from cobalt and nickel through activated cementation*. Hydrometallurgy, 2004. **73**(1–2): p. 163-168.
53. Jun, D., De-quan, Wang, Lan, Jiang, Man, Jin, *Removal of cobalt from zinc sulphate solution using rude antimony trioxide as additive*. Trans. Nonferrous Met. Soc. , 2002. **12**(6): p. 1172-1175.
54. BØrve, K. and T. Østvold, *Norzink removal of cobalt from zinc sulphate electrolytes*, in *Hydrometallurgy '94*. 1994, Springer Netherlands. p. 563-577.
55. Tozawa, K., et al., *Comparison between purification processes for zinc leach solutions with arsenic and antimony trioxides*. Hydrometallurgy, 1992. **30**(1–3): p. 445-461.
56. Bratsch, S.G., *Standard Electrode Potentials and Temperature Coefficients in Water at 298.15 K*. Journal of Physical and Chemical Reference Data, 1989. **18**(1): p. 1-21.
57. Younesi, S.R., et al., *Kinetic mechanisms of cementation of cadmium ions by zinc powder from sulphate solutions*. Hydrometallurgy, 2006. **84**(3–4): p. 155-164.
58. Yang, D., et al., *Mechanism of cobalt removal from zinc sulfate solutions in the presence of cadmium*. Hydrometallurgy, 2006. **81**(1): p. 62-66.
59. van der Pas, V. and D.B. Dreisinger, *A fundamental study of cobalt cementation by zinc dust in the presence of copper and antimony additives*. Hydrometallurgy, 1996. **43**(1–3): p. 187-205.
60. Singh, V., *Technological innovation in the zinc electrolyte purification process of a hydrometallurgical zinc plant through reduction in zinc dust consumption*. Hydrometallurgy, 1996. **40**(1–2): p. 247-262.
61. Zaghoul, A.A., El-Subruiti, G. M., and Ahmed, A.M. , *Kinetic Study of Cementation of Copper on Zinc Metal in Ethanol-Water Mixtures*. J. Mater. Sci. Technol., 1996. **12**: p. 41-45.
62. Dreher, T.M., et al., *The kinetics of cobalt removal by cementation from an industrial zinc electrolyte in the presence of Cu, Cd, Pb, Sb and Sn additives*. Hydrometallurgy, 2001. **60**(2): p. 105-116.
63. Truesdale, E.C. and R.K. Waring, *Reduction Equilibria of Zinc Oxide and Carbon Monoxide I*. Journal of the American Chemical Society, 1941. **63**(6): p. 1610-1621.
64. Atkins, P. and L. Jones, *Chemical Principles The Quest for Insight*. 5 ed. 2009, New York, NY: W. H. Freeman; 5th edition 1024.
65. Flynn, J.H. and L.A. Wall, *A quick, direct method for the determination of activation energy from thermogravimetric data*. Journal of Polymer Science Part B: Polymer Letters, 1966. **4**(5): p. 323-328.
66. Flynn, J., *The isoconversional method for determination of energy of activation at constant heating rates*. Journal of Thermal Analysis and Calorimetry, 1983. **27**(1): p. 95-102.
67. Hollas, J.M., *Modern Spectroscopy*. 2003: John Wiley & Sons Ltd.
68. Hou, X., Jones, B. T, *Inductively Coupled Plasma/Optical Emission Spectrometry*, in *Encyclopedia of Analytical Chemistry*. 2000, John Wiley & Sons Ltd, Chichester, 2000. p. 9468-9485.
69. Echlin, P., *Introduction*, in *Handbook of Sample Preparation for Scanning Electron Microscopy and X-Ray Microanalysis*. 2009, Springer US. p. 1-9.
70. Mittemeijer, E., *Analysis of the Microstructure; Analysis of Lattice Imperfections: Light and Electron Microscopical and X-Ray Diffraction Methods*, in *Fundamentals of Materials Science*. 2011, Springer Berlin Heidelberg. p. 245-302.
71. *Joint Committee of Powder Diffraction Standards*, in *JCPDS-ICCD 2010*: Philadelphia, USA.
72. Haines, P.J., *Thermogravimetry*, in *Thermal Methods of Analysis*. 1995, Springer Netherlands. p. 22-62.
73. Verdonck, E., *TGA Training Course*, in *Thermogravimetry (TGA) Theoretical Training Course*. 2014, TA Instruments.

74. Interactive, P., *Implements PHREEQC 3.1.2*, in 3.1.2.8538, USGS, Editor. 2014.
75. Daniel Saalfeld, C.B., *MINTEQ database*. 2003, Jon Petter Gustafsson: Stockholm, SE.
76. Olsson, E., *Interfacial Microstructure in ZnO Varistor Materials*, in *Physics*. 1988, Chalmers University of Technology: Göteborg, SE. p. 50.
77. Pourbaix, M., *Atlas of electrochemical equilibria in aqueous solutions*. 1974: National Association of Corrosion Engineers.
78. Gutknecht, T., et al., *Investigations into Recycling Zinc from Used Metal Oxide Varistors via pH Selective Leaching: Characterization, Leaching, and Residue Analysis*. The Scientific World Journal, 2015.
79. B. Boyanov, V.K.a.N.K., *Removal of cobalt and nickel from zinc sulphate using activated cementation*. Journal of Mining and Metallurgy, Section B: Metallurgy, 2004. **40**(1): p. 41-55.
80. Kroleva, V., Metallurgiya Sofia, 1980.
81. Krause, B. and R.F. Sandenbergh, *Optimization of cobalt removal from an aqueous sulfate zinc leach solution for zinc electrowinning*. Hydrometallurgy, 2015. **155**(0): p. 132-140.
82. Lew, R., *The removal of cobalt from zinc sulphate electrolytes using the copper-antimony process*, in *Materials Engineering*. 1994, The University of British Columbia: Vancouver, Canada.
83. Bøckman, O. and T. Østvold, *Products formed during cobalt cementation on zinc in zinc sulfate electrolytes*. Hydrometallurgy, 2000. **54**(2-3): p. 65-78.
84. Raghavan, R., P.K. Mohanan, and S.K. Verma, *Modified zinc sulphate solution purification technique to obtain low levels of cobalt for the zinc electrowinning process*. Hydrometallurgy, 1999. **51**(2): p. 187-206.
85. Chen, H.-K., *Kinetic study on the carbothermic reduction of zinc oxide*. Scandinavian Journal of Metallurgy, 2001. **30**(5): p. 292-296.
86. Guger, C.E. and F.S. Manning, *Kinetics of zinc oxide reduction with carbon monoxide*. Metallurgical and Materials Transactions B, 1971. **2**(11): p. 3083-3090.
87. Bottom, R., *Thermogravimetric Analysis*, in *Principles and Applications of Thermal Analysis*. 2008, Blackwell Publishing Ltd. p. 87-118.
88. Golunski, S.E. and D. Jackson, *Antimony Oxides: A guide to phase changes during catalyst preparation*. Applied Catalysis, 1989. **48**(1): p. 123-135.
89. Jones, S.A., J. Fenerty, and J. Pearce, *The enantiotropic phase transition of antimony(III) oxide*. Thermochemica Acta, 1987. **114**(1): p. 61-66.
90. Trofimov, V.G., Sheinkman, A.I., Kleshchev, G.V., *Izv. Vyssh. Uchebn. Zaved. Fiz.*, 3, 1973: p. 135-137.
91. Centers, P.W., *Sublimation-controlled oxidation of antimony trioxide*. Journal of Solid State Chemistry, 1988. **72**(2): p. 303-308.
92. Cody, C.A., L. DiCarlo, and R.K. Darlington, *Vibrational and thermal study of antimony oxides*. Inorganic Chemistry, 1979. **18**(6): p. 1572-1576.
93. Orman, R.G. and D. Holland, *Thermal phase transitions in antimony (III) oxides*. Journal of Solid State Chemistry, 2007. **180**(9): p. 2587-2596.
94. Agrawal, Y.K., A.L. Shashimohan, and A.B. Biswas, *Studies on antimony oxides: Part I*. Journal of thermal analysis, 1975. **7**(3): p. 635-641.
95. Golunski, S.E., T.G. Nevell, and M.I. Pope, *Thermal stability and phase transitions of the oxides of antimony*. Thermochemica Acta, 1981. **51**(2-3): p. 153-168.